Structural and functional studies on nucleotide binding to AMP-activated protein kinase

A thesis submitted by

Peter Saiu

June 2010

Molecular Structure
MRC National Institute for Medical Research
The Ridgeway, Mill Hill, NW7 1AA
London

Research Department of Structural &
Molecular Biology
University College London

This thesis is submitted to University College London
for the degree of
Doctor of Philosophy

Declaration:

I, Peter Saiu, confirm that the work presented in this thesis is my own. Where information has been derived from other sources, I confirm that this has been indicated in the thesis

I have not submitted any portion of the work referred to in this thesis in support of any other qualification at this or any other institute of higher learning

Student

Signed:……..

Date:…….

(Dedicated to my parents)

Abstract

AMP-activated protein kinase (AMPK) is an enzyme that senses and regulates cellular energy balance thus playing a key role in homeostasis. As such it is a target for treatment of metabolic disorders such as type II diabetes. AMPK is a hetero-trimeric complex composed of an α, β and γ subunit. α contains the catalytic kinase domain, β is a scaffolding subunit that enables complex formation and γ monitors cellular energy via nucleotide binding to its CBS domains. AMPK is primarily activated by phosphorylation at Thr-172 on the activation loop in the kinase domain. It exerts its cellular effects via phosphorylation of a range of downstream targets involved in different aspects of energy production & utilization.

The aim of this thesis is to characterize the mechanistic basis of energy regulation of mammalian AMPK via structural and binding measurements. Fluorescence studies have been facilitated by the use of *N*-methylanthraniloyl (mant) labelled AMP and of β-Nicotinamide adenine dinucleotide 2'-phosphate (NADPH) to monitor competition with AMP, ADP and ATP. A number of mutations in the γ subunit, which interfere with the normal function of AMPK and cause Wolff-Parkinson-White (WPW) syndrome, have also assessed for changes in nucleotide binding affinities and potential implications for the regulation of kinase activity.

Thermal denaturation experiments are used to investigate the stabilizing effects of nucleotides and other small molecule ligands. This method was used in a low throughput screen against an enriched list of compounds selected from an *in silico* screen to try to identify novel activators.

I have also determined the structure of the regulatory fragment of the enzyme bound to 5-aminoimidazole-4-carboximide riboside monophosphate (ZMP), an intermediate on the biosynthetic route to AMP, the fluorescence reporter mant-AMP and the WPW mutants Arg298→Gly, Arg69→Gln and His150→Arg. The structures of the mutants have revealed that nucleotide binding is impaired due to a reduced affinity for the nucleotides thus affecting the regulation of the kinase.

Acknowledgements

First I would like to thank Steve Gamblin who gave me the opportunity to work in his lab and the MRC for funding my PhD. A special thank goes to my lab colleagues especially Bing, Jing, Lazy Lizzie & Phil. I kind of thank Rich "*the Mighty*" for humor, DVDs, insults, abuses, unfinished sentences, nicking markers & occasional help. Dave Goldstone for his immense patience in updating me with the new crystallographic softwares etc. I also acknowledge Lesley & Roxanne for setting up some initial trays and Valeria & Vangelis for help in chemistry.

I am grate to Jasveen from MRC Technology for carrying out the *in silico* screen and to Chris Toseland, John Eccleston, Colin Davis & John Offer from Physical Biochemistry for help in the nucleotide bound experiments. Thanks to Guy Dodson, although he never remembers my name (!), for helping me in structuring my thesis. The tremendous help, comments and patience in teaching me the basis of my binding studies by Stephen Martin are gratefully acknowledged. Thanks also to Dave Carling's lab for their collaboration and in particular to Dave for helpful comments on my thesis.

My particular thanks to everybody in the Molecular Structure Division for the enjoyable tea/beer times and to my farmville neighbors. Thanks to the Chirac's Worms & the footy crew for the immense quality football played in these 3 years (and thanks to Cyprian for playing as bad as me at pool!). Thanks to the canteen for the roast dinner on Wednesdays, burgers on Thursdays & English breakfast on Fridays. Finally, I would like to thank my friends from Leafield Cottage and my coffee-time acquaintances … (what's her name?!?) … for the distractions that made the last 3 years particularly enjoyable! … Now the serious part …

When I first joined this project I worked on several aspects of the work described in Xiao *et al* 2007 but because of my level of experience I was not principally directing these studies. Later in the project, although advised and guided, I carried out the work described here independently.

List of abbreviations

ACC1	Acetyl-CoA carboxylase 1
ACC2	Acetyl-CoA carboxylase 2
ADP	Adenosine diphosphate
AICAR	5-Aminoimidazole-4-carboxamide-1-β-D-ribofuranosyl
AMP	5'-Adenosine monophosphate
AMPK	AMP-activated protein kinase
AMPK-RK	AMPK-related kinases
AMPKK	AMPK upstream kinases
Arg	Arginine
Asp	Aspartic acid
AS160	Akt Substrate 160
ATP	5'-Adenosine triphosphate
AXP	AMP, ADP or ATP
CaMKKs	Ca^{2+}/Calmodulin-dependent protein Kinase Kinases
CBS	Cystathionine β-synthase domain
CD	Circular Dichroism
CD36	Fatty acid translocase
CLCs	chloride channels
CNTF	Ciliary neurotrophic factor
DLS	Dynamic Light Scattering
DMSO	Dimethyl sulfoxide
EDTA	Ethylenediaminetetraacetic acid
EF-2 kinase	Elongation factor-2 kinase
F-1,6-P_2	Fructose-1,6-bisphosphate
FRET	Förster resonance energy transfer
GBD	Glycogen-binding domain
GF	Gel filtration
Gln	Glutamine
GLUTs	Glucose transporters
GLUT4	Glucose transport 4
Gly	Glycine
GP	Glycogen phosphorylase
GS	Glycogen synthase
GSD	Glycogen storage diseases
HCl	Hydrochloric acid
His	Histidine
HMGR	HMG-CoA reductase
HPLC	High-performance liquid-chromatography
HSL	Hormone-sensitive lipase
IL-6	Interluekin-6
IPTG	Isopropyl-β-D-thiogalactopyranoside
K_a	Association constant
K_d	Dissociation constant
KO	Knock-out
Lys	Lysine

Mant	*N*-methylanthraniloyl
MEF-2	Myocyte enhancer factor-2
Mg^{2+}	Magnesium
MO25	Mouse protein 25
MPD	2-Methyl-2,4-pentanediol
MRCT	MRC technology
NADH	β-nicotinamide adenine dinucleotide
NADPH	β-nicotinamide adenine dinucleotide 2'-phosphate
NIMR	The National Institute for Medical Research
PFK2	6-phosphofructo-2-kinase
PGC-1α	PPAR-γ coactivators-1α
PP	Protein phosphatase
r.m.s.	Root mean square
SAM	S-adenosyl methionine
SDS-PAGE	Sodium Dodecylsulfate Polyacrylamide Gel Electrophoresis
SNF1	Sucrose Non-Fermenting-1
STRADα	STE20-related adaptor protein α
TAK1	Transforming growth factor-β-activated kinase 1
TCEP	Tris(2-carboxyethyl) phosphine hydrochloride
Thr	Threonine
T_m	Melting temperature
TNF-α	Tumor necrosis factor α
TOR	Target-of-rapamycin
TORC 1	mTOR complex 1
TSC2	Tuberus Sclerosis complex 2
Tu-MP	Tubercidin 5'-monophosphate
WHO	World Health Organisation
WPW	Wolff-Parkinson-White
wt	Wild type
ZMP	AICAR 5'-monophosphate

List of contents

List of figures

List of tables

List of appendices

INTRODUCTION

1. Introduction

Living organisms need energy in order to carry out vital cellular processes such as synthesis of macromolecules, cell division and movement. In mammalians, energy is derived from foods such as carbohydrates, fatty acids and proteins. These nutrients are absorbed from the gut and dispersed through the blood stream from where they are taken up by cells throughout the body. A key molecule used as a source of energy in cells is glucose. Excess glucose is stored by conversion into glycogen. When energy is needed, glucose, through a series of cellular processes such as glycolysis, the Krebs cycle and oxidative phosphorylation, is used to regenerate 5'-Adenosine triphosphate (ATP). ATP is an immediately available nucleotide that liberates large amounts of energy when it is hydrolyzed to 5'-Adenosine diphosphate (ADP) and phosphate [1].

In a typical cell, there is a continuous turnover of ATP and it is clearly vital to have an efficient mechanism for monitoring ATP consumption and regulating its regeneration so that cellular homeostasis is not compromised.

1.1 AMP-activated protein kinase (AMPK)

AMPK is an ubiquitously expressed protein kinase that senses and regulates cellular energy balance, playing a central role in regulating cellular metabolism [2]. AMPK activity in cells is relatively low in situations where glucose and oxygen levels are optimal and the cell is not under metabolic stress (e.g. myocytes at rest). Under these conditions, ATP, ADP & AMP concentration are around 2-5 mM, 200-500 μM and 2-5 μM, respectively [3]. AMPK is thought to be activated by a number of stimuli that act to increase the AMP:ATP ratio [4-5]. Once AMPK is activated, it works on a wide range of target enzymes to restore energy levels by inhibiting energy-requiring pathways such as protein or fatty acid synthesis and at the same time, it enhances ATP-producing pathways such as glycolysis and fatty acid oxidation.

1.1.1 Structure of AMPK

AMPK is a hetero-trimeric complex composed of one copy each of α, β and γ subunits (**Fig 1.1**). Homologues of all three subunits have been identified in yeasts, which form the SNF1 (Sucrose Non-Fermenting-1) complex in *S. Cerevisiae* and SNF-like protein in *S. Pombe* (see **section 1.1.3.2**) [6-7]. In mammals, two isoforms each for α and β are known (α1, α2, β1 and β2) and three different isoforms of γ (γ1, γ2 and γ3) together with alternate splicing forms [8]. Different combinations of isoforms allow the formation of distinct hetero-trimeric complexes which have been suggested to be tissue-specific [8-11]. α is the catalytic subunit which has a conventional kinase domain at its amino terminus including a regulatory phosphorylation site at Thr-172 (**Fig 1.1**). The crystal structure of the kinase domain of AMPK has been published [12], but the activation loop is largely disordered, presumably because it is not phosphorylated. The α subunit also interacts with the β-subunit through its C-terminus. The β-subunit acts as a scaffold to which the other two subunits bind; it also contains a so-called glycogen-binding domain (GBD) towards its amino terminus, which has been proposed to play a role in sensing glycogen availability [11,13] (see **section 1.1.2.3**)**.** A crystal structure of the isolated GBD from mammalian AMPK has been published revealing the carbohydrate binding pocket responsible for binding to glycogen [14-15]. The γ subunit of AMPK is responsible for the energy sensing properties of the complex because it binds competitively to either AMP, ADP or ATP via its two Bateman domains [16]. A Bateman domain is made up from a pair of CBS motifs [17], termed after cystathionine β-synthase, the human protein where this domain was initially found. A CBS motif is a conserved domain of about 60 amino acids which are present in over a thousand other known proteins. The crystal structures of several proteins containing CBS domains have been solved [18-20]. Although the function of CBS motifs in most of these proteins remains to be established, they often occur in the context of metabolic enzymes, transcriptional regulators, ion channels and transporters [21]. In some proteins CBS motifs are responsible for binding to adenosine-containing ligands such as AMP, ATP or S-adenosyl methionine [22]. In AMPK, the four CBS motifs that

make up the γ subunit have been found to be responsible for monitoring cellular energy by binding competitively to either AMP or ATP [16].

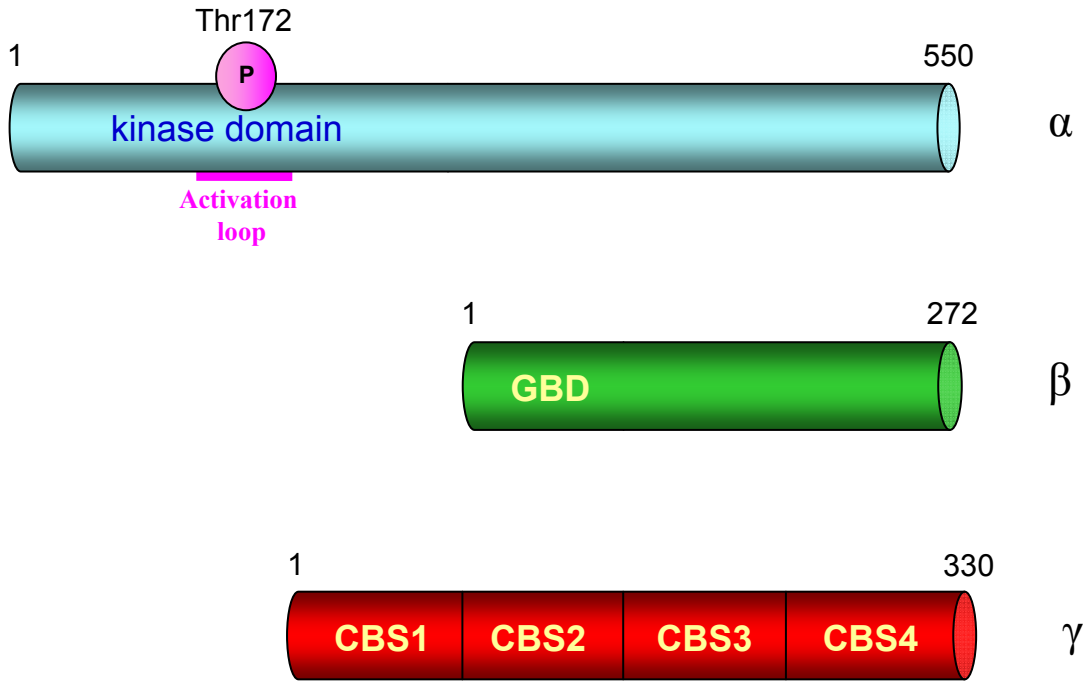

Figure 1.1: Diagrammatic representation of the hetero-trimeric complex of AMPK: the α subunit is indicated in cyan, β in green and γ in red.

1.1.2 Regulation of AMPK

The enzyme activity of AMPK is highly dependant on the phosphorylation status of the activation loop of the kinase domain. Activity increases 100-fold upon phosphorylation by upstream kinases [4]. AMPK is activated by various stimuli such as hypoxia [23], oxidative stress [24], glucose deprivation [25], ischemia [26-27] and physical exercise [28-29]. The outcome of all of these effects is to increase the cellular AMP/ATP ratio. AMPK has also been found to be regulated by glycogen and hormones [30].

1.1.2.1 Reversible phosphorylation

The activity of many proteins is modulated by post translational modification. Acetylation, glycosylation and phosphorylation are all common covalent modifications. Protein phosphorylation refers to the reversible attachment of a phosphate group to hydroxyl side chains of serine, threonine and tyrosine, and is some cases to the side chain of histidine residues [31-32]. The phosphorylation cycle is catalyzed by a protein kinase and a protein phosphatase (PP).

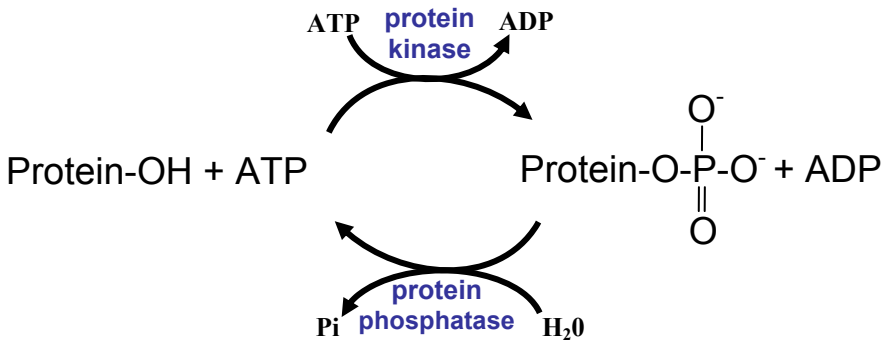

Figure 1.2: Regulation of phosphorylation: phosphorylation and dephosphorylation are highly favourable reactions driven ultimately by the hydrolysis of ATP**.**

In animal cells reversible phosphorylation is the major intracellular mechanism by which cells respond to first messengers, which include growth factors, nutrients and hormones etc. [33]. These extracellular stimuli can then give rise to the sequential phosphorylation of protein kinases inside the cell in a protein kinase cascade which amplifies the original signal. Second messengers can be formed in micromolar concentrations in response to nanomolar levels of external signal molecules [34]. To date, about 518 protein kinases have been identified in the human genome which are involved in a myriad of cellular processes; their misregulation often results in disease [35]. The development of specific activators and inhibitors for protein kinases is increasing and kinases are now the second most important group of drug targets, after G-protein-coupled receptors [35]. As a consequence a lot of effort has been

invested in determining their 3-dimensional structures and currently there are about 50 unique protein kinase crystal structures [36].

AMPK belongs to a well characterized protein kinase cascade. Two of the upstream kinases (AMPKKs) that catalyze the phosphorylation of AMPK at Thr-172 are LKB1 and Ca^{2+}/Calmodulin-dependent protein Kinase Kinases (CaMKKs) [37-40] (**Fig.1.3**). LKB1 is the major upstream kinase and is a tumor suppressor which is mutated in Peutz-Jeghers cancer predisposition syndrome. Peutz-Jeghers syndrome patients are characterized by the development of numerous benign intestinal polyps (hamartomas). The LKB1 gene generates two alternative splicing patterns whose protein products have different C-terminal sequences: a long 50 kDa form, LKB1L, and a short 48-kDa form, LKB1S [41]. LKB1L is widely expressed in mammalian tissues, whereas LKB1S is primarily expressed in the testis. It appears that the physiological role of the two distinct alternative splice forms of LKB1 is not directly connected to divergences in the carboxyl terminal sequences but probably because of differences in tissue distribution [41]. In order to be active, it is essential also for LKB1 to form a heterotrimeric complex with two regulatory subunits, namely the pseudokinase STE20-related adaptor protein α (STRADα) and Mouse protein 25 (MO25) [42-43]. AMPK activity is significantly reduced in a tissue-specific knockout model of LKB1 in myocytes, cardiocytes and hepatocytes indicating that LKB1 plays a key role in AMPK activation [44-46].

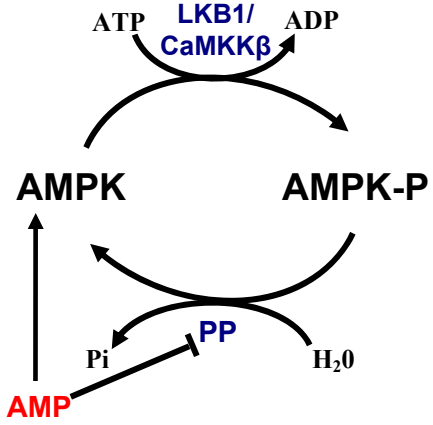

Figure 1.3: Regulation of AMPK: LKB1 and CaMKKβ activate AMPK by phosphorylation at Thr-172. AMP allosterically activates AMPK and also protects the activation loop from dephosphorylation by protein phosphatases.

CaMKKs were initially shown to phosphorylate Calmodulin-dependent protein kinases I and IV [47]. Their physiological role as an activator of AMPK was revealed when in HeLa cells, which do not express LKB1, the basal activity of AMPK was diminished by the CaMKK inhibitor STO-609. In contrast, when incubated with the Ca^{2+} ionophore A23187, AMPK activity increased [39]. Two isoforms of CaMKK, which are primarily found in neural tissue, have been identified, α and β, but it was shown that only CaMKKβ, plays a major role in phosphorylating and activating AMPK *in vitro* and in mammalian cells [39,48-49]**.** Hence, there appear to be at least two signaling pathways that trigger AMPK activity, one dependent on LKB1 and the other induced by increases in calcium, mediated by CaMKKβ.

Recently, it has been reported that transforming growth factor-β-activated kinase-1 (TAK1) activates AMPK in rodents, but the physiological role of TAK1 as an AMPKK is not well documented [50-51]. Further, auto-phosphorylation on the α and β subunits may additionally affect enzymatic activity [52-53], but their precise role is also still unclear. It has been suggested that these additional auto-phosphorylation sites might play a role in AMPK activity or cellular localization.

AMPK is down-regulated when de-phosphorylated by a protein phosphatase (PP). The identity of the protein phosphatase responsible for AMPK dephosphorylation *in vivo* has not been determined. Although all the PP tested de-phosphorylated AMPK *in vitro*, the likely physiological candidates are PP2A and PP2C (the latter is also referred as PPM) [54]. The yeast homologue of AMPK, SNF1 complex has been shown to be de-phosphorylated by the Glc7-Reg1 protein phosphatase complex [55]. Glc7 is the catalytic subunit of the complex and belongs to the type I PPs (PP1) [56]. Reg1 interacts with the catalytic subunit of the SNF1 complex, Snf1, leading to the inactivation of SNF1 complex through dephosphorylation of the activation loop by Glc7. By analogy this suggests that PP1 might play a role in the regulation of mammalian AMPK, although this issue has yet to be confirmed.

Mutation of Thr-172 to a negatively charged residue such as a glutamic acid (Thr-172→Glu) can, to some extent, mimic the phosphorylation event resulting in constitutive activity that is about 50% of the corresponding activated wild-type AMPK [57]. Conversely, mutation of Thr-172 (Thr-172→Ala), abolishes AMPK activity almost entirely.

AMPK phosphorylates, and differentially regulates numerous targets. Some of these include: acetyl-CoA carboxylase 1 (ACC1), HMG-CoA reductase (HMGR) and muscle glycogen synthase (GS) phosphorylation of which inactivates the synthesis of fatty acid, cholesterol and glycogen, respectively (**Table 1.1**) [4,58-60]. AMPK also inhibits protein synthesis in different ways, either by activating elongation factor-2 kinase (EF-2 kinase) [61], therefore inhibiting the elongation step, or by inhibiting the mammalian target of rapamycin (mTOR), which enhances translational initiation. mTOR is inhibited by AMPK either directly, by phosphorylating the mTOR binding partner, raptor, or by phosphorylating Tuberus Sclerosis complex 2 (TSC2) which lies upstream of mTOR [62-65].

Other AMPK targets include proteins involved in the production of energy such as acetyl-CoA carboxylase 2 (ACC2), 6-phosphofructo-2-kinase (PFK2), hormone-sensitive lipase (HSL), fatty acid translocase (FAT/CD36). Their phosphorylation enhances fatty acid oxidation, glycolysis, triglyceride breakdown and fatty acid uptake, respectively (**Table 1.1**) [23,66-72]. AMPK also enhances glucose uptake by enabling the translocation of GLUT4 vesicles. This appears to be mediated by AMPK by targeting the Akt Substrate 160 (AS160), although recently it has been suggested that AS160 is not directly phosphorylated by AMPK but TBC1D1 appears to be the true downstream substrate for AMPK (explained in more detail in **section 1.1.4.1**) [71,73-75].

AMPK therefore plays a dual role in re-establishing cellular energy homeostasis by the inhibition of ATP-consuming processes and by enhancing ATP-producing pathways. In addition, AMPK also exerts long-term effects on fatty acid synthesis and gluconeogenesis altering gene expression [76-78] and these effects are probably mediated by down-regulating transcription factors such as HNF-4α or GLUT4 [79-80]. GLUT4 expression in myocytes, for example, is enhanced by AMPK by stimulating the binding of the transcription factor myocyte enhancer factor-2 (MEF-2) to the GLUT4 promoter [80]. Alternatively, AMPK exerts its effects at the transcriptional level by directly phosphorylating transcriptional coactivators such as PPAR-γ coactivators-1α (PGC-1α; [81]), at Thr-177 & Ser-538, or as transducer of regulated CREB activity 2 (TORC2; [82]), at Ser-171. AMPK phopshorylation of PGC-1α results in upregulation of several transcription factors involved in mitochondrial biogenesis [83], whereas phosphorylation of TORC2 by AMPK results in a reduction in gluconeogenesis by blocking its nuclear accumulation [82].

Substrate	Residue	Effect on activity/Role	Ref
ATP-requiring pathways			
HMGR	Ser-871	↓ cholesterol synthesis	4; 59
ACC1	Ser-79; Ser-1200; Ser-1215	↓ fatty acids synthesis	59
GS	Ser-7	↓ glycogen synthesis	58; 60
EF-2 kinase	Ser-366; Ser-398	↓ protein synthesis	61
TSC2	Thr-1227; Ser-1345	↓ protein synthesis	64
Raptor	Ser-722; Ser-792	↓ protein synthesis	63
TORC2	Ser-171	↓ gluconeogenesis	82
ATP-producing pathways			
ACC2	Ser-222	↑ fatty acid oxidation	66; 70
PFK-2	Ser-466	↑ glycolysis	23
HSL	Ser-565	↑ triglyceride breakdown	67; 68
FAT/CD36		↑ fatty acid uptake	69
AS160	Ser-588	↑ glucose uptake	71; 74
TBC1D1	Ser-231; Ser-660; Ser-700	↑ glucose uptake	73-75
PGC-1α	Thr-177; Ser-538	↑ mitochondrial biogenesis	81; 83

Table 1.1: Downstream targets of AMPK**:** the phosphorylation sites are shown together with the effect on metabolism.

1.1.2.2 Regulation of AMPK by AMP

The binding of a ligand to a site on a protein, that is not the active site, which alters enzyme activity is termed allosteric regulation. Such ligands may enhance the activity of the enzyme and be referred to as allosteric activators, or they may decrease the enzyme's activity and are described as allosteric inhibitors [84]. Allosteric regulation can occur within one subunit or between subunits. AMP-activated protein kinase was so-named because early studies showed that this protein kinase was allosterically activated by AMP [85]. AMPK purified from rat tissues was shown to be

activated by AMP around 3-fold *in vitro*. Later it was shown that AMP bound to the regulatory γ subunit and that the level of activation depended on the combination of isoforms making up the heterotrimer [86]. Specifically, AMPK containing a γ2 subunit is more sensitive to AMP than γ1- or γ3-containing heterotrimers; γ3 being the least AMP responsive. Neither ADP and ATP allosterically activate AMPK but bind to the AMP site, thus by competing with AMP, ATP inhibits activation of AMPK.

AMP also acts to protect AMPK from dephosphorylation of Thr-172 [5,54] (**Fig 1.3**). Initially it was believed that AMP facilitated a third mechanism for AMPK activation by promoting phosphorylation of Thr-172. However, a recent paper has suggested that initial data were misinterpreted because AMPK samples were only partially purified and some PP2C was present in the preparation [87].

5-aminoimidazole-4-carboximide ribonucleoside (AICAR) has been a valuable tool for studying AMPK regulation in cells [4]. AICAR is an adenosine analogue that enters the cells via adenosine transporters [88]. It is then converted by adenosine kinase to 5-aminoimidazole-4-carboximide riboside monophosphate (ZMP), by the addition of a phosphate group [89] (**Fig 1.4**). ZMP mimics both of the effects of AMP on AMPK (i.e. allosteric activation and reduced dephosphorylation), but its potency is poorer than AMP [59,90]. Additionally, this compound is not completely specific for AMPK, as ZMP interacts with other AMP-sensitive enzymes such as fructose-1,6-bisphosphatase (FBPase) and muscle glycogen phosphorylase [89,91] (see **section 1.1.3.3**).

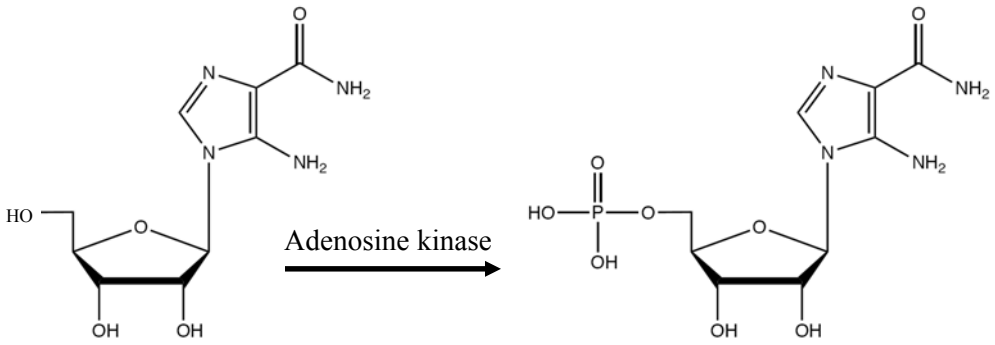

Figure 1.4: Structure of AICAR (left) which is converted to ZMP (right) by adenosine kinase.

1.1.2.3 Putative allosteric inhibition of AMPK by glycogen

Previous studies have shown connections between AMPK and glycogen metabolism [30]. Among the downstream targets of AMPK is glycogen synthase, which is responsible for the synthesis of glycogen from glucose-6-phosphate. The synthesis of glycogen is a process that requires larges amount of energy, therefore when there is high utilization of ATP, AMPK phosphorylates glycogen synthase, inhibiting its activity, leaving the metabolized glucose free to enter glycolysis [58,92]. An additional connection between AMPK and glycogen metabolism is shown in myocytes, where high glycogen levels repress contraction-induced AMPK activation [92-93]. Interestingly, naturally occurring mutations in the human γ2 subunit of AMPK causes a glycogen storage cardiomyopathy.

Recently, McBride and Hardie suggested that AMPK might play a direct role in glycogen storage and utilization, by acting as a glycogen storage sensor [94]. As mentioned above, the β subunit of AMPK contains a GBD. The GBD has been proposed to regulate AMPK activity in response to cellular glycogen content. Specifically, McBride and Hardie proposed that glycogen could allosterically inhibit AMPK. This might explain why, in response to exercise, high glycogen levels in myocytes reduce AMPK activity without apparently changing adenine nucleotide concentration [92]. McBride and Hardie additionally suggested that glycogen inhibited the phosphorylation of Thr-172 phosphorylation of AMPK by upstream kinases [94].

1.1.2.4 Regulation by hormones and cytokines

AMPK is also involved in the regulation of whole-body energy metabolism as it regulates both energy expenditure and appetite. AMPK activity in different tissues is coordinated via the secretion of various hormones and cytokines. For example, adipocytes secrete hormones such as leptin, adiponectin and resistin, whereas stomach cells secrete ghrelin [95]. Cytokines such as interluekin-6 (IL-6), ciliary

neurotrophic factor (CNTF) and tumor necrosis factor α (TNF- α) are also secreted by specific cells of the immune system [95]. Leptin and adiponectin appear to enhance insulin sensitivity by influencing weight gain, feeding behavior and glucose homeostasis. Activation of AMPK by these hormones in peripheral tissues causes an increase in fatty acid oxidation and an increase in glycolysis (**Table 1.2**) [96-97]. Leptin and adiponectin are unable to regulate glucose homeostasis in the livers of AMPK knock-out mice, suggesting that these effects may be partly mediated by AMPK activation [98]. Additionally, expression of a dominant negative mutant of AMPK using an adenoviral vector lead to a reduction of gluconeogenesis in the liver, and reduction of glucose levels *in vivo*, confirming that stimulation of glucose utilization and fatty-acid oxidation by adiponectin occurs via AMPK activation [97].

While leptin and adiponectin appear to enhance insulin sensitivity, other hormones and cytokines seem to have the opposite effect on insulin sensitivity [95,99-102]. For example, the level of AMPK phosphorylation in the liver of resistin knock-out mice is higher compared to wild type, indicating that resistin might down-regulate hepatic AMPK [103]. It is thought that inappropriate secretion of these hormones and cytokines play an important role in the development of obesity and metabolic syndrome [95]. Therefore it will be important to determine the exact roles of AMPK in influencing the effects brought about by these hormones and cytokines, and to understand the connection between AMPK and whole energy homeostasis.

	Hypothalamus	Skeletal muscles	Adipocytes
Hormones			
Leptin	↓	↑	↑
Adiponectin	↑	↑	↑
Ghrelin	↑	no effect	↓
Resistin	?	↓	↓
Cytokines			
IL-6	?	↑	↑
TNF- α	?	↓	?

Table 1.2: Summary of the effects of hormones and cytokines on AMPK activity in three different tissues. This is consistent with a crucial role of AMPK in regulating whole body energy homeostasis.

1.1.3 AMPK across the kinome

1.1.3.1 AMPK-related kinases (AMPK-RK)

Sequence homology analysis has revealed thirteen human protein kinases closely related to the catalytic subunit of AMPK that are referred to as the AMPK-RK family. They comprise: BRSK1, BRSK2, MARK1, MARK2, MARK3, MARK4, MELK, NUAK1, NUAK2, QIK, QSK, SIK and SNRK [104] (**Fig 1.5**). Like AMPK they are regulated via phosphorylation of a threonine residue on their activation loops by LKB1. The specificity of these AMPK-RK to the upstream activation is somewhat different to AMPK in that the activation loops contains a leucine residue at the -2 position [46]. Interestingly, AMPK-RK do not appear to be regulated by CaMKKs. For some of them, phosphorylation enhances their activity as much as 50-fold [105]. In contrast, MELK is the only protein of this family that is not phosphorylated by LKB1 but is instead activated by auto-phosphorylation [105]. SNRK is the least conserved member of the AMPK-RKs and belongs to an additional family of 8 protein kinases, referred to as the SNRK family [106]. Interestingly, only SNRK from this group is activated by LKB1 possibly because it is the only protein

among the SNRK family that contains a leucine at the -2 position in the activation loop.

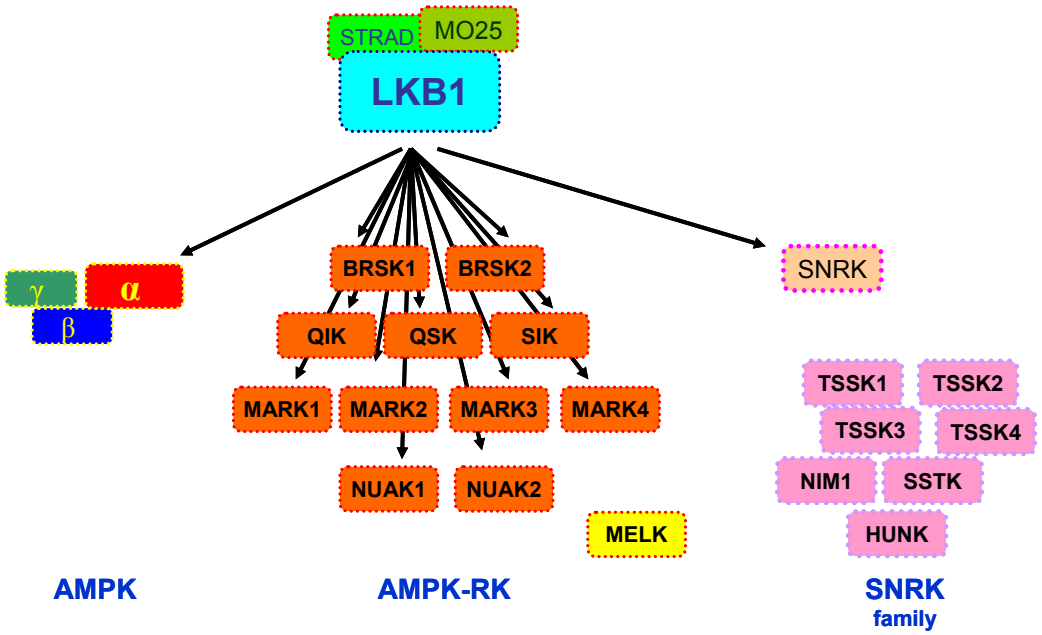

Figure 1.5: LKB1 is the master regulator of 13 protein kinases. The activity and cellular localization of LKB1 is controlled through its interaction with STRAD and MO25. α, the catalytic subunit of AMPK, is related to AMPK-RK and SNRK. MELK, although belongs to AMPK-RK, is not activated by LKB1 but by auto-phosphorylation. The SNRK family comprises NIM1, TSSK1, TSSK2, TSSK3, TSSK4, SSTK, HUNK and SNRK. Only the latter is phosphorylated by LKB1.

The sequences of the α subunit of AMPK and AMPK-RKs, are similar and all contain an amino-terminal kinase domain. Except for NUAK-1 & -2, the kinase domain of AMPK-RK is followed by an ubiquitin-associated (UBA) domain. A UBA domain is a sequence of about 45 amino acid residues present in various enzymes, although the AMPK-RKs are the only family of kinase proteins in the human genome to contain a UBA domain [104,107]. In proteins other than kinases, UBA domains function as ubiquitin- or polyubiquitin-interacting motifs, whereas in AMPK-RKs they do not interact with ubiquitin-like molecules, but appear to be necessary for LKB1 phosphorylation [104,106,108]. The effect of UBA domains in AMPK-RK is achieved not by associating with the LKB1–STRAD–MO25 complex,

but by directly interacting with the catalytic domain of these AMPK-RKs, facilitating an optimal conformation for phosphorylation by LKB1 [107].

1.1.3.2 Yeast homologues of AMPK

AMPK is highly conserved across species and many insightful studies have been carried out on the yeast homologue of AMPK, SNF1 from *S. Cerevisiae* [6]. Homologues of the mammalian α, β and γ subunits are present in *S. Cerevisiae*. Snf1 is the catalytic subunit that contains the kinase domain; Sip1, Sip2 and Gal83 proteins are scaffolding subunit equivalent to β [109], and Snf4 corresponds to the γ subunit and contains four CBS motifs. Interestingly, SNF1 is not AMP regulated but it performs the role of cellular energy monitor by phosphorylating targets involved in the regulation of gene transcription in response to intracellular changes in glucose levels [110]. No full-length structures have been solved for SNF1, but truncated constructs, similar to the one used in our lab, have been crystallized (**see section 3.2.2**). The structure of the kinase domain alone of Snf1, was solved in 2005 at about the same time as the human α2 AMPK kinase domain [111]. The crystal structure of the regulatory domain of SNF1, and of the SNF1 protein from *S. Cerevisiae*, were both published in 2007, at the same time as our mammalian version. These structures showed similar domain arrangement as ours and, additionally, the SNF-like protein contained a GBD which interacts with the γ subunit equivalent [112-113] (see **section 5.6**).

1.1.3.3 Other AMP-regulated enzymes

AMPK is not the only AMP-dependant enzyme in mammalian cells. The widespread use of AICAR in AMPK studies revealed that other AMPK-independent pathways are affected. Further studies with liver specific AMPK knock-out mice (AMPKα1α2$^{-/-}$) demonstrated that AICAR inhibited glucose-induced translocation of glucokinase from the nucleus [114]. In liver cells from AMPKα1α2$^{-/-}$ mice AICAR also inhibited cellular respiration in association with a decrease in cellular ATP concentrations [115]. This inhibition resulted partly from an ATP-mediated

phosphorylation of AICAR which leads to a reduction in intracellular phosphate, which is one of the main cofactors in mitochondrial oxidative phosphorylation (OXPHOS) [115]. ZMP accumulation also affects many enzymes with AMP-binding sites, such as glycogen phosphorylase, glycogen synthase, or fructose 1,6-bisphosphatase, glucokinase and phosphofructokinase-1 [89,91,116-118], their respective K_ms for ZMP being generally in the range of the cellular nucleotide concentration. These results clearly show that some of the effects of AICAR in cells are not caused by AMPK and the results that come with its use need to be carefully interpreted.

Glycogen phosphorylase (GP) is a good example of a structurally well documented enzyme whose activity is regulated by AMP (**Fig 1.6**). Glycogen phosphorylase catalyses the first step of glycogenolysis which is the intracellular degradation of glycogen into glucose-1-phosphate [119]. It exists in a non-phosphorylated GPb form (T state) which is less active and in an active phosphorylated form GPa (R state) [120]. Hormonal or neuronal signals stimulate the phosphorylation on a serine residue at the amino terminal (Ser-14) located on the surface of the protein. The non-phosphorylated form of glycogen phosphorylase is also allosterically activated by micromolar concentrations of AMP and the level of activity achieved by phosphorylation and allostery are comparable [119]. Therefore, during physical exercise for example, AMP concentration increases and glycogen phosphorylase is allosterically activated. By enhancing glycolysis, glycogen phosphorylase enhances ATP supply. Consequently, ATP opposes the allosteric activation by displacing AMP from the binding pocket. This indicates the re-establishment of energy homeostasis.

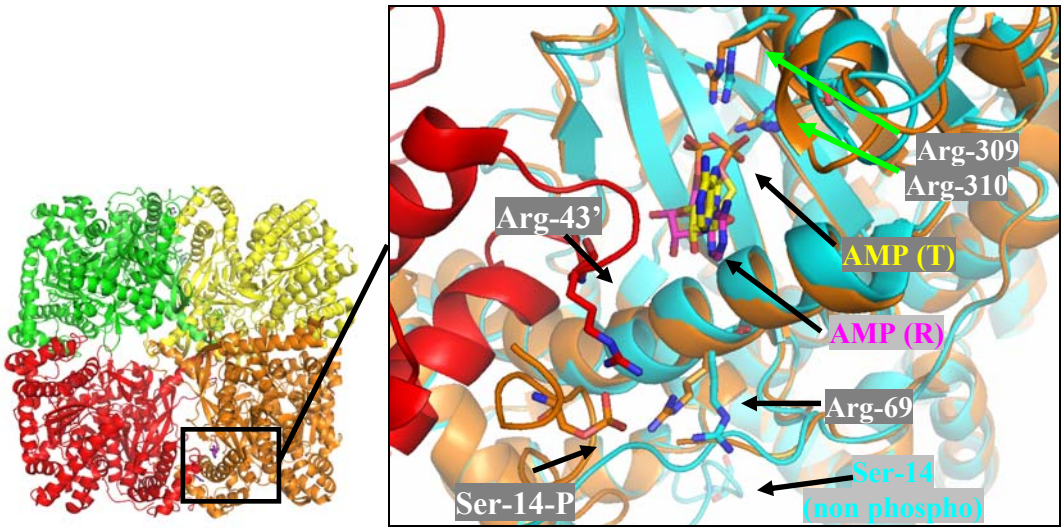

Figure 1.6: Cartoon representation of glycogen phosphorylase in the R state (PDB: 7GPB). In the unbound state, the non-phosphorylated form of glycogen phosphorylase is a dimer. (A) Once AMP binds, or the enzyme is phosphorylated, two dimers associate to produce a tetramer. (B) Superposition between the R state (protein colored in orange with AMP in sticks with carbon atoms in magenta) and T state (protein in cyan with AMP in sticks with carbon atoms in yellow – PDB: 8GPB). Arg-43 belongs to the other subunit of the enzyme which is in red).

When non-phosphorylated, glycogen phosphorylase has low affinity for substrates, but when phosphorylated the affinity for substrates and allosteric activators increases [119]. The catalytic site is at the centre of the protein distinct from the surface where AMP binds at the interface of the two subunits. The low affinity of AMP for the T state can be structurally explained by the relatively few contacts formed between the phosphate moiety of the nucleotide and two basic residues in the allosteric binding pocket (Arg-309 & Arg-310). Thus the specificity for ligand binding arises from other parts of the nucleotide, hence other ligands such as ADP, ATP, ZMP can also bind [121]. When non-phosphorylated, the N-terminal part containing Ser-14 blocks access to the catalytic site. But, in the R state, once Ser-14 is phosphorylated it shifts approximately 34 Å and it interacts with two other basic residues at the subunit interface (Arg-69 from one subunit & Arg-43' from the other) and liberates the catalytic site [122]. This causes AMP to shift a few Å and its ribose and adenosine

moiety form new interactions with the protein. This binding site therefore becomes more extensive following phosphorylation creating a more favorable binding site for AMP.

Another example, in less detail, of an enzyme which is regulated by AMP is fructose FBPase (**Fig 1.7**). FBPase catalyzes an important step of gluconeogenesis by hydrolyzing fructose-1,6-bisphosphate (F-1,6-P_2) to fructose-6-phosphate and inorganic phosphate [123]. FBPase is very sensitive (micromolar range) to allosteric inhibition by AMP and its believed to be constantly inhibited in the presence of normal physiological AMP concentrations [124]. In contrast, when, glyconeogenesis or gluconeogenesis is needed, the substrate for FBPase is supplied by aldolase. In myocytes, aldolase strongly interacts with FBPase forming a complex which is then insensitive to AMP [125].

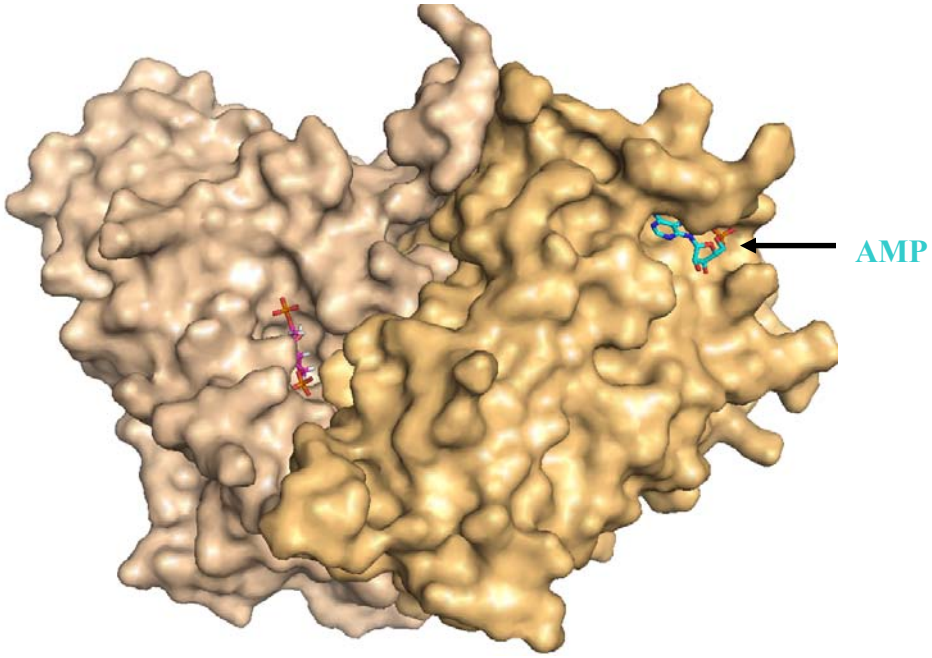

Figure 1.7: Surface representation of the dimeric complex of two FBPases (PDB: 1FPF). Mammalian FBPase exists as a tetramer where each monomer is composed of two domains, the F-1,6-P_2 domain containing the active site and AMP-binding site domain [126]. AMP and 2,5-anhydroglucitol-1,6-biphosphate (an F-1,6-P_2-analogue) are shown in sticks with carbon atoms colored in cyan and magenta, respectively.

Similarly to AMPK, misregulation of the activity of glycogen metabolism enzymes may result in defects leading to glycogen storage diseases (GSD) [127] (see **section 1.1.4.3**). There are eleven distinct conditions that are commonly considered to be glycogen storage diseases and malfunction in the activity of glycogen synthase, muscle glycogen phosphorylase, liver glycogen phosphorylase and muscle phosphofructokinase-1 correspond to GSD types 0, 5, 6 and 7, respectively.

1.1.4 Connection to diseases

As AMPK is implicated in the regulation of food intake and energy expenditure at the systemic level, it is considered a promising target for the treatment of metabolic disorders including cardiovascular disease, obesity, type II diabetes and, recently, cancer. Additionally, AMPK regulation is linked to other human disorders as naturally occurring mutations in its γ subunit are also responsible for Wolff-Parkinson-White (WPW) syndrome.

1.1.4.1 Diabetes mellitus

The World Health Organisation (WHO) estimates that more than 180 million people worldwide have diabetes and this number is increasing rapidly. Approximately 1.1 million people died from diabetes in 2005 and this number is projected to increase by over 50% in the next 10 years. 10% of the cases of diabetes mellitus belong to type I, whereas 90% are attributed to type II [128]. The former type is more acutely life-threatening than the type II form and is characterized by insulin deficiency due to autoimmune destruction of β-cells from the pancreas which secrete it. It has an early onset and is treated with insulin injections. Type II diabetes instead has an adult-onset and, although there seems to be genetic factors that influence predisposition, it is strongly associated with a sedentary lifestyle and an unbalanced

diet. Both forms, if untreated lead to long-term complications, including retinal damage, nerve damage and kidney & cardiovascular disease [128-129].

Type II diabetes is associated with increased insulin, glucose and lipid concentrations in the blood together with insulin resistance of tissues. Patients have reduced glucose uptake in peripheral tissues and increased gluconeogenesis. Cellular glucose uptake is mediated by glucose transporters (GLUTs) of which thirteen isoforms are currently known, and their relative abundance is tissue-specific [130]. GLUT4 is mostly found in skeletal muscles and adipose tissues, which together comprise about 60% of body mass [131]. One of the main cellular effects of insulin is to stimulate glucose uptake from the blood into cells following a carbohydrate-rich meal by mediating the translocation of GLUT4 to the plasma membrane [132]. Diabetic patients have a dysfunctional insulin pathway that leads to poor GLUT4 translocation to the plasma membrane [132]. However, a parallel, insulin-independent, pathway for glucose uptake can still be activated via physical exercise which mimics some of the cellular effects of insulin [29,133] (**Fig 1.8**). One of the key players in the exercise-induced GLUT4 recruitment is AMPK [134-135]. Numerous studies showed that the exercise-induced pathway is insulin-independent as incubation with wortmannin, an inhibitor of PI3-Kinase (a kinase triggered by insulin), does not block this pathway [136]. Additionally, the insulin-induced and exercise-induced glucose uptakes are additive [137]. The two pathways converge at the point where the protein TBC1D1 is phosphorylated. This protein is involved in regulating GLUT4 translocation [138]. Interestingly, when glucose uptake is triggered by AMPK activation, the glucose is destined for glycolysis/oxidation, whereas when insulin stimulated, the sugar is destined for glycogen synthesis [139].

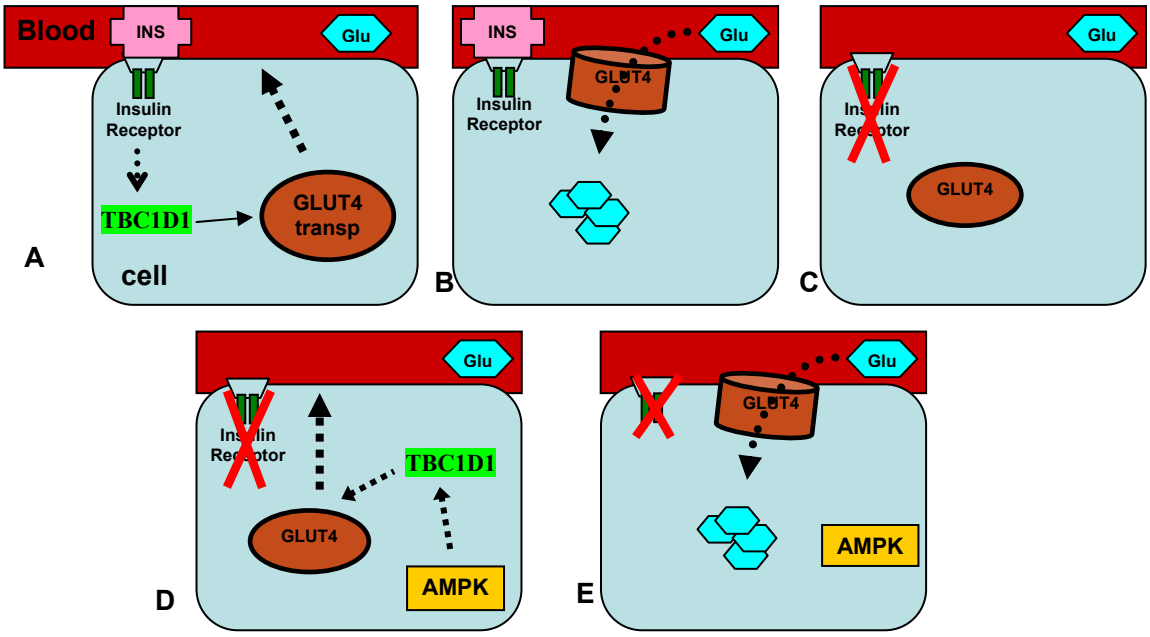

Figure 1.8: Two parallel signaling pathways exist which mediate glucose uptake in skeletal and adipose tissues. One of these two pathways is insulin-dependent and the other is exercise-induced. (A) Following a carbohydrate-rich meal the blood has increased levels of glucose. When insulin binds to the insulin-receptor a cascade of signals lead to the translocation of GLUT4 transporters to the plasma membrane. (B) Glucose can then enter into the cell. (C) In diabetic patients, where insulin signalling is compromised, glucose remains in the blood, reaching toxic levels which are responsible for the symptoms of the disease. (D) AMPK, via an exercise-induced mechanism, also leads to the phosphorylating of AS160, enhancing GLUT4 recruitment. (E) Glucose can now enter the cell via this alternative mechanism which is insulin-independent [139].

Some of the most widely prescribed diabetic drugs are the thiazolidinediones (e.g. rosiglitazone and pioglitazone) and biguanide (e.g. phenformin and metformin) [140-144]. Although AMPK was not the primary target of the study, these drugs have been found to activate AMPK, leading to the identification of the enzyme as a good potential target for the treatment of diabetes. Since these drugs have been reported to have undesirable side effects such as heart failure and lactic acidosis they had to be

withdrawn from the market [145-148]. In contrast, although metformin causes gastrointenstinal upset, it remains the most widely prescribed drug for type II diabetes. Metformin is an oral drug which improves insulin sensitivity in type II diabetic patients, and decreases plasma glucose and lipids by decreasing gluconeogenesis and, to a minor extent, by increasing glucose uptake into skeletal muscle [149-150]. These effects appear to be mediated via hepatic AMPK activation by inhibiting the mitochondrial respiratory complex. This in turn causes inhibition of mitochondrial respiration and inhibition of β-oxidation of fatty acids [151-153].

However, all these drugs activate AMPK indirectly and have only modest potency. One of the aims of current research is to find a drug that directly and potently activates AMPK. This approach might combine therapeutic benefits while eliminating unwanted side effects.

In 2006, Cool *et al* discovered a small molecule activator of AMPK, A-769662, a compound from the thienopyridone family, which is conventionally referred to as Abbott compound (from the name of the labs where it was synthesized) [154]. Although A-769662 is thought to bind directly to AMPK, its binding site has not been identified. A-769662 is not an AMP mimetic, though it produces the same effects as AMP, i.e. allosteric activation and protection against dephosphorylation. As a consequence it is more specific than AICAR, as it does not affect fructose-1,6-bisphosphatase or glycogen phosphorylase [154]. Unfortunately, the therapeutic use of A-769662 is not promising as it has a poor oral absorption [154-155], therefore there is a strong impetus to identify a direct, specific and potent activator of AMPK that has good pharmokinetic properties.

1.1.4.2 Cancer

The role of AMPK as a potential target to treat diabetes is well established, but in these last few years AMPK has been revealed as a potential target for cancer treatment. Its involvement in cancer incidence was noted when patients who were

treated with metformin (**section 1.1.4.1**) were found to have a decreased rate of cancer compared with untreated patients [156]. It has been shown that breast cancer cell growth is inhibited by metformin in an AMPK-dependent way and by down-regulating the mammalian target of rapamycin (mTOR) activity [157-158]. mTOR is a major player in cell growth and proliferation, which is over-activated in many different types of cancer [159]. The mTOR signaling pathway is triggered in response to growth factors, such as insulin and insulin-like growth factor, and it mediates ribosomal biogenesis and protein translation [160]. Since processes such as protein synthesis require larges amount of energy, increases in cellular AMP/ATP ratio lead to an AMPK inhibition of mTOR signaling. AMPK indirectly inhibits mTOR by activating the TSC1/TSC2 heterodimer, a complex between two tumor suppressors that lie upstream of mTOR [161]. More precisely, TSC2 is phosphorylated at Ser-1345 and it appears to activate the GTPase-activating protein activity of TSC2 towards Rheb, a Ras family GTPase that activates mTOR complex 1 (mTORC1) [64,162]. Thus, Rheb-GTP levels, and therefore mTOR activity, are decreased. It has been recently shown that AMPK inhibits mTOR signaling by an alternative pathway by directly phosphorylating Raptor, a subunit of TORC1, at Ser-722 and Ser-792 which are two phosphorylation sites important for the down-regulation of mTORC1 [63].

Other evidence that supports a role for AMPK in human cancer is that the tumor suppressor LKB1 is itself involved in different types of cancer [161]. Impaired LKB1 activity is not only implicated for Peutz–Jeghers syndrome but is also responsible for pancreatic and biliary cancers, malignant melanomas, human non-small cell lung cancer and other lung cancer cell lines [163-167]. Additionally, in humans, LKB1 is involved in cell polarity, another energy-consuming process whose deregulation is often linked to tumor invasion [42-43]. Studies in Drosophila have showed that deletion of either AMPK or LKB1 produced a similar phenotype; disrupted cellular structure & cell polarity, suggesting that the effects of LKB1 in cell polarity are, at least in part, mediated by AMPK [168-169]. More specifically, AMPK plays a key role in the regulation of epithelial tight junction assembly and trans-epithelial resistance through activation of a calcium switch which prevents tight junction disassembly

[170-171]. The molecular mechanisms and phosphorylation events involved in this process are unclear.

1.1.4.3 Wolff-Parkinson-White (WPW) syndrome

Naturally occurring mutations in the human γ2 isoform of AMPK, encoded by the *PRKAG2* gene, causes a cardiomyopathy characterized by a marked accumulation of glycogen in cardiac muscle cells. A mutation in the γ3 subunit of AMPK in Hampshire pigs is associated with elevated glycogen content in skeletal muscles [172]. Interestingly, no natural mutations in the γ1 subunit have been identified, presumably because they would be embryonically lethal since the γ1 isoform provides the majority of AMPK activity in most cell types [173]. The mutations found in the γ2 subunit comprise one insertion of a leucine residue between Arg-350 and Glu-351 and ten missense mutations (Arg302Gln, Leu351Ins, His383Arg, Arg384Thr, Thr400Asn, Asn488Ile, Tyr487His, Glu506Lys, Arg531Gly, Arg531Gln and Ser548Pro (**Table 1.3**) [174-183].

Mutation	No. of patients (families)	Age of onset	Left ventricular hypertrophy	Sudden cardiac death	Reference
Arg302Gln	78 (8)	Adolescence to Adult	Y	Y	175,180
Leu351Ins	5 (1)	Adult	Y	Common	178
His383Arg	3 (1)	Paediatric	Y	-	178
Arg384Thr	1	Paediatric	Y	-	174
Thr400Asn	1 (1)	Adult	Y	-	175
Asn488Ile	40 (1)	Adolescence to Adult	Y	Rare	175
Tyr487His	2 (1)	Juvenile	Y	Y	176
Glu506Lys	8 (1)	Adult	Y	-	177
Arg531Gly	4 (1)	Paediatric	N	Y	180
Arg531Gln	3 (3)	Neonatal	Y	Y	179
Ser548Pro	1 (1)	Adult	Y	Possible	182

Table 1.3: List of mutations that have been identified to date in the human AMPK γ2 subunit that give rise to WPW syndrome.

The data in the literature regarding the effects of these mutations on AMPK activity are incomplete, unclear and sometimes contradictory (summarized in **Table 1.4**). Overexpression studies in pulmonary fibroblasts and COS cells showed that by mutating the equivalent of γ2-Arg302Gln in γ1 and γ3 (Arg70Gln and Arg225Gln, respectively) resulted in the basal activity of AMPK being increased but sensitivity to AMP was impaired [184-185]. In contrast, studies performed with CCL13 cells with Arg302Gln, His383Arg, Thr-400Asn and Arg531Gly displayed a reduced AMPK activity [16,186]. Interestingly, in the same study, the insertion of a leucine (Leu351-Ins) had no effect on AMP sensitivity and enzyme activity. It has been suggested that the discrepancies in these results arises because of the different cell lines used, which contain different amounts of LKB1 [179]. Subsequent to submission Hawley *et al* published some results using stably transfected isogenic cell lines, the effect of which could be quantified in a more reliable manner. They showed that although the expression levels of the wild type and Arg531Gln mutant of AMPK were identical, the mutant was insensitive to AMP but had a 2-fold higher basal activity [187].

Transgenic mice overexpressing tissue-specific AMPK-γ2 have also been employed [188-189]. The heart-specific mutant animals expressing Arg302Gln, Asn488Ile, Thr400Asn or Arg531Gly displayed cardiac hypertrophy and increased glycogen storage [190-193]. Interestingly the mutations affecting the basic residues (Arg302Gln & Arg531Gly) resulted in decreased AMPK activity, whereas the Asn488Ile and Thr400Asn mutations displayed increased activity and biphasic changes in activity, respectively (**Table 1.4**).

Subunit	Phenotype		Reference
Whole body knockout			
γ3 KO	Impaired glycogen synthesis after exercise		184
Trangenic (heart)			
γ2 Arg302Gln	Cardiac hypertrophy, glycogen storage ↓ activity		193
γ2 Asn488Ile	Cardiac hypertrophy, glycogen storage ↑ activity		190
γ2 Thr400Asn	Cardiac hypertrophy, glycogen storage Biphasic changes in activity		191
γ2 Arg531Gly	Cardiac hypertrophy, glycogen storage ↓ activity and AMP stimulation		192
Trangenic (muscle)			
γ3 Arg200Gln	↑ Muscle glycogen ↑ activity and ↓ AMP stimulation		189
γ1 Arg70Gln	↑ Muscle glycogen		188
Overexpression in cells		**Cell type**	
γ1 Arg70Gln	↑ Basal activity; ↓ AMP stimulation	COS7	185
γ2 Arg302Gln	↓ activity; ↓ AMP stimulation	CCL13	16; 186
γ3 Arg225Gln	↑ Basal activity; ↓ AMP stimulation	COS7	180
γ2 Leu351ins	No effect	CCL13	16; 186
γ2 His383Arg	↓ activity; ↓ AMP stimulation	CCL13	16; 186
γ2 Thr400Asn	↓ activity; ↓ AMP stimulation	CCL13	16
γ2 Arg531Gly	↓ activity; ↓ AMP stimulation	CCL13	16; 184
	↑ Basal activity; ↓ AMP stimulation	HEK293	187

Table 1.4: Genetic models of mutant AMPK that have been generated to date. Knock-out (KO) and overexpression of mutants of AMPK have been used to study their effects *in vivo* and in cells. In transgenic mice the same phenotype is observed as in human patients with cardiac hypertrophy and increased cardiac glycogen stores.

Overall it can be concluded that mutations in γ2 seem to interfere with the normal activation of AMPK by AMP [175,179,186,190,194]. Consistent with these findings, Scott *et al* reported that such mutations in the γ subunit cause a significant decrease in AMP binding to AMPK [16]. Abnormal regulation of AMPK could result in an imbalance in glucose uptake and glycogen synthesis which could explain the increased glycogen content in myocytes associated with this syndrome [129].

The excess storage of glycogen in the heart appears to create an insulating layer which causes abnormal electrical conductance characterized by ventricular premature excitation (abnormal activation of the ventricles by-passing the atrio-ventricular node) and an unexplained mild-to-severe cardiac hypertrophy. These traits are referred as WPW syndrome [190,194]. Patients with cardiac hypertrophy have an unusual electrocardiogram pattern and might be asymptomatic or experience chest pain, shortness of breath, congestive heart failure, syncope, and malignant ventricular arrhythmia. WPW is associated with an increased risk of sudden fatal arrhythmias in midlife and has an autosomal dominant inheritance [175,179].

Numerous groups have investigated whether the glycogen that accumulates in WPW syndrome is available as an energy source. Studies have shown that *PRKAG2* transgenic mice, either mutant or wild type, can utilize their stored glycogen in cardiomyocytes for energy production during exercise [195]. Likewise, enhanced glycogen storage in myocytes in Arg70Gln γ1 transgenic mice helped improving exercise tolerance [188]. These results indicate that therapeutic approaches to decrease glycogen accumulation in these patients may help to treat the disease [194].

As mentioned in **section 1.1.1**, conserved pairs of CBS motifs occur in metabolic enzymes, kinases, and channels [16,21]. Several human diseases are associated with point mutants in CBS motifs from these proteins. Mutations in the Bateman domains from cystathionine β-synthase and IMP dehydrogenase-1 result in homocystinuria and retinitis pigmentosa, respectively [196-197]. Additionally, mutations in the chloride

channels CLC1, CLC2, CLC5, CLC7 and CLCKB causes congenital myotonia, idiopathic generalized epilepsy, Dent's disease, Albers-Schonberg disease and Bartter syndrome, respectively [198-202].

An important question is how AMP binding to CBS motifs affects the regulation of these enzymes and in particular of AMPK. Understanding the molecular basis of AMP binding to wild type and WPW mutant proteins will likely help us to understand the phenotypes associated with this syndrome and perhaps new ways of treating them.

1.2 Project aim

The main objective of this thesis was to characterize the mechanisms by which AMPK is regulated by AMP.

In chapter 3 I describe the crystal structures of a regulatory fragment of AMPK in complex with the activator ZMP (a mimic of AMP) and with mant-AMP (fluorescent reporter used for my binding studies). Additionally, I report the crystal structures of three common WPW syndrome mutants (Arg69→Gln, His150→Arg and Arg298→Gly) and their complexes with nucleotides.

In Chapter 4 I present fluorescent binding studies aimed at determining the affinities of natural nucleotides, fluorescent reporters and activators for the two exchangeable sites of AMPK. The affinities of AXPs were also tested in the three WPW mutants of AMPK. HPLC studies were carried out on WPW mutants to see if the non-exchangeable AMP site was affected by these mutations. I also present thermal denaturation studies carried out on AMPK to screen a panel of putative binding partners that could be used for activity studies.

MATERIALS & METHODS

2. Materials & Methods

2.1 Molecular biology

Two pET3a tri-cistronic *E. Coli* expression vectors were used. The vectors encoded full-length His-α1β2γ1 and truncated AMPK His-α1(396-550)β2(187-272)γ1 constructs. These vectors were provided by Dr. Richard Heath. The templates were used to generate the wild type and mutant AMPK constructs. All DNA stocks were stored at -20°C.

2.1.1 Materials

pET3a tri-cistronic *E. Coli* expression vectors were from Novagen. The QuikChange Site-Directed Mutagenesis Kit was from Stratagene. All mutagenic primers were synthesized by Sigma genosis**.** PCR reactions were carried out using a Mastercycler personal (Eppendorf). PCR tubes were from Elkay. QIAquick PCR Purification kit from Qiagen. *E. coli* TOP10 Competent Cells AND *E. coli* BL21 DE3 were from Invitrogen. IPTG from VWR International.

2.1.2 Site-directed mutagenesis

Three site-directed mutagenesis experiments were carried out to insert single point mutations to the γ-subunit of AMPK. The residues that have been mutated are Arg-69→Gln, His-150→Arg and Arg-298→Gly. These experiments were done using the QuikChange Site-Directed Mutagenesis Kit according to the manufacturer's instructions. Constructs were generated by PCR and standard cloning techniques. All mutant DNA clones were thoroughly sequenced to verify correctness by Hammersmith Hospital. Sequences were aligned and analyzed using Chroma [203].

2.1.3 Bacterial strains

E. coli TOP10 Competent Cells were transformed for the cloning of single point mutations and DNA purification procedures. *E. coli* BL21 DE3 competent cells were used in the expression of all protein constructs. The DE3 contains the T7 polymerase gene under the control of the *lacUV5* promoter. Addition of isopropyl-β-D-thiogalactopyranoside (IPTG) induces constitutive expression of T7 polymerase which results in overexpression of the protein of interest. The plasmid encodes an in-frame amino terminal six-histidine peptide (His-tag) connected to the protein by a spacer and a six amino acid protease recognition sequence for identification and cleavage by thrombin protease (CATGAGCCATCATCATCATCATCACAGC AGCGGCCTGGTGCCGCGCGGCTCC). The His-tag will bind metal ions such as Nickel and therefore allows for protein purification via Nickel affinity chromatography (see **section 2.2.3.1***)*.

2.1.4 Transformations

Transformation is the process that enables the uptake of exogenous DNA by a bacteria cell. The foreign DNA integrates with the altered genome of the bacteria and can be used to express a recombinant protein. Transformations were carried out by adding 1µl of 100 ng/µl DNA solution to the *E. coli* competent cell aliquot. The cells were incubated on ice for 10 min, heat-shocked at 42°C for 50 sec and quickly placed on ice. 250 µl SOC medium was added. Following 1 hour incubation at 37°C the sample was plated on LB Agar media with ampicillin antibiotic. All plates were incubated overnight at 37°C.

2.2 Protein biochemistry

2.2.1 Materials

Ampicillin, B-mercaptoethanol (BME) and Imidazole were from Sigma. Complete EDTA-free protease inhibitor cocktail tablets from Roche, Benzonase Nuclease

from Novagen. Cells were incubated during protein expression in a Multitron 2 incubator (Infors HT) and centrifuged either in a Beckman Avanti J-25 or Beckman J6-MC centrifuge. Cell lysis was carried out in a Branson Sonifier 450 (Branson). Sterile Minisart filters (Sartorius stedim biotech) were used before and after purification. The P1 pump was from Amersham. Nickel-affinity purification was performed in a 5 ml HisTrap HP column (GE Healthcare), ion-exchange purification either in a Mono Q or a Mono S column (Pharmacia Biotech) and Gel filtration purification in a 120 ml volume Superdex 200 column (Pharmacia Biotech). All three chromatography techniques were carried out in columns attached to an AKTA Prime (Amersham) with fractionation system. Human alpha thrombin (1 mg) was purchased from Haematologic technologies Inc at of 36 U/µl and diluted to 0.72 U/µl before storage at -20˚C. 4X LDS sample buffer is from Invitrogen. Ppack was from Calbiochem. Protein was concentrated down in Vivaspin membranes (Vivascience) via centrifugation carried out in Sorvall legend RT centrifuges (Sorvall). Instant Blue was from Expedeon. NuPage 4-12% Bis-Tris gel (15 well) and Mark12 Unstained Standard were from Invitrogen. Protein concentration was measured by using either a NanoDrop or a Cary 50 Bio spectrophotometer. Dynamic Light Scattering measurements of protein samples were made using Viscotek 802 DLS Instrument (Viscotek).

2.2.2 Protein expression

One colony from a plate with transformed *E. coli* expression cells was used to start a bacterial culture in 250 ml of LB Luria-Bertani medium (LB). Ampicillin was prepared by dissolving in dH_2O and was added as an antibiotic in the media. The final concentration of ampicillin was 100 µg/ml. Incubation was carried out overnight at a temperature of 37ºC and at a shaking rate of 200 rpm. These 250ml of culture were used to start a large scale expression of the proteins consisting of six flasks of 750ml Terrific Broth (TB) medium each, with ampicillin. When the optical density at a wavelength of 600 nm (OD_{600}) reached 1.5 (4-5 hours), temperature was dropped to 25ºC and IPTG was added to induce cells to express AMPK protein from

pET3a vector (5 hours). The final concentration of IPTG was 1 mM. Cells were harvested by centrifugation at a speed of 4000 rpm for 30 min at 4ºC and the supernatant was discarded. The pellet was washed in 100 ml of 0.9% NaCl and recentrifuged with the same parameters as before. The supernatant was discarded again and the dry pellet was frozen at -20°C until cell lysis.

2.2.3 Cell lysis

Stored cell were thawed, kept on ice and resuspended in 250 ml of lysis buffer (50mM Tris-HCl, 100 mM NaCl, 20 mM Imidazole, 2 mM BME, 4 complete protease inhibitor tablets (EDTA-free), 1 mM MgCl2, 4 KU Benzonase Nuclease). The pH of the buffer depended on the isoelectric point (pI) of the protein expressed: for full-length AMPK buffer with pH 8.0 was used whereas pH 7.0 was used for the truncated version. Cells were lysed by sonication at 40% power in 30 s pulses for a total of 3 min. The insoluble fraction of the sonicate was removed by centrifugation at 20,000 rpm for 30 min at 4ºC. The supernatant containing the cleared lysate with the soluble protein was kept for further purification. An aliquot of the insoluble pellet was used for SDS-PAGE analysis (see **section 3.1**).

2.2.4 Protein purification

2.2.4.1 Nickel affinity purification

The His-tag in the amino-terminal of AMPK has high affinity for divalent cations, such as Nickel, which are tightly bound to the protein purification column, whereas non-specific proteins are washed away. The 5 ml Nickel-column was pre-washed with binding buffer (50 mM Tris, 100 mM NaCl, 20 mM imidazole and 2 mM BME). As mentioned above (**section 2.2.2**), the pH of the buffer depended on the pI. of the protein construct. The cleared lysate was filtered (0.45 μm membrane) and loaded with a P1 pump onto the Nickel-column at a flow rate of 2 ml/min. Non-binding proteins were washed off with 100 ml binding buffer at a flow rate of

2 ml/min. Small aliquots of the flow-through from the loading and washing steps were collected and used later for SDS-PAGE analysis. The recombinant protein was eluted with a gradient that went from 0% to 100% Elution buffer (same as the binding buffer except for 200 mM imidazole) over 150 ml at the same flow rate as before. 2 ml fractions were collected over the elution procedure. If the SDS-PAGE gel showed a readily clean sample, gel filtration was carried out; otherwise an extra step of ion exchange purification was performed.

2.2.4.2 Ion Exchange Chromatography

Ion exchange chromatography enables the separation of different proteins according to differences in their charge. The pI of a protein is the pH at which the protein carries no net electrical charge. A mono-Q column, a strong anion exchanger, is used when the pH of the protein buffer is higher than the pI, or a mono-S column, a strong cation exchanger, is used when the opposite occurs. Therefore a 40 ml mono-Q column was used for the full-length AMPK construct (pI = 6.7, protein buffer pH 8.0) and a 40 ml mono-S column for the truncated AMPK construct (pI = 8.0, protein buffer pH 7.0). The column was pre-washed with 100 ml buffer B (50 mM Tris, 1 M NaCl, 2 mM BME) and 100 ml buffer A (50 mM Tris, 100 mM NaCl, 2 mM BME). The protein sample was loaded in the column with a P1 pump at a flow-rate of 2 ml/min and the column washed with 100 ml of buffer A. The proteins was eluted by increasing the salt concentration of the elution buffer B with a gradient that went from 0% to 100% buffer B over 150 ml. 2 ml fractions were collected during the gradient and analyzed by SDS-PAGE. The fractions that contain a clean, concentrated recombinant protein were pulled together.

2.2.4.3 His-Tag Cleavage

A small scale His-tag cleavage by thrombin was carried out to determine optimal incubation time with the protease. The experiment was carried out at room temperature. 4 U of thrombin per mg of recombinant protein is used during

proteolytic incubation and AMPK concentration 1 mg/ml. Reactions at different time points of the small-scale incubation were stopped with 2x loading buffer, whereas the large scale reaction was stopped with the Ppack, a thrombin inhibitor [204].

2.2.4.4 Size Exclusion Chromatography

Size exclusion chromatography separates molecules according to their size via a column containing porous beads. This technique is referred to as gel filtration (GF) chromatography, if an aqueous solution is used for diffusion of the sample through the column. Larger molecules travel faster along the column because they enter to fewer porous beads and thus diffuse to the bottom of the column before the small molecules which enter into a greater number of beads and therefore elute at a later stage. The gel filtration column was pre-washed with 100 ml GF buffer (50 mM Tris, 100 mM NaCl, 2 mM BME). The protein sample collected from the previous stage of purification was concentrated down via centrifugation (3000 rpm) to a volume below 5 ml and it was then filtered (0.2 μm membrane). The protein sample was then loaded to the 120 ml GF S200 column, washed (20 ml) and eluted at 1 ml/min. 2 ml fractions were collected during elution and analyzed by SDS-PAGE.

2.2.4.5 SDS-PAGE

The different proteins from the aliquots of the insoluble pellet during bacterial cell lysis, the cleared lysate and aliquots resulting from various protein purification steps, e.g. wash and elution, were separated according to size using Sodium Dodecylsulfate Polyacrylamide Gel Electrophoresis (SDS-PAGE) [205]. Protein samples were heated to 100ºC for 5 min with 4X loading buffer before loading into the gel wells. The gel was run at 200 V with a current of 20 mA for 40 min. The different protein bands were visualized by staining with Instant Blue, a Coomassie based staining solution. The molecular mass of the protein bands were initially determined by comparison with Mark12 Unstained Standard and confirmed by mass spectrometry.

2.2.4.6 Determination of protein concentration

Protein concentration was measured by UV-visible spectroscopy. The GF buffer which is used to store the protein was used as a blank. The concentration was then calculated using the Beer-Lambert equation:

$A = \varepsilon c l$

where "A" is the absorbance, "ε" is the theoretical extinction coefficient, "c" is the concentration in molarity (M) and "l" is the path length in cm.

ε was calculated from the amino acid sequence of a protein via the ExPASy ProtParam tool software [206] based on the amount of residues such as phenylalanine, tryptophan and tyrosine that absorb light at 280 nm [207].

2.2.4.7 Dynamic Light Scattering (DLS)

If the purified protein was destined for crystallization trials, a DLS measurement was carried out to determine the oligomeric state and molecular size of the protein [208-209]. It has been established that monodispersity of proteins measured using DLS correlated well with the ability to grow crystals, in fact the more polydisperse a protein sample is, the less likely it is to crystallize. 30 µl protein samples at 0.5 mg/ml were centrifuged (14000 rpm for 15 min) and 15 µl placed in the cuvette. 10 measurements per sample were made for statistical validity. Proteins with a molecular weight that did not exceed 20% of the expected size and a polidispersity lower than of 20% were considered optimal samples and were used for crystal trials, otherwise the protein was used for binding studies.

2.3 Crystallization

2.3.1 Materials

48- and 24-well trays were from Hampton research. MES, PEG 3350, PEG 4000 and MPD were from Sigma.

2.3.2 Co-crystallization of wild type AMPK with ZMP

Crystals of truncated AMPK, α1 (rat; 396-550), β2(human; 187-272), γ1(rat) in complex with ZMP were grown by vapour diffusion technique at 18 ºC in a hanging drops tray of 48 wells. The volume in each well was 200 µl. ZMP was added to the protein at a final concentration of 2 mM. The protein concentration was 10 mg/ml. Drops were prepared by mixing equal volumes of AMPK-ZMP with well solution (100 mM MES pH 5.5, 7% PEG 3350) in a 2 µl drop.

2.3.3 Wild type AMPK crystals soaks with mant-AMP

Crystals of truncated AMPK were grown by vapour diffusion at 18 ºC in hanging drops. The 48-well tray contained 200 µl of reservoir solution. Drops were prepared by mixing 1 µl of AMPK sample (11.4 mg/ml protein) with 0.5 µl well solution (100 mM MES pH 6.4, 6% PEG 3350). Suitable crystals were transferred using a nylon loop into reservoir solution containing 0.5 mM mant-AMP and soaked overnight prior to freezing.

2.3.4 AMPK-R298G mutant crystals

Crystals of truncated AMPK with a single point mutation (Arg298→Gly) were grown by vapour diffusion at 18 ºC in sitting drops either in complex with AMP or with no nucleotide. The 24-wells sitting drop tray had a volume of 500 µl of reservoir solution. Drops were prepared by mixing 1µl of protein sample AMPK-AMP (9 mg/ml protein; 340 µM AMP) with 0.5 µl well solution (100 mM MES pH 6.0, 8% PEG 3350). Crystals grown with AMP were transferred and soaked overnight in the same well reservoir with 2 mM of either ADP or ATP.

2.3.5 AMPK-R69Q mutant crystals

Crystals of truncated AMPK-R69Q were grown by vapour diffusion at 18 ºC in sitting drops either with no nucleotide or in complex with AMP. The 24-well sitting drop tray had a volume of 500 µl of reservoir solution. Drops were prepared by

mixing 1 µl of AMPK-AMP sample (8 mg/ml protein; 300 µM AMP) with 0.5 µl well solution (100 mM MES pH 6.0, 5% PEG 3350).

2.3.6 Co-crystallization of AMPK-H150R mutant with AMP

Crystals of truncated AMPK-H150R in complex with AMP were grown by vapour diffusion at 18 ºC in sitting drops. The 24-well sitting drop tray contained 500 µl of reservoir solution. Drops were prepared by mixing 1 µl of protein sample AMPK-AMP (9 mg/ml protein; 340 µM AMP) with 0.5 µl well solution (13% 2-Methyl-2,4-pentanediol (MPD), 3% PEG 4000).

2.3.7 Freezing of crystals

Crystals appeared in two days and grew to maximal size over 7 days. Crystals that reached a size of at least 50 µm in width (unless otherwise specified) were selected for X-ray exposure. They were cryo-protected in two steps to avoid crystal cracking. Crystals were harvested with a loop and transferred into a drop of reservoir solution with 10% ethylene glycol and then into a second drop with 25% ethylene glycol, before being plunged into liquid nitrogen. Frozen crystals were stored under liquid nitrogen until required.

2.3.8 Data collection, processing and refinement

Crystals were screened for diffraction in-house on a MicroMax 007HF rotating anode coupled to a RaxisIV^{++} detector. Crystals were maintained at 100K using a cryostream and were exposed for 2 min at 0.5° oscillation at 1.54 Å λ in two orientations 90˚ apart. If these two images autoindexed normally, a full data set was collected by the oscillation method (0.5°/frame, 2 sec/frame, 0.97 Å λ) at the Diamond Synchrotron Light Source (UK). Only one crystal was used for each data set. X-ray diffraction data were processed using Denzo and Scalepack [210]. The structures were solved by molecular replacement with Amore [211] or Phaser [212] using wild type AMPK in complex with AMP as a search model (PDB entry: 2V8Q; [213]). Iterative cycles of refinement were done with Refmac5 interspersed with manual

rebuilding using Coot [214-215] (see **section 3.2.1**). The geometry was verified with the program packages PROCHECK [216] and with Molprobity [217]. Root mean square deviation (r.m.s.d.) in Cα positions was calculated with LSQMAN [218]. Molecular graphics were generated with the software Pymol [219] and Grasp [220].

2.4 Binding studies

A variety of different experimental approaches may be used to characterize the interaction of small molecule ligands with a protein: isothermal titration calorimetry (ITC), surface plasmon resonance (SPR), equilibrium dialysis, and several different spectroscopic (or optical) methods. The small amount of sample required and the short data collection time make the optical methods particularly useful tools in such studies as well as in the study of protein stability. A series of fluorescence based binding studies have been carried out to characterize the interaction of AMPK with the adenine nucleotides: AMP, ADP and ATP. For some proteins the binding of adenine nucleotides has been monitored though their effects on the intrinsic (generally tryptophan) fluorescence of the protein. However, such studies are generally of limited applicability because of the strong absorption of the nucleotides at the wavelengths used to excite intrinsic protein fluorescence [221]. An alternative approach is to use fluorescent analogues to monitor binding and then to use either competition or displacement experiments to characterize the binding of the natural nucleotides. In this study, *N*-methylanthraniloyl (mant)-nucleotides and NADPH (or NADH) have been used as the fluorescent reporters.

2.4.1 Materials

Mant-AMP and mant-ATP were kind gifts from Dr John Eccleston. AMP, ADP and ATP were all purchased from Sigma and ZMP was purchased from Calbiochem. Stock solutions of these nucleotides were prepared in GF buffer and stored at -20˚C. NADH, NADPH, NAD+ and NADP+ (Sigma) were freshly prepared each day because of potential stability problems [222]. Concentrations of all nucleotide stock

solutions were determined using published extinction coefficients. The A-769662 compound was a gift from AstraZeneca and was dissolved in dimethyl sulfoxide (DMSO). The phosphopeptide was synthesized by Dr Graham Bloomberg at the University of Bristol and was dissolved in GF buffer. The 413 compounds used in the thermal binding assays were provided by the MRC Technology Division and were dissolved in DMSO at a final concentration of approximately 1mM.
The Partisil 10 SAX column used in the nucleotide assays was from Whatman. Fluorescence measurements were made using two spectrofluorimeters: an ISS photon counting instrument and a Jasco FP 6300. Thermal unfolding assays were carried out using a temperature-controlled Jasco V-550 UV/Vis spectrophotometer. The 3 mm and 5mm light path cuvettes used for fluorescence spectroscopy and the micro-cuvette with a 10 mm path-length used for thermal denaturation experiments were from Hellma

Ligand binding to AMPK was tested using the full-length protein (phosphorylated and non-phosphorylated forms), and a truncated AMPK α1(396-548)β2(187-272)γ1 construct. Protein concentrations were routinely determined using calculated extinction coefficients (117580 $M^{-1}cm^{-1}$ at 280 nm for the full length protein and 59250 $M^{-1}cm^{-1}$ at 280 nm for the truncated construct).

2.4.2 Fluorescent binding studies

Uncorrected fluorescence emission spectra of the *N*-methylanthraniloyl (mant)-nucleotides and their complexes with AMPK were recorded at 20ºC (unless otherwise specified) with an excitation wavelength of 380 nm (bandwidth 2.5 nm) and emission scanned from 400 to 550 nm (bandwidth 10 nm). The free (uncomplexed) mant-nucleotides have an emission maximum at 446 nm. In the presence of saturating AMPK the emission maximum is blue-shifted to approximately 430 nm and the fluorescence intensity is increased up to 5-fold. Binding of mant-AMP was generally monitored by adding AMPK to a solution of the nucleotide in a buffer containing 25mM Tris-HCl (pH depending on the pI of the

construct used) and 100 mM NaCl. Due to the unstable nature of AMPK, following each titration the sample was mixed not by stirring but by gently pipetting in and out the solution. Some experiments were also performed at low temperature and/or in the absence of salt (conditions expected to strengthen binding of the nucleotide) in order to establish the stoichiometry of the interaction. Competition assays in the presence of 50 μM AMP, ADP or ATP were used to determine the K_d values for the adenine nucleotides. The binding of A-769662 and ZMP to AMPK were assessed using a similar approach.

For the mant-nucleotides it is possible to use a different, but complementary, approach in which binding is monitored by adding the nucleotide to a solution of AMPK in ISS buffer (25mM Tris-HCl [pH depending on the pI of the construct used], 100 mM NaCl), rather than by adding the AMPK to the nucleotide. In this case the excitation wavelength used is 290 nm rather than 380 nm. At this shorter wavelength there is relatively little direct excitation of the mant fluorophore but significant excitation of the tryptophan residues in AMPK. The signal monitored in this experiment is the mant fluorescence (400-550 nm) which arises through Förster resonance energy transfer (FRET) from AMPK's tryptophan(s) to the mant group. Electronic excitation energy can be transferred by this dipole-dipole resonance interaction between donor and acceptor fluorophores over distances that extend to 30 Å and more [223] and several groups have used this FRET based approach to study protein-ligand interactions [221,224-225].

Fluorescence emission spectra of the reduced forms of β-nicotinamide adenine dinucleotide (NADH) and β-nicotinamide adenine dinucleotide 2'-phosphate (NADPH) and their complexes with AMPK were recorded with an excitation wavelength of 340 nm (bandwidth 2.5 nm) and emission scanned from 400 to 550 nm (bandwidth 10 nm). Free (uncomplexed) NADPH has an emission maximum at 461 nm. In the presence of saturating AMPK the fluorescence intensity is increased by 4-10 fold (depending on the AMPK construct used) and the emission maximum is blue-shifted to approximately 428 nm. Binding of NADPH was monitored by

adding AMPK to a 10 μM solution of the nucleotide in ISS buffer (25mM Tris-HCl [pH depending on the pI of the construct used], 100 mM NaCl). Some experiments were also performed at low temperature and/or in the absence of salt (conditions expected strengthen binding) in order to establish the stoichiometry of the interaction. Competition assays in the presence of either 12.5 μM or 25 μM AMP, ADP or ATP were used to determine the K_d values for the adenine nucleotides. Competition assays in the presence of NAD^+ or $NADP^+$ were done with either 250 μM or 500 μM nucleotide concentrations. The binding of ZMP to AMPK was assessed using a similar approach. FRET based measurements with NADPH could not be performed because excitation at 290 nm would produce far too much direct excitation of NADPH.

2.4.3 Bound nucleotide analysis

Solutions of AMPK at known concentration were denatured with perchloric acid and sodium acetate and then centrifuged to remove the protein. The supernatant was applied to Partisil 10 SAX (strong anion-exchange) column and eluted with 0.6M $NH_4H_2PO_4$ at 1 ml/min with absorbance monitoring at 260 nm. The concentrations of the different nucleotides present in the protein sample were estimated by integrating peaks and comparing the areas with those produced by nucleotide standards with known concentration.

2.4.4 Thermal stability measurements

The stability of a protein can be assessed by monitoring any of several optical signals (e.g. circular dichroism) that change when the protein unfolds at high temperature. If a ligand binds only to the folded form of the protein then it will increases its stability and unfolding will occur at a higher temperature. Such studies have become an increasingly important tool in the search for new drugs [226-227]. The AMPK construct used here was the trimeric complex α1(396-550)β2(187-272) with

full-length γ1. Protein samples were prepared in GF buffer (50 mM Tris-HCl pH 7.0, 100mM NaCl) at a concentration of 1.5 μM and then heated at 1 degree/minute from 40 to 70˚C in a UV/Vis spectrophotometer. It is important to note that what is being monitored here (absorbance at 400 nm) is the turbidity increase associated with protein aggregation. Despite the irreversible nature of protein unfolding for many large proteins, it has been suggested that irreversible unfolding may be treated as two discrete steps; where a relatively fast folded to unfolded reaction is uncoupled from a much slower aggregation step. Under this condition, an apparently irreversible process may be treated as a reversible unfolding transition [227]. Determination of the mid-point for unfolding was performed using in-house software written by Dr Stephen Martin (Division of Physical Biochemistry, NIMR).

2.4.5 Statistics

Unless otherwise specified, experiments shown are representative of two or three studies that gave similar results. Results of averaged experiments are given as means ± SD.

RESULTS

3. Results - crystallography

3.1 Protein purification

AMPK was overexpressed in *E. coli*. The bacterial cells were harvested by centrifugation, lysed by sonification, and the soluble lysate was loaded onto a Nickel-affinity column (**section 2.2.1**). The column was washed with an imidazole gradient from 20 mM to 200 mM and the protein eluted at approximately 100 mM imidazole. Fractions containing AMPK were analyzed by SDS-PAGE and then appropriately pooled (**section 2.2.3.1**) (**Fig 3.1A**). Samples of the pellet, lysate, flow-through and wash were also analyzed.

The pooled fractions were loaded onto an ion exchange chromatography column. Proteins were eluted by increasing the salt concentration from 100 mM to 1 M NaCl (**section 2.2.3.2**). AMPK eluted at approximately 250 mM NaCl. SDS-PAGE analysis of various fractions are shown in **Figure 3.1B**.

The N-terminal His-tag was removed from recombinant AMPK by proteolytic cleavage with thrombin. In order to determine the minimum amount of thrombin needed to cleave the His-tag, without beginning to cleave the protein at other sites, a pilot scale (80 µl) thrombin cleavage experiment was done. Different time points were taken (0, 1, 2, 5, 10, 30 min) and subsequently analyzed by SDS-PAGE (**Fig 3.1C**). The optimal time length of incubation of AMPK with thrombin was then used for the large-scale prep and the reaction was stopped with Ppack, a potent small molecule thrombin inhibitor [204]. The un-tagged AMPK was separated from the His-tag, Ppack and Thrombin in the subsequent gel filtration step.

The protein was concentrated by centrifugation using Vivaspin concentrators (3000 rpm) to approximately 5 ml and loaded onto a S200 size exclusion column. The buffer used to elute the protein is the same as used to store the protein after purification (**Fig 3.1D**). The yield of purified protein from one litre of culture was approximately 5 mg.

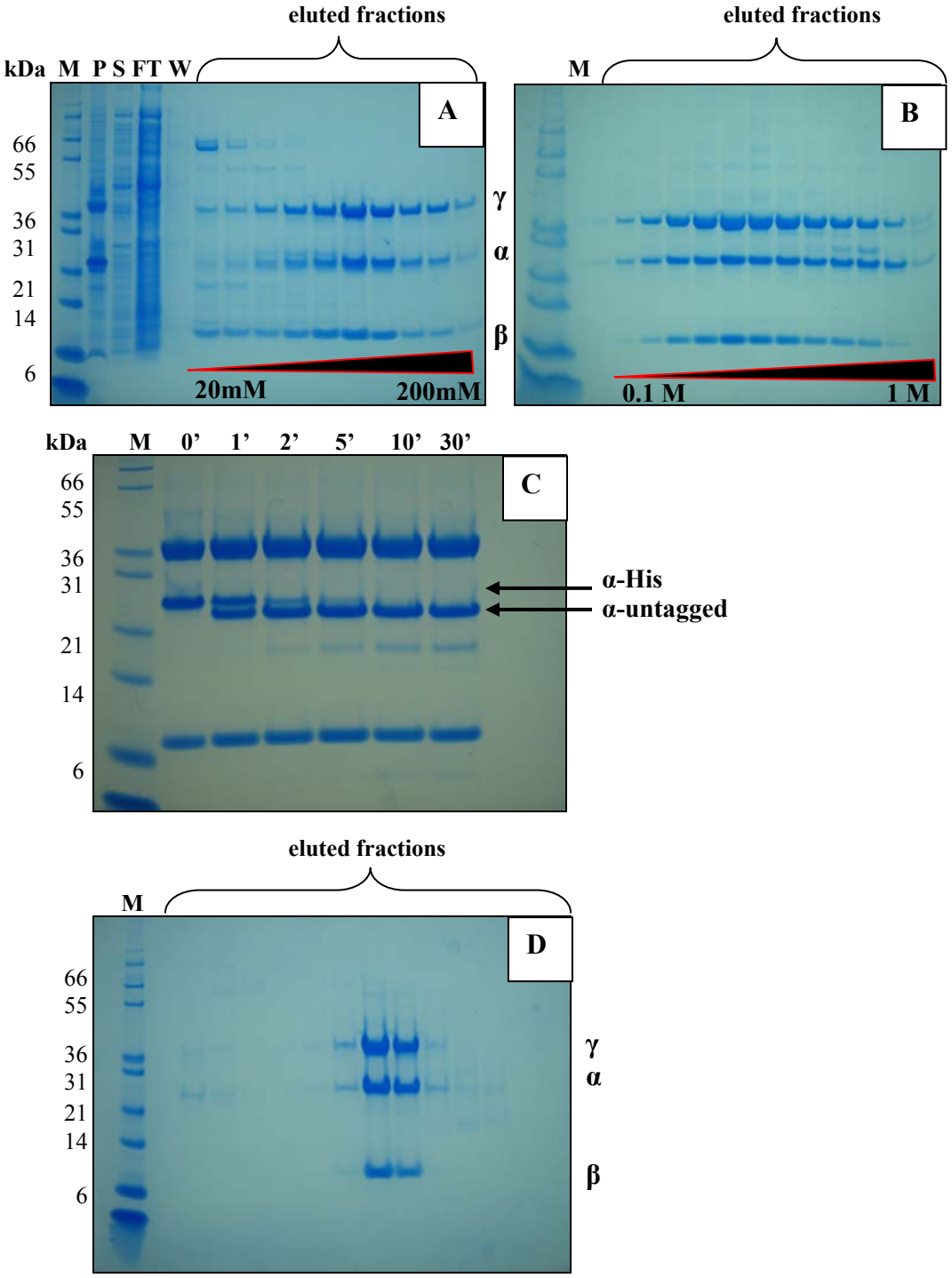

Figure 3.1: SDS-PAGE analysis of (A) Nickel purification, (B) ion exchange, (C) small scale thrombin incubation and (D) Gel filtration of the truncated construct of AMPK. The molecular weight of α, β and γ subunits are 19, 10 and 37 kDa. In C, the time points taken were 0, 1, 2, 5, 10, and 30 min. M, marker; P, pellet; L, lysate; FT, flow-through; W, wash. Arrows indicate the position of cleaved and uncleaved α subunit from the His-tag.

3.2 Crystallography

3.2.1 Overview

In this thesis I describe the structure of a number of different complexes of either wild type or mutant AMPK. The wild-type is in complex with the activator ZMP, an intermediate on the biosynthetic route to AMP, or with mant-AMP, the fluorescent reporter used in binding studies (see **section 3.4.3**). In addition, I present the crystal structures of three AMPK mutants which carry single point mutations in the γ subunit responsible for Wolff-Parkinson-White syndrome: Arg-69→Gln (R69Q), His-150→Arg (H150R) and Arg-298→Gly (R298G). The structures of the mutants reveal that nucleotide binding is impaired in one of the two exchangeable sites, which might explain the dysregulation of the kinase in patients with WPW disease.

Since initial crystallization trials using full-length mammalian AMPK were unsuccessful, a truncated protein was designed from the results of limited proteolysis and sequence analysis. The construct used contains the carboxyl terminus of α1 (rat; 396-550) and β2 (human; 187-272) with full-length γ1 (rat) (**Fig 3.2A**). The protein was co-crystallized with AMP, although further soaking experiments with ADP, Mg^{2+}-free ATP and Mg^{2+}-ATP also took place. Crystals of this protein construct commonly grow in a tetragonal habit (**Fig 3.2B**) but belong to the orthorhombic space group $P2_12_12_1$. The diffraction limit of the different protein crystals ranges from 2.0 Å to 2.6 Å Bragg spacing. Diffraction data were processed using Denzo and Scalepack [210]. The structures were solved by molecular replacement using Amore or Phaser [211-212]. The starting phases for the calculation of initial electron density map were obtained from the model of wild type AMPK in complex with AMP which was solved in our lab and was refined at 2.1 Å resolution (PDB entry: 2V8Q) [213]. All three nucleotides, as well as water molecules, were omitted from the molecular replacement and phase calculations. Crystallographic refinement was carried out using the rigid body, simulated annealing and TLS protocol of the

program package Phenix [228]. After each round of refinement, the models were manually adjusted using the computer graphics program Coot where necessary [215]. In cases where the electron density for some residues or segments was ambiguous the following procedure was followed. Selected residues were given zero occupancy in the coordinate files prior to some cycles of refinement, the resulting phases were then used calculate less biased electron density maps which were often useful in identifying the correct build. Water molecules were initially incorporated by Coot and then manually added into remaining positive electron density peaks. Water molecules closer than 2.2 Å to each other or 2.5 Å from nitrogen and oxygen or 3.5 Å from carbons atoms of the protein complex were removed. B-factor values were refined but atom occupancies were left at 1.0 during refinement. Other rounds of refinement were carried out using the program package Refmac5 [214]. Temperature factor refinement and manual adjustment of side-chains and solvent positions were carried on until the R_{Free} did not decrease any further and no interpretable features were left in the difference electron density maps.

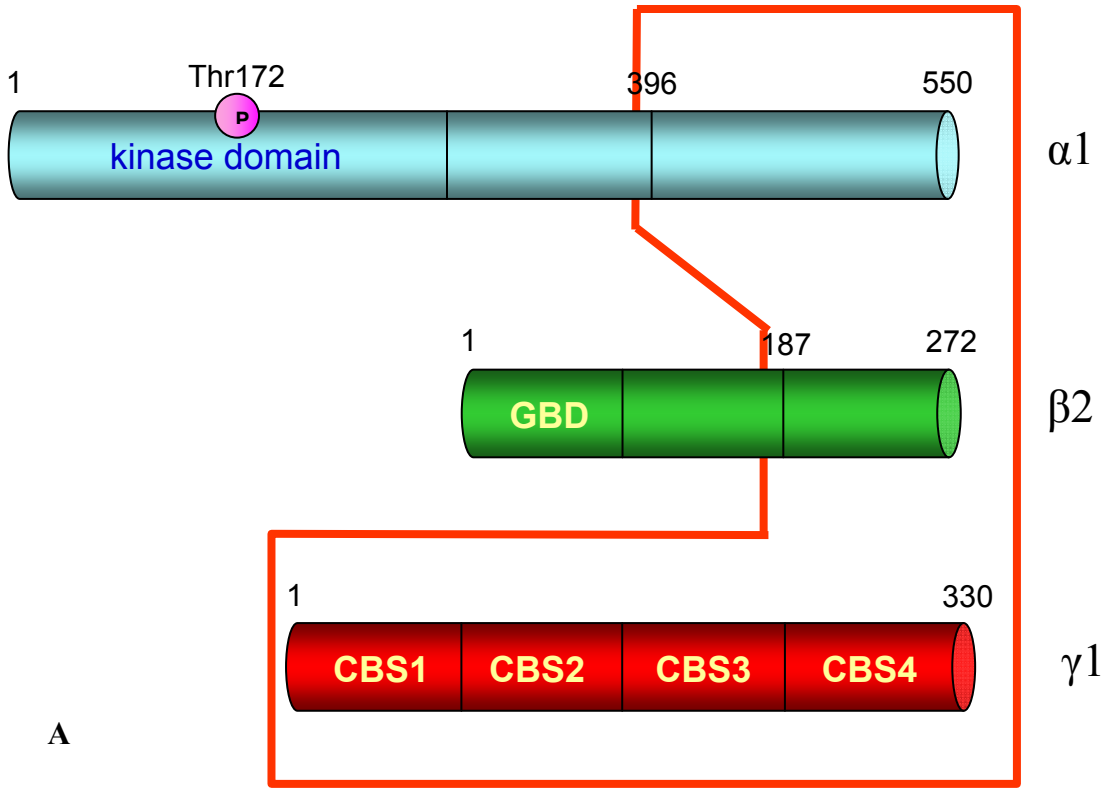

B

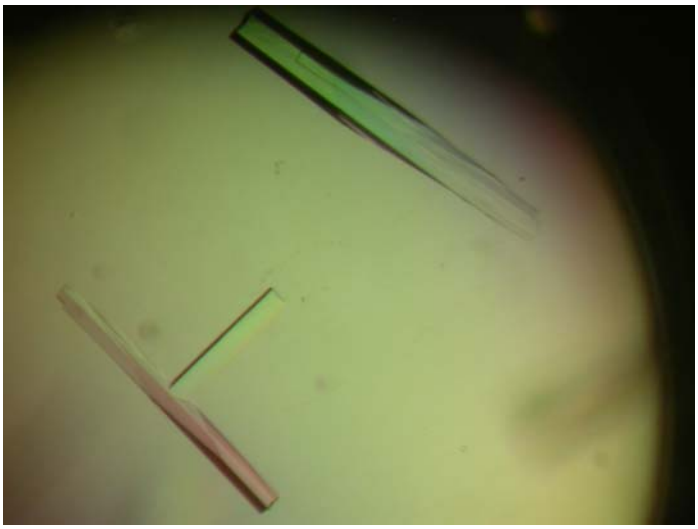

Figure 3.2: (A) Diagrammatic representation of the three subunits of the heterotrimer. The construct used for crystallography is outlined in red. (B) Typical crystals of truncated AMPK which grow in a tetragonal shape.

3.2.2 Overall structure

The inter-subunit interactions between the three subunits are primarily mediated by the last two anti-parallel strands of the beta subunit (β 249-272, colored in green) with a strand from the N-terminal of the gamma subunit (γ 42-76, colored in red) and a loop at the C-terminus of the alpha subunit (α 530-544, colored in cyan) (**Fig 3.3A**). The gamma subunit is disk-shaped and approximately 60 Å in diameter and with a thickness of 30 Å. The γ subunit is made up of four CBS motifs arranged as two Bateman domains [16-17]. As observed in several crystal structures of CBS motifs, in our truncated AMPK structure, each one of the four CBS motifs consists of a conserved α1-β2-β3-α4 pattern in an anti-parallel arrangement [21] (**Fig 3.3B**). Each pair of CBS domains is associated via hydrophobic interactions between homologous β sheets, making it unlikely that single domains would be stable in solution (**Fig 3.3B**). The packing of these four pseudo-symmetric motifs generates four potential adenyl binding sites. The truncated wild type structure of AMPK was first solved as a complex with AMP, then crystals were soaked in ATP. The structure shows how one nucleotide binds between CBS 1-2 (site-1) and two nucleotides between CBS 3-4 (site-2 and site-3) (**Fig 3.3B**). Between CBS 1-2 there is a potential fourth nucleotide binding site, but thus far no nucleotide has been seen to bind at this site; this issue will be discussed in more detail in **section 5.6**. Each of the three nucleotides sits in a partially basic pocket formed at the interface between a pair of CBS domains (**Fig 3.3C&D**). Interestingly, binding site-3 does not undergo nucleotide exchange and seems to exclusively bind an AMP molecule which has been shown to co-purify with the protein (see **section 3.3**) [213]. The other two nucleotide binding sites can exchange between AMP, ADP or ATP.

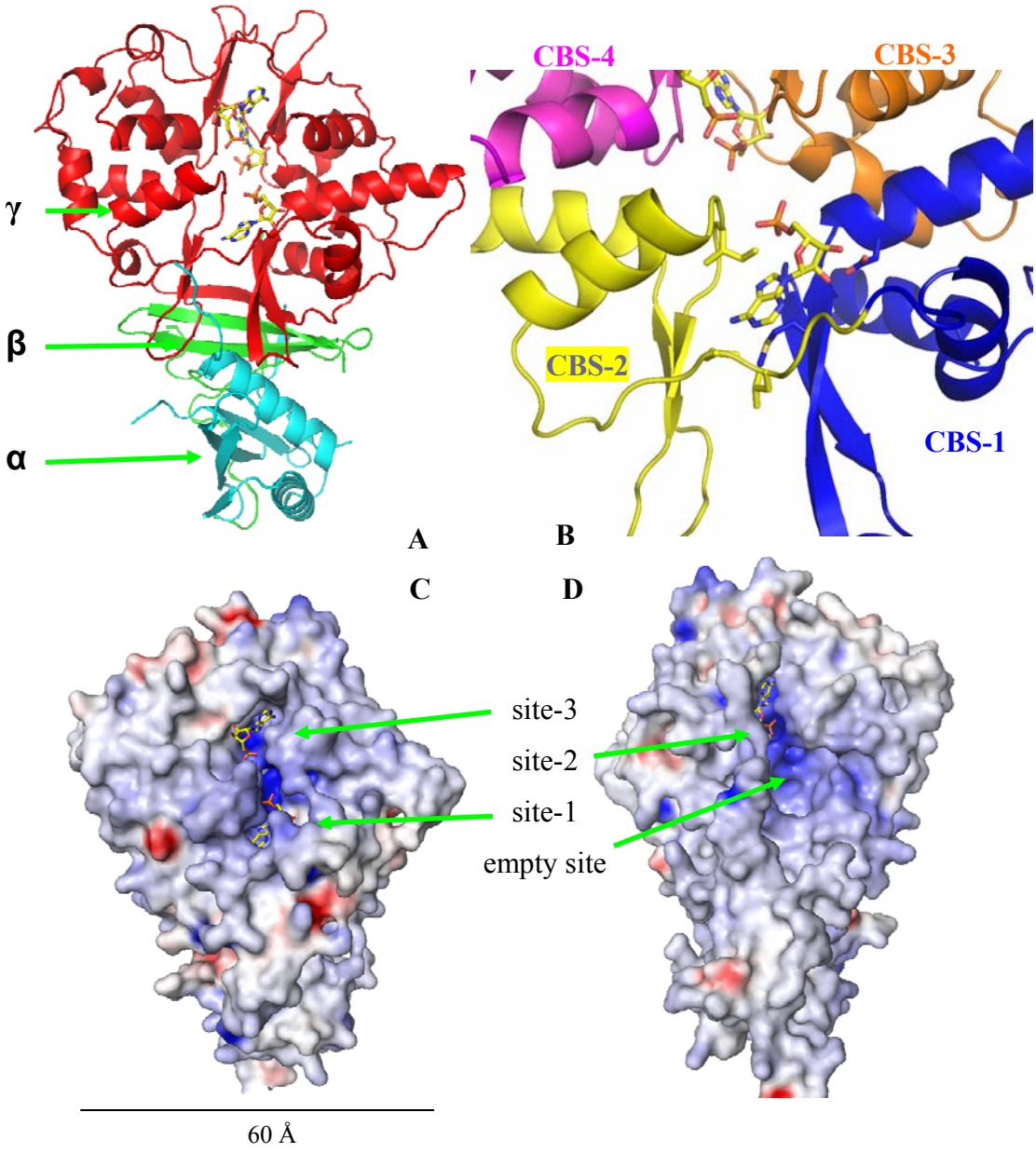

Figure 3.3: Ribbons (A&B) and surface (C&D) representation of AMPK in complex with three AMP molecules. In (A, B & C) the same view is shown. The three subunits in (A) are colored according to **Fig 3.2A**. Bateman 1 is shown in more detail in (B). CBS 1-2 (Bateman 1) are colored in blue and yellow, whereas CBS 3-4 (Bateman 2) are in orange and magenta, respectively. (C) Front view with site-1 and site-3; (D) Reverse view showing site-2. The surface is colored according to the electrostatic potential [blue, positive (contour level +30.0 K_bT / e_c); red, negative (-30.0 K_bT / e_c)]. AMP molecules are in stick representation with carbon atoms in yellow.

One of the key features of the binding site is the hydrogen bonding of the two hydroxyl groups of the ribose with the side chain of an aspartate residue (Asp 89 with site-1, Asp 244 with site-2 and Asp 316 with site-3) (**Fig 3.4A**).

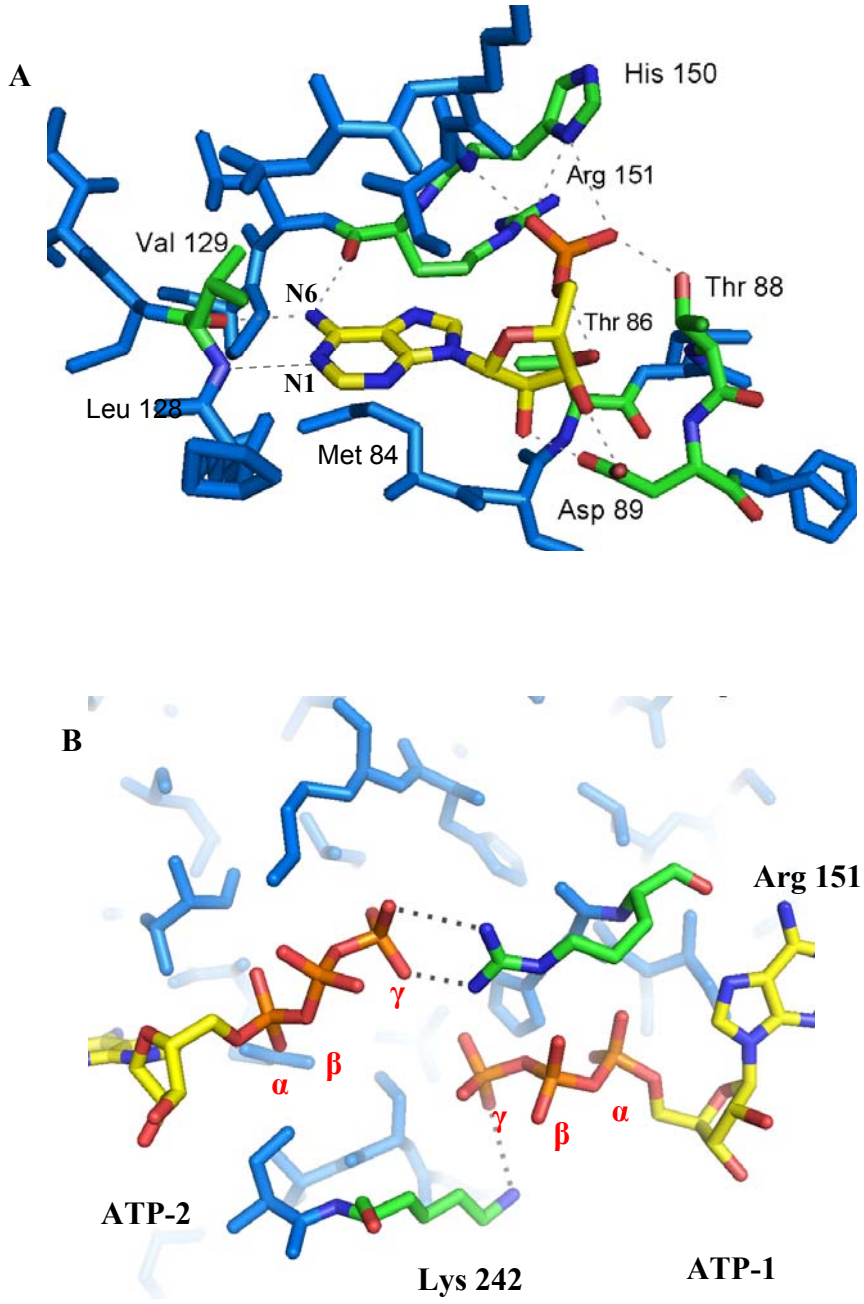

Figure 3.4: (A) Typical interaction between an AMP molecule and residues from the γ subunit. The binding site represented here is site-1. (B) Additional interaction between ATP and side chains of the protein (Lys 242 with ATP-1 and Arg 151 with ATP-2). The three phosphates of ATP are labelled in red. The AMP & ATP molecules are in stick representation with carbon atoms in yellow, the protein is in blue with the carbon atoms of residues that hydrogen bond with the nucleotide in green.

On the adenosine moiety, the amino group at N6 acts as a hydrogen bond donor to two main chain carbonyl groups from the enzyme (Val-129 and Arg-151 in site-1; Leu-276 and Arg-298 in site-2; Ala-204 and Ala-226 in site-3) (**Fig 3.4A**). The N1 atom hydrogen bonds with the amino group from the main chain of AMPK (Val-129, Leu-276 and Ala-204 with site-1, site-2 and site-3, respectively) (**Fig 3.4A**). The phosphate groups interact with the hydroxyl groups of serine or threonine residues (Thr-86 and Thr-88 in site-1; Ser-241 in site-2; Ser-225, Ser-313 and Ser-315 in site-3) and with the positively charged side chains of a number of different residues (His-150 and Arg-151 in site-1; Arg-69, Lys-169, Arg-298 and His-297 in site-2; His-150 and His-297 in site-3). Turning to the ATP complex, the γ phosphate of ATP makes an extra interaction with Lys-242 in site-1 and with Arg-151 in site-2, which is not possible when either AMP or ADP is bound (**Fig 3.4B**).

Hydrophobic interactions also contribute significantly to nucleotide binding, including the interactions from the carbon atoms of the adenosine moiety with Met-84 and Leu-128 (in site-1), Ile-236, Val-275 and Val-296 (site-2) and Ile-203 and Val-224 (site-3) (**Fig 3.4A**).

Although the nucleotides bind at the interface of two CBS motifs that make up a Bateman domain, there are some interactions of the nucleotides with amino acids from the "other" Bateman domain; for example AMP-2 interacts with residues predominantly from CBS3-4, but also with Arg-69 and Lys-169 (which belong to CBS-1 and -2, respectively); AMP-3 interacts with residues from CBS3-4 but also with His150 (CBS-2) (**Fig 3.5**).

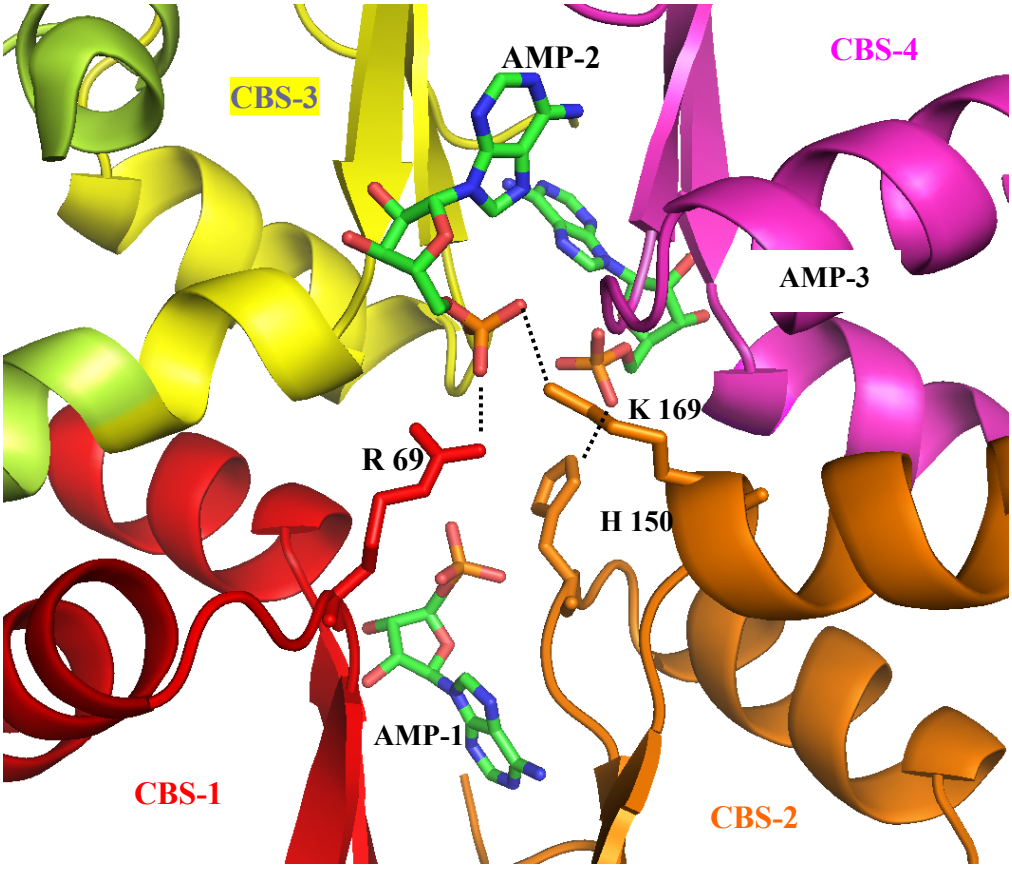

Figure 3.5: Ribbons representation of AMPK in complex with three AMP molecules. CBS 1-2 (Bateman 1) are colored in red and orange, whereas CBS 3-4 (Bateman 2) are in yellow and magenta, respectively. AMP molecules are in stick representation with carbon atoms in green.

There are disordered loops in both the α- and β-subunits: α-470 to α-523 and β-223 to β-232. Two loops in the γ subunit that are close to the two exchangeable AXP binding sites also show relatively poor electron density; γ-120 to γ-128 and γ-265 to γ-278 being adjacent to site-1 and -2, respectively.

3.2.3 Wild type AMPK structure in complex with ZMP

To study the binding of ZMP, an AMP mimic that has been investigated as a potential therapeutic agent, I carried out a series co-crystallization experiments of

AMPK with ZMP. Crystals were initially obtained with a protein concentration of 10 mg/ml and 2mM ZMP. The precipitant used contained MES, isopropanol and glycyl-glycyl-glycine and crystals grew up to 35 μm in width, and diffracted to about 2.9 Å. (**Table 3.1**). The merging statistics of the data were relatively poor (R_{merge} in the resolution shell between 3.0 Å and 2.9 Å was 0.32). Data merging and refinement statistics are given in **Table 3.1**. The relatively poor quality of this data is evident from these statistics.

Data collection		**Refinement**	
method	Co-crystallization	No. relections	17035
Space group	$P2_12_12_1$	No. atoms: Protein	3896
		Ligand	45
		Water	66
Cell dimension: a, b, c (Å)	48.3 123.8 124.4	R_{Work}/R_{Free} (%)	24.2/32.4
α, β, γ (˚)	90, 90, 90		
		B-factors (Å^2): Protein	41.4
Resolution (Å)	30-2.9 (3.0-2.9)	ZMP-1	38.8
		ZMP-2	no
		AMP-3	32.5
		Water	43.0
R_{merge}	11.2 (32.0)	R.m.s deviations from standard geometry:	
I/σ	9.3 (1.4)	Bond length (Å)	0.015
Completeness (%)	95.3 (87.9)	Bond angles (˚)	1.738
Redundancy	3.0 (2.5)		

Table 3.1: Crystallographic statistics of the AMPK/ZMP complex. The highest resolution shell is shown in parenthesis.

Although there was some electron density for three nucleotides in the binding sites, the structures of AMP and ZMP are too similar to adequately differentiate at this resolution (**Fig 3.6**). Therefore further crystallization trials using 100 mM MES pH 5.5 and 7% PEG 3350 as a precipitant were undertaken that resulted in the growth of larger crystals (55 μm). These crystals diffracted to higher resolution and were processed to 2.1 Å. Crystallographic statistics are shown in **Table 3.2**.

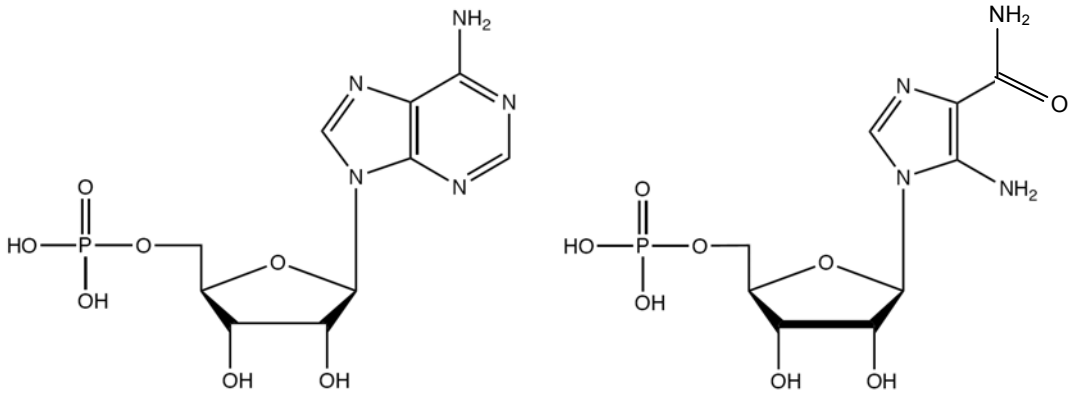

Figure 3.6: Structures of AMP (left) and ZMP (right). The only differences appear in the base moiety: AMP has an adenosine whereas ZMP has an imidazole group.

Data collection		**Refinement**	
Method	Co-crystallization	No. unique relections	44170
Space group	$P2_12_12_1$	No, atoms: Protein	3881
		Ligand	67
		Water	203
Cell dimension: a, b, c (Å)	48.6, 124.7, 124	R_{Work}/R_{Free} (%)	23.9/27.1
α, β, γ (˚)	90, 90, 90		
		B-factors (Å^2): Protein	42.8
Resolution (Å)	30-2.1	ZMP-1	40.9
	(2.20-2.10)	ZMP-2	55.2
		AMP-3	36.5
R_{merge}	7.1 (53.1)	Water	37.9
		R.m.s deviations from standard geometry:	
I/σ	19 (3.2)	Bond length (Å)	0.008
		Bond angles (˚)	1.589
Completeness (%)	98.7 (98.5)	Ramachandran plot (%):	
		favored	94.9
Redundancy	5.1 (5.2)	outliers	0.8

Table 3.2: Crystallographic statistics of the AMPK/ZMP complex using a crystal grown in MES, and PEG 3350. The highest resolution shell is shown in parenthesis.

The structure was solved by molecular replacement. The R_{factor} of the initial model was 33.4 %. Following refinement the final R_{work} and R_{Free} were 23.9 % and 27.1 %. The average protein B factor is 42.8 Å^2, and the B factor for the ZMPs in site-1 and site-2 and AMP-3 are 40.9, 55.2 and 36.5 Å^2, respectively. The geometry of the model is within the normal range for refined structures. The root mean square deviations (r.m.s.d.) from standard geometry is 0.008 Å for bond length and 1.6º for

bond angles. Analysis of the final Ramachandran plot revealed that more than 94.9 % of the residues adopted the most favorable conformational angles whereas less than 0.8 % lie in additional disallowed regions.

Good quality electron density for two ZMP molecules in the exchangeable nucleotide sites (site-1 and site-2) was evident from the initial difference (F_{obs} - F_{calc}) map (**Fig 3.7A&B**). Site-3 is again occupied by an AMP molecule (**Fig 3.7C**). The ZMP I built into the site previously referred to as AMP-1 I will refer to as ZMP-1 and likewise for AMP-2/ZMP-2. The non-exchangeable AMP-3 site retains its nomenclature. The structures of AMPK/AXP and AMPK/ZMP complexes are very similar over the α- and β-subunits (with a root mean square (r.m.s.) deviation of 0.26 and 0.65 Å respectively). In contrast, the γ-subunit shows differences in the conformation of some loops associated with the two exchangeable nucleotide-binding sites (**Fig 3.7D**). The loops close to site-1 (residues γ-121 to γ-127) and site-2 (residues γ-268 to γ-275), seem to be in a more closed conformation when ZMP binds respect to when AXPs bind. The biggest shift involves phenylalanine residue γ-125 in site-1 and γ-272 in site-2 which move 6.8 and 3.9 Å respectively. The environment of the binding site containing the non-exchangeable AMP-3 sits remains unchanged.

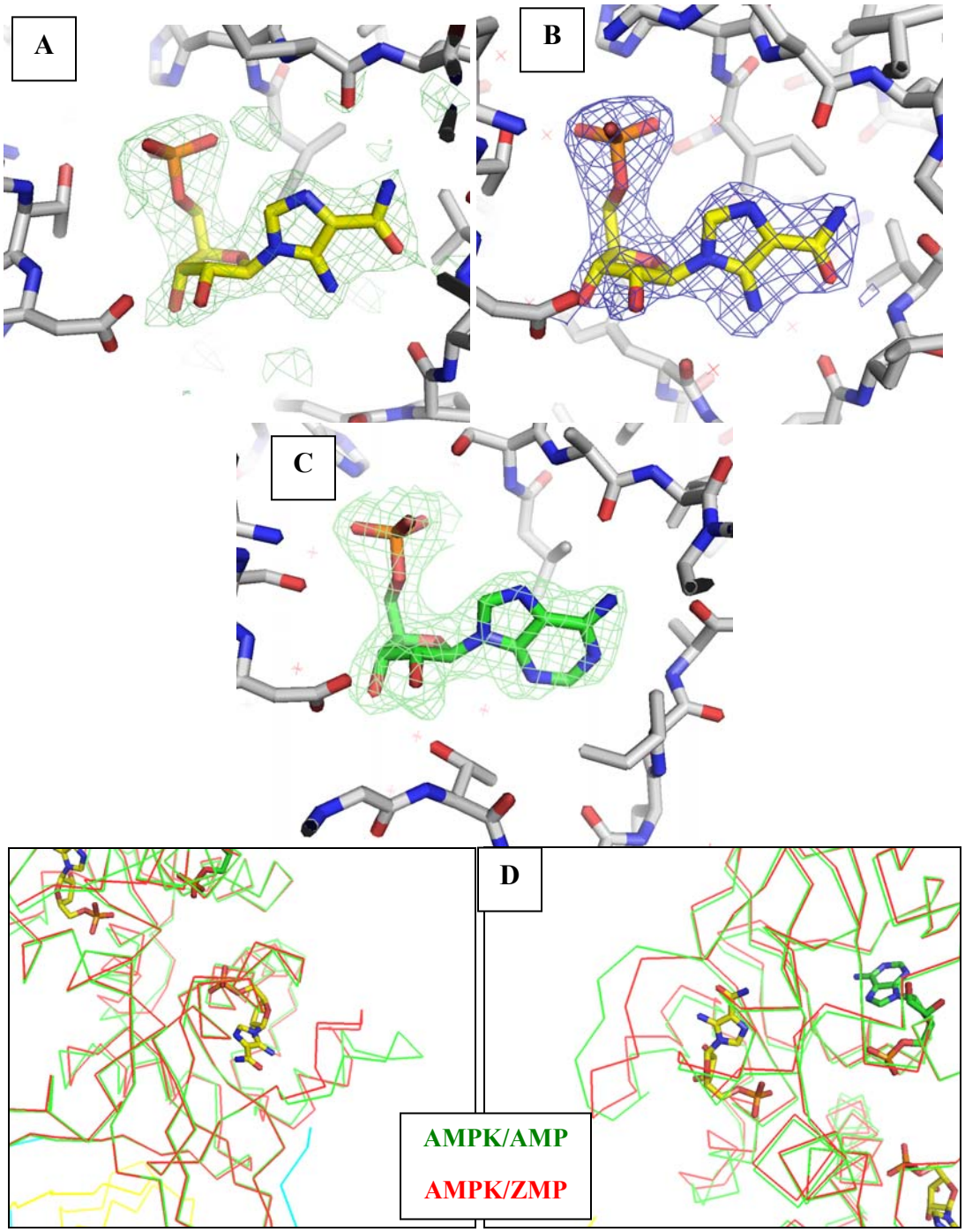

Figure 3.7: Structure of AMPK/ZMP complex: Electron density maps surrounding the exchangeable binding pocket site-1 before [A, (F_{obs} - F_{calc})] and after [B, ($2F_{obs}$ - F_{calc}) modeling in a ZMP molecule. The (F_{obs} - F_{calc}) map is contoured at 2.5 σ for ZMP-1 (A) and AMP-3 (C) whereas the ($2F_{obs}$ - F_{calc}) is at 1.5 σ (B); the electron density has been selected on the basis of being 1.6 Å from the coordinates of the ligand. (D) Superposition of the γ subunit from the AMPK/AMP (green) and AMPK/ZMP (red) complexes (left, site-1; right, site-2). ZMP and AMP molecules are represented with carbon atoms in yellow and green sticks, respectively.

Overlap of the AMPK/ZMP and the AMPK/AXP complexes reveals that the ZMPs and AMPs do not superpose exactly (**Fig 3.8A**). The phosphate groups of the three nucleotides shows some differences, between AMP and ZMP, interacting with basic residues of the protein; the interaction between Arg-69 and Lys-169 with ZMP-2 is lost due to a rearrangement of the side chains of these two residues. Interestingly, the imidazole group of His-297 is rotated about 120˚ away from AMP-3, and in its new rotamer conformation, His-297 interacts with the phosphate from ZMP-2. Due to the slight shift of the ZMP molecule in the pocket, the new rotamer of His-297 does not clash with the phosphate group of AMP-2 as seen in the WPW mutant AMPK described later (**section 3.2.5**). Otherwise the residues that interact with ZMP are largely the same as with the AMPK/AXP complex, although there are some changes in bond lengths (**Fig 3.8B**). The interaction between the adenosine part in the AMPK/ZMP complex involves two hydrogen bonds between the amino group at position 2 (equivalent to N6 of AMP) with the carbonyl group of the main chain of Val-129 and Arg-151 in site-1 and Leu-276 and Arg-298 in site-2. The O5 atom of ZMP (corresponding to N1 of AMP) hydrogen bonds with the main chain amide of the enzyme (Val-129 and Leu-276 in site-1 and site-2, respectively) (**Fig 3.8B**). The two loops close to the exchangeable binding sites contain residues that are outliers in the Ramachandran plot: Ser-124 and Lys-126 close to site-1 and His-270, Tyr-271 and Val-275 in the loop close to site-2. Residues Thr-253 and Tyr-254 have been deleted from the model as the electron density is unclear, and the use of an omit map did not help in building them.

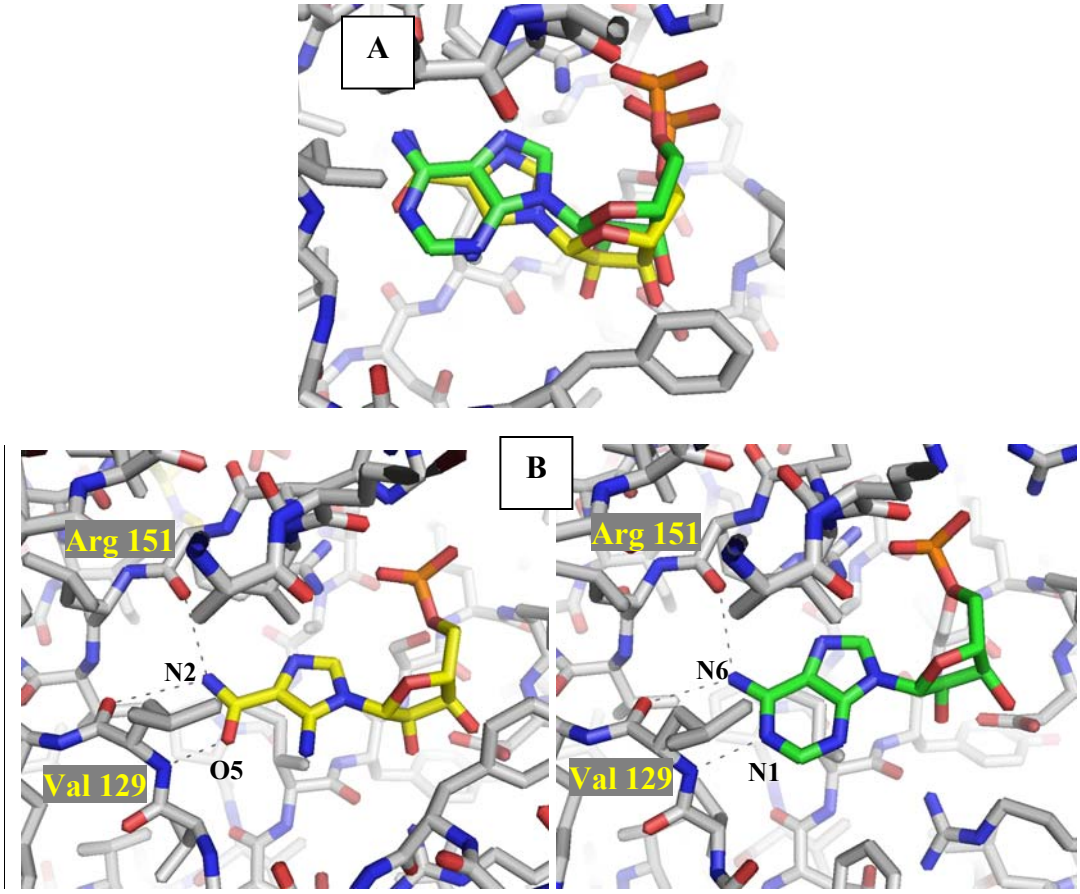

Figure 3.8: (A) Overlap of AMP-2 from the AMPK/AXP complex with ZMP-2 from the AMPK/ZMP. (B) Hydrogen bonding between the base of ZMP-1 (left) and AMP-1 (right) with main chain atoms of Val 129 and Arg 151. ZMP and AMP molecules are represented with carbon atoms in yellow and green sticks, respectively.

A free 6-NH2 group in the nucleobase in AMP may be critical for ligand binding to the nucleotide binding sites and the structure of AMPK with ZMP shows the same interactions with the protein explaining why ZMP, and not other nucleotides in the cell other than AMP, bind and activate AMPK (discussed in detail in **section 4.2; Fig 3.8B**). The loss of interaction betweens basic residues and ZMP probably explain the reduced affinity of this compound for AMPK (detailed fluorescent binding studies are in **section 3.4.7**), and hence the reduced potency of this drug for AMPK compared to AMP.

3.2.4 Wild type AMPK structure in complex with mant-AMP

To confirm that the fluorescent reporters used for later binding studies (see **section 4.2**) are binding in a similar and thus competitive manner with unlabelled AMP, I carried out a series of soaking experiments of AMPK with mant-AMP. Crystals obtained from 11.4 mg/ml protein with 100 mM MES pH 6.4 and 6% PEG 3350 were soaked overnight with 0.5 mM mant-AMP. The soaked crystal diffracted to 2.1 Å and the crystallographic statistics for data collection and refinement are given in **Table 3.3**.

Data collection		**Refinement**	
Method	Soaking	No. unique relections	44456
Space group	$P2_12_12_1$	No. atoms: Protein	3804
		Ligand	89
		Water	241
Cell dimension: a, b, c (Å)	49, 123.6, 124.9	R_{Work}/R_{Free} (%)	23.0/26.3
α, β, γ (˚)	90, 90, 90		
Resolution (Å)	30-2.1 (2.20-2.10)	B-factors (Å^2): Protein	43.4
		mAMP-1	48.6
		mAMP-2	67.9
		AMP-3	36.5
		Water	41.0
R_{merge}	6.2 (42.9)	R.m.s deviations from standard geometry:	
I/σ	16 (2.1)	Bond length (Å)	0.008
Completeness (%)	99.5 (100)	Bond angles (˚)	1.321
Redundancy	3.7 (3.7)	Ramachandran plot (%):	
		favored	97.4
		outliers	0.2

Table 3.3: Crystallographic statistics for the AMPK/mant-AMP complex. The highest resolution shell is shown in parenthesis.

The structure was solved by molecular replacement as before using 2V8Q as a model. The starting R_{factor} was 30.9%. Following refinement the final R_{WORK} and R_{FREE} were 23.0 and 26.3%, respectively. The average protein B factor is 43.4 $Å^2$, and the B factor for mant-AMP-1, mant-AMP-2 and AMP-3 are 48.6, 67.9 and 36.5 $Å^2$, respectively. The geometry of the model is within the normal range for refined structures. The r.m.s. deviation from standard geometry is 0.008 Å in bond length and 1.3º in bond angles. Analysis of the final Ramachandran plot revealed that greater than 97.4 % of the residues adopt the most favorable conformational angles and just 1 residue, Thr-253 lies in the additional disallowed regions.

The electron density for the mant-AMP in site-1 and site-2 was clear from the first map with strong positive ($F_{obs} - F_{calc}$) electron density for the AMP and mant moieties (**Fig 3.9A**). The mant-nucleotides were built into the electron density maps and subsequently refined as part of the atomic model. As expected, site-3 showed electron density for AMP.

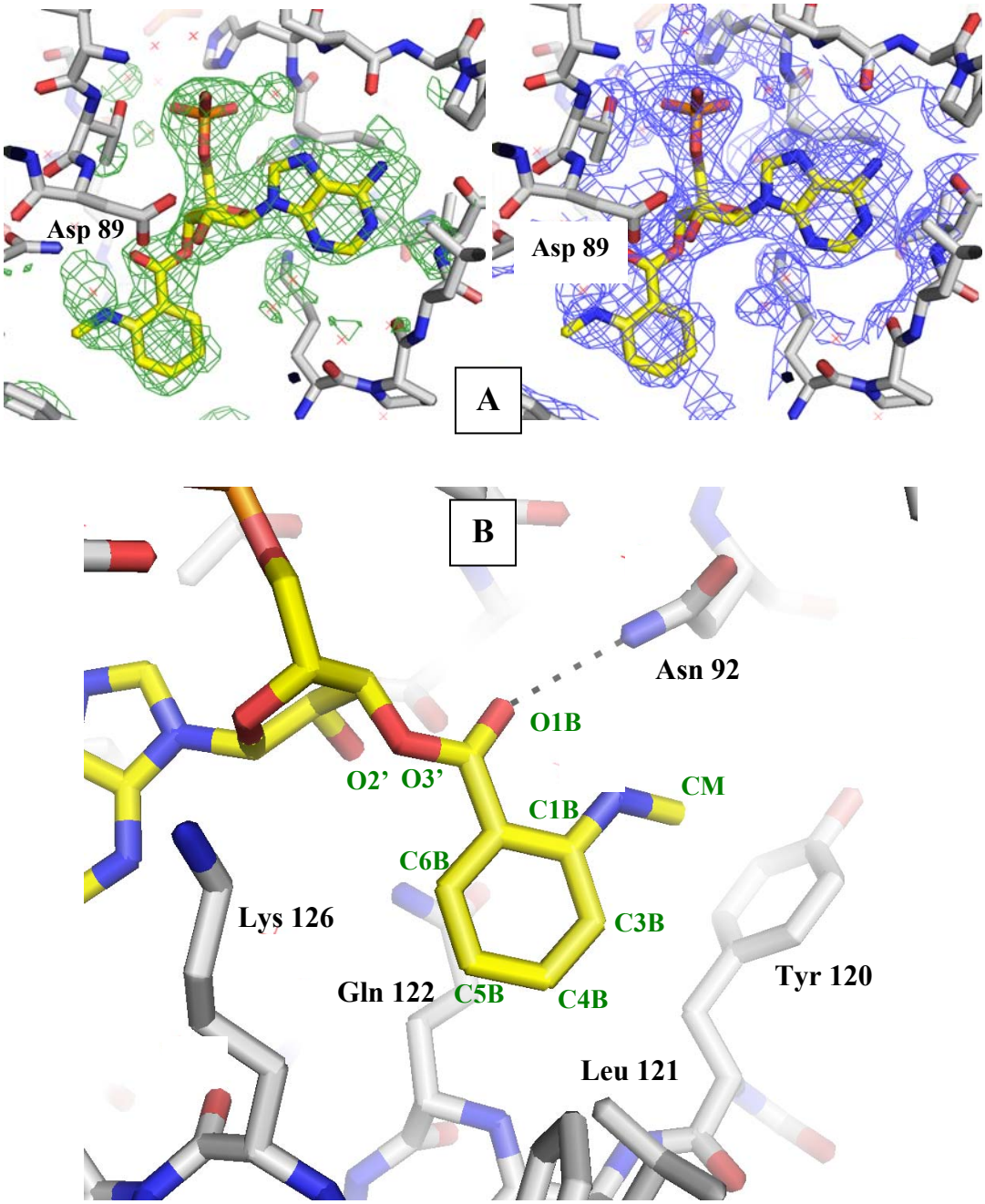

Figure 3.9: (A) Electron density of the initial difference map (F_{obs} - F_{calc}) contoured at 2.5 σ is on the left. A portion of the electron density map ($2F_{obs}$ - F_{calc}) after mant-AMP had been refined in the atomic model is contoured at 1.0 σ, right. (B) Atomic model of mant moiety with numbered positions. The binding pocket shown is site-1. Carbon atoms of the mant-AMP are in yellow sticks.

The monophosphate and the adenyl parts of the mant-nucleotide adopt similar conformations to those observed in the AMP complex with AMPK. The structure of mant-nucleotide consists of an AXP molecule with a mant group linked to the ribose at the 3' position (**Fig 3.9B**). The usual bi-dentate interaction that is formed between the 2' and 3' hydroxyl groups of the ribose with an aspartic acid can not be formed in the presence of the mant substituent. Instead, the side chain of the aspartate makes a single hydrogen bond interaction with the 2'-OH.

There are limited contacts between the fluorescent mant group and the protein and it does not seem to cause any changes to the structure of the protein. The mant group from the nucleotide in site-1 hydrogen bonds with Asn-92 through the carbonyl oxygen labelled O1B in **Fig 3.9A**. Hydrophobic interactions between the mant moiety and the protein include the methylamine group interacting with the aromatic ring of the side chain of Tyr-120, atom C4B with the side chain of Leu-121, atom C5B with the Cβ of Gln-122 and C6B with the alkyl part of the side chain of Lys-126 (**Fig 3.9B**). In site-2, the carbonyl in the mant moiety does not hydrogen bond with the protein, but hydrophobic interactions stabilize the binding of the mant moiety in a similar manner to site-1: the methylamine makes hydrophobic contact with the Cγ of Arg-268 and the carboxyl group from the main chain of Tyr-271. Atom C2B makes hydrophobic contact with the side chain of His-270, C3B with the amino group of the main chain of Ser-269, C4B with Cβ from Ser-269 and atom C6B interacts with Phe-243. The mant group extends outside the normal binding pocket and therefore does not alter the binding of the adenyl moiety (**Fig 3.10**). Interestingly, the loops close to the two exchangeable binding sites that are usually poorly defined are, in this case, well ordered enabling them to be built into the atomic model.

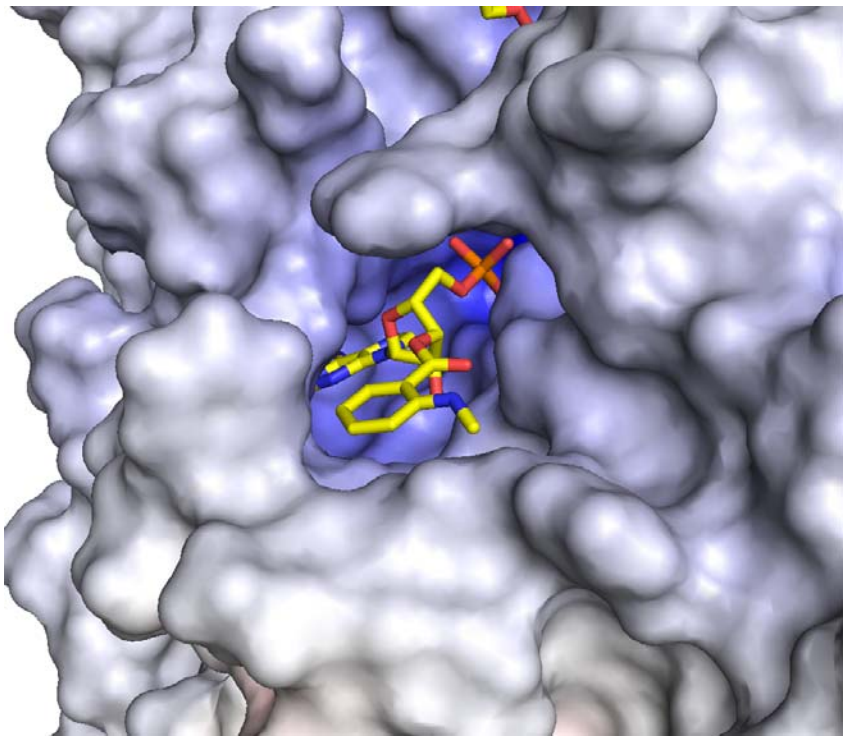

Figure 3.10: Surface representation of AMPK in complex with mant-AMP. The pocket shown is site-1. The surface is colored according to the electrostatic potential [blue, positive (contour level +30.0 K_bT / e_c); red, negative (-30.0 K_bT / e_c)]. Mant-AMP is in stick representation with carbon atoms in yellow.

Detailed fluorescence binding studies using mant-AMP are described in **section 4.2.3**. The binding data suggests a stoichiometry of 2:1 (mant-AMP/AMPK). The crystal structure of the regulatory subunit of AMPK in complex with mant-AMP presented here confirms that the binding of the fluorescence reporter is specific, i.e. two molecules of mant-AMP bind to the exchangeable nucleotide binding sites and that this reporter binds competitively with the unlabelled nucleotide, whereas site-3 remains non-exchangeable.

3.2.5 Structures of Wolff-Parkinson-White (WPW) mutants

To gain insight into the mechanism of WPW mutations of AMPK, I undertook a series of crystallization experiments to determine the structures of Arg69→Gln, His150→Arg and Arg298→Gly –three of the naturally occurring mutants that cause WPW. Protein crystals grew in sitting and hanging drops by vapour diffusion with a protein concentration ranging from 8 mg/ml (for His150→Arg and Arg298→Gly) to 9 mg/ml (for Arg69→Gln). Arg69→Gln crystals grew in 100 mM MES, pH 6.0 and 5% PEG 3350 to a width of 120 μm. Arg298→Gly crystals grew in 100 mM MES, pH 6.0 and 8% PEG 3350. Apo crystals for Arg298→Gly grew up to 200 μm in width but in complex with AMP were only about 90 μm (**Fig 3.11**). In the case of the His150→Arg mutant, crystallization was problematic and after much screening only a precipitant containing AMP, 13 % MPD and 3 % PEG 4000 produced single crystals which grew to 40 μm. See **section 2.3.5** for more details. I could not grow crystals of the apo form for the His150→Arg mutant. For Arg69→Gln and Arg298→Gly, apo protein produced the largest crystals. My experience, not uncommon, was that larger crystals resulted in higher resolution diffraction (e.g. the 200 μm apo crystal of Arg298→Gly diffracted to 2.0 Å resolution, whereas the 40 μm crystal of His150→Arg to only 2.6 Å Bragg spacing.

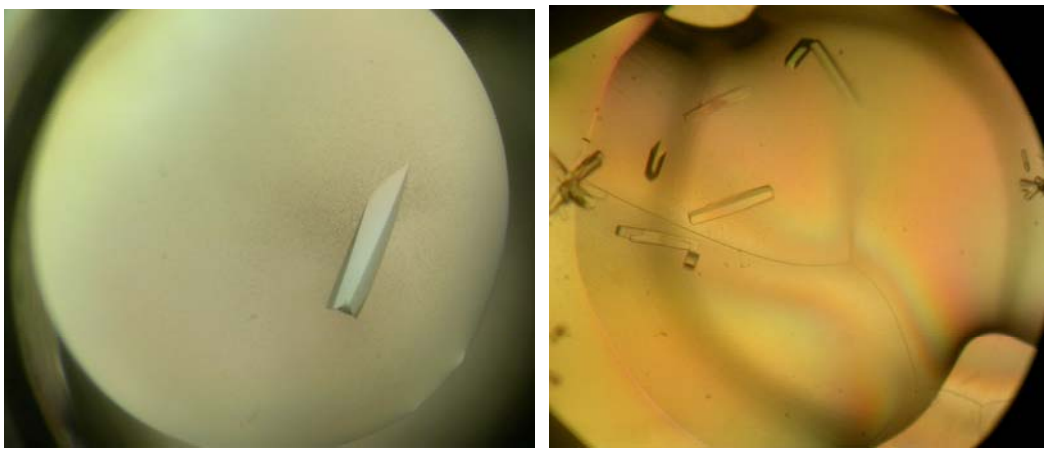

Figure 3.11: Typical crystals of WPW mutant AMPK. Apo crystals reached 200 μm in width (left), whereas protein in complex with AMP produced crystals of about 90 μm (right).

Summary of the crystallographic statistics for the three mutants AMPKs in complex with AMP are listed in **Table 3.4A**. Arg298→Gly is also presented in the apo form and in complex with ADP or ATP in **Table 3.4B**.

Data collection	R69Q	H150R	R298G
Space group	$P2_12_12_1$	$P2_12_12_1$	$P2_12_12_1$
Cell dimension: a, b, c (Å)	48.5, 119.2, 128.5	48.9, 124.3, 123.8	48.5, 121.7, 126.6
α, β, γ (˚)	90, 90, 90	90, 90, 90	90, 90, 90
Resolution (Å)	30-2.1 (2.20-2.10)	30-2.6 (2.72-2.60)	30-2.4 (2.41-2.40)
R_{merge}	7.1 (50.3)	3.1 (37.3)	6.2 (34.9)
I/σ	18.7 (2.4)	30.2 (3)	16.3 (2.2)
Completeness (%)	98.4 (99.7)	97.1 (85.1)	98.4 (99.8)
Redundancy	5.3 (5.4)	3.7 (3.7)	3.7 (3.7)

Refinement	R69Q	H150R	R298G
No. unique relections	43429	23048	29647
No. atoms: Protein	3848	3714	3703
Ligand	69	46	46
Water	216	161	133
R_{Work}/R_{Free}	24.5/27.4	24.0/30.0	27.5/29.5
B-factors (Å^2): Protein	45.3	53.3	43.9
AMP-1	39.9	56.9	38.5
AMP-2	40.2	N.B.	N.B.
AMP-3	39.3	38.5	43.0
Water	34.4	48.5	28.3
R.m.s deviations from standard geometry:			
Bond length (Å)	0.010	0.009	0.011
Bond angles (˚)	1.457	1.215	1.331
Ramachandran plot (%):			
favored	96.1	93	96.4
outliers	0	1.5	0

Table 3.4A: Crystallographic statistics of the Arg69→Gln (R69Q), His150→Arg (H150R) and Arg298→Gly (R298G) mutant models in complex with AMP. The highest resolution shell is shown in parenthesis. N.B., no binding.

Data collection	R298G	R298G	R298G	R298G
Method	apo	AMP co-cryst	ADP soak	ATP soak
Space group	$P2_12_12_1$	$P2_12_12_1$	$P2_12_12_1$	$P2_12_12_1$
Cell dimension:				
a, b, c (Å)	48.3, 118.7, 129.2	48.5, 121.7, 126.6	48.6, 124.7, 124	49, 123.6, 124.9
α, β, γ (˚)	90, 90, 90	90, 90, 90	90, 90, 90	90, 90, 90
Resolution (Å)	30-2.0 (2.09-2.00)	30-2.4 (2.41-2.40)	30-2.6 (2.72-2.60)	30-2.5 (2.61-2.50)
R_{merge}	5.8 (43.7)	6.2 (34.9)	5.4 (42.1)	9.2 (44.7)
I/σ	18.9 (2.5)	16.3 (2.2)	18.1 (2.5)	15 (4.3)
Completeness (%)	99 (99.3)	98.4 (99.8)	99.1 (99.2)	98.1 (100)
Redundancy	3.6 (3.6)	3.7 (3.7)	3.6 (3.6)	7.1 (7.3)

Refinement	R298G **Apo**	R298G **AMP**	R298G **ADP**	R298G **ATP**
No. unique relections	51114	29647	23482	24947
No. atoms: Protein	3837	3703	3768	3801
Ligand	46	46	77	85
Water	280	133	147	85
R_{Work}/R_{Free}	24.8/26.3	27.5/29.5	24.2/26.1	27.2/30.7
B-factors (Å^2): Protein	45.2	43.9	54.3	71.7
AXP-1	43.1	66.1	57.1	64.5
AXP-2	N.B.	N.B.	58	61.6
AMP-3	43.2	63.8	50.4	62.5
Water	41.3	28.3	45.2	61.9
R.m.s deviations from standard geometry:				
Bond length (Å)	0.008	0.011	0.009	0.010
Bond angles (˚)	1.576	1.331	1.304	1.526
Ramachandran plot (%):				
favored	94.6	96.4	95.15	94.8
outliers	1.7	0	0.4	1.5

Table 3.4B: Crystallographic statistics of the AMPK-R298G models in the apo form or in complex with nucleotides. The highest resolution shell is shown in parenthesis. N.B., no binding.

The data was processed using Denzo and Scalepack [210]. All crystals belonged to the space group $P2_12_12_1$. The structures were solved by molecular replacement. The starting R_{Work}/R_{Free} were 35/36.6 for Arg69→Gln, 37.5/38.4 for His150→Arg and 35.4/34.9 for Arg298→Gly.

All three mutant structures are very similar in overall structure to wild type AMPK. The most significant differences occur in the γ-subunit with r.m.s.d. in Cα positions of 0.4 Å for Arg69→Gln, 0.7 Å for His150→Arg and 0.4 Å for Arg298→Gly. The most significant differences occur in the conformation of loops close to the two exchangeable nucleotide-binding sites. In His150→Arg the loop close to site-2 (residues γ-268 to γ-275) partially occupies the pocket of site-2 which is empty in this mutant. In the case of R298G/AMP, the density for some of the residues in this loop is poorly defined and these residues were removed from the atomic model. The environment of the pockets where AMP-1 and the non-exchangeable AMP-3 are situated remains similar.

To summarize, for all three mutant structures, the nucleotide occupancy is unambiguous in site-1 and site-3. At site-3 only AMP bound whereas at site-1 AMP, ADP or ATP could bind. When I superimpose the mutant structures with wild type AMPK, the position of AMP-1 and AMP-3 overlap closely. The fluorescent binding studies presented below (see **section 4.2.5**), will show that the Arg69→Gln, His150→Arg and Arg298→Gly mutant AMPK, have reduced affinity for nucleotides in one of the two exchangeable nucleotide sites (but that Arg69→Gln is less affected than the other two mutants). The structure of Arg69→Gln shows clear electron density for all three AMP molecules, in contrast there is no electron density for AMP in site-2 of the His150→Arg or Arg298→Gly structures (**Fig 3.12A**&**B**). In addition to AMP, Arg298→Gly was also crystallized with ADP and ATP to verify that neither of these nucleotides binds at site-2 (**Fig 3.12C**). Taken together, these data suggests that site-2 is the "weak" site and site-1 is the "tight" site, seen in binding measurements (see **section 4.2**).

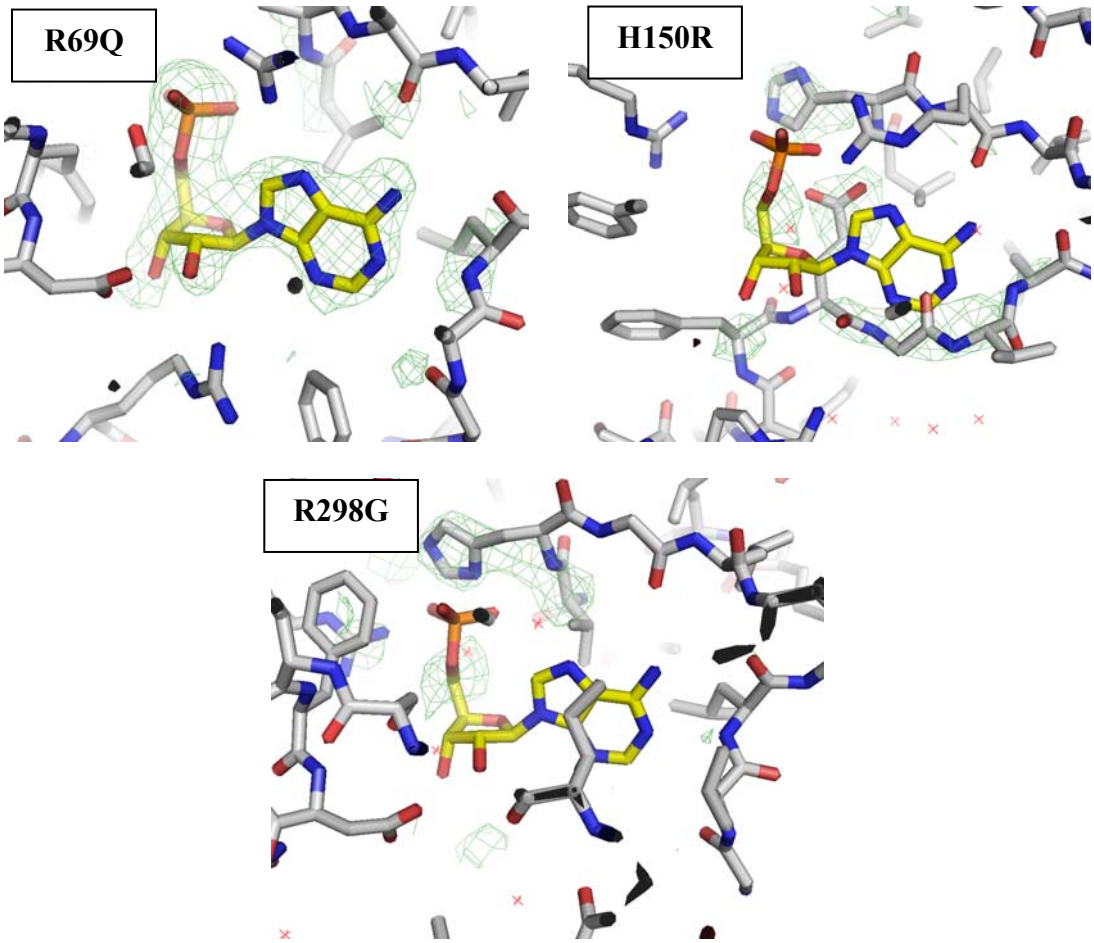

Figure 3.12: Electron density from initial (Fobs - Fcalc) maps of the AMPK mutants: Arg69→Gln, His150→Arg and Arg298→Gly. The binding pocket shown is site-2 and the map is contoured at 2.5 σ. The AMP molecules, coloured with carbon atoms in yellow sticks, have been transferred from the wild type complex to show where the electron density for the nucleotide might be expected, but for the His150→Arg and Arg298→Gly structures there is no clear electron density for AMP. In contrast, Arg69→Gln does show clear electron density for an AMP molecule in site-2.

When the wild type structure is compared to the His150→Arg and Arg298→Gly mutants, an interesting difference is observed in the side chain rotamer of His-297. In the wild type structure, the main chain amino group of His-297 hydrogen bonds with the phosphate group of the nucleotide in site-2, whereas its side chain interacts

with the phosphate of the non-exchangeable AMP-3. In the case of His150→Arg and Arg298→Gly the side chain of His-297 is rotated 120˚ with respect to the wild type and occupies a position that would sterically clash with the phosphate of AMP-2 **if it were occupied**. (**Fig 3.13**). In contrast, in the structure of Arg69→Gln, His-297 adopts the same side chain rotamer as wild type.

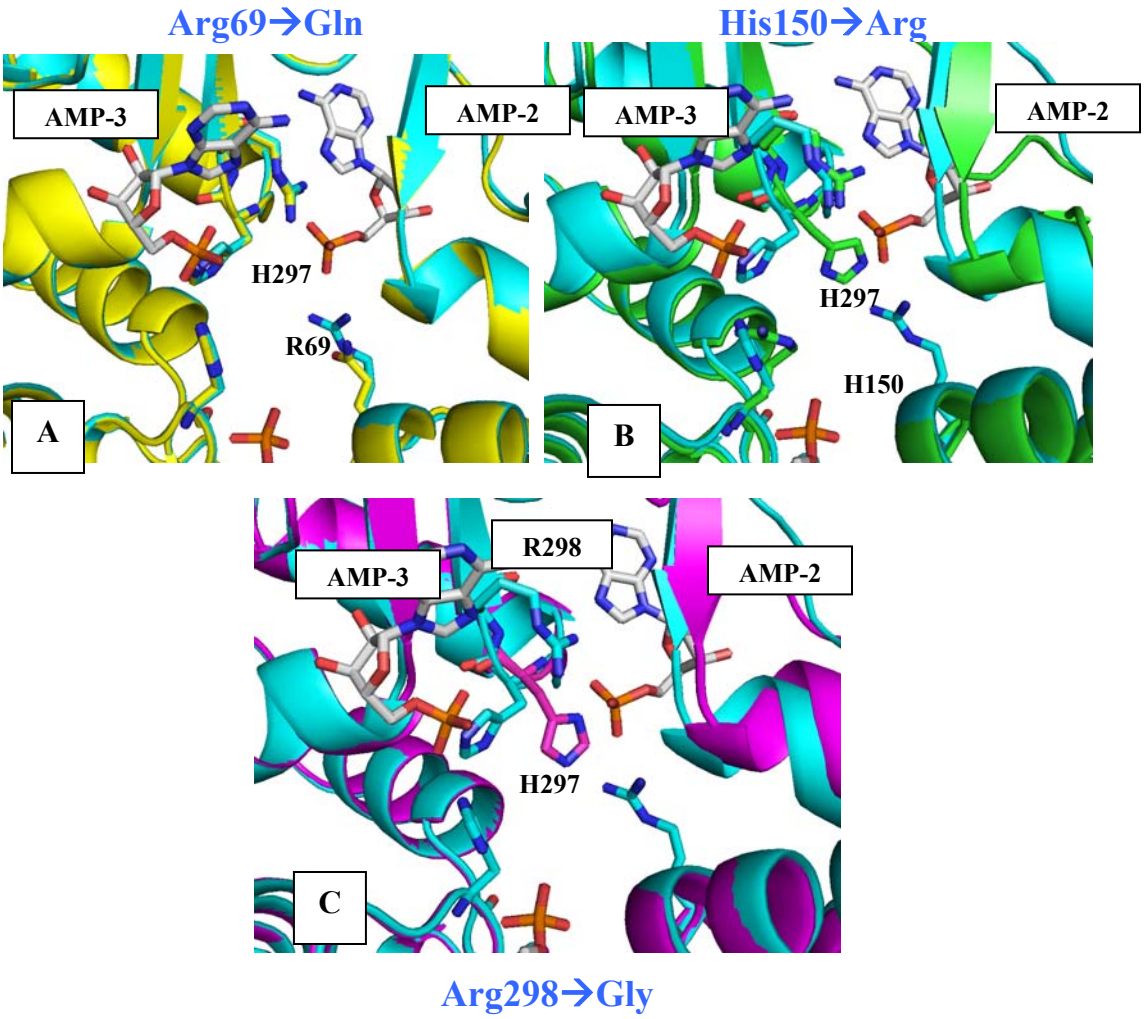

Figure 3.13: Ribbons representation of the superposition between wild type and mutant mammalian AMPK structures: wt protein is in cyan; a) Arg69→Gln in yellow b) His150→Arg is in green. c) Arg298→Gly is in purple. AMP molecules are shown in stick representation together with residues important in nucleotide binding.

The crystal structures of the three WPW mutants complement the results from the binding studies in **section 4.2.5**. My binding data was produced with the use of two fluorescence reporters, mant-AMP and NADPH, and suggests that the two exchangeable nucleotide binding sites have different affinities. Additionally, in WPW mutants AMP has a reduced affinity for the "weaker" site, compared to wild type protein. Arg69→Gln appears to be the protein that is least affected by the mutation. Since the crystal structures in this chapter show no nucleotide bound in site-2 for Arg298→Gly and His150→Arg, I can speculate that, at least in the truncated construct, the weaker site is site-2, whereas the tighter site is site-1.

4. Results – binding studies

4.1 Identification & quantification of nucleotide bound to WPW mutant AMPK

Bound nucleotide analysis on a purified wild type AMPK sample, shows that for every wild type protein molecule there is approximately 0.85 molecules of AMP and 0.15 of ADP [213]. These nucleotides therefore bind sufficiently tightly that they co-purify with the enzyme through the various steps of protein purification. To determine whether the WPW mutations affect the binding of AMP in the non-exchangeable site-3, I carried out the same analysis on the Arg-298→ Gly, His-150→Arg and Arg-69→Gln mutants. AMPK mutants were denatured, protein removed by centrifugation and the supernatant analyzed by high-performance liquid-chromatography (HPLC). In the three mutants, about 75% of the adenyl-nucleotide present is AMP and about 17% is ADP (**Fig 4.1**). This suggests that in WPW mutants, as seen wild type protein, AMPK co-purifies with one AMP molecule.

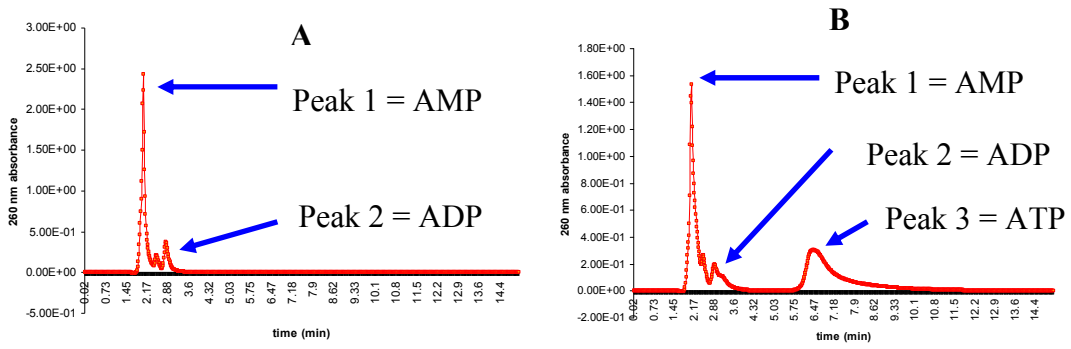

Figure 4.1: The elution profile for the supernatant from the Arg-298→Gly protein only is shown. (A) The protein is in the apo form and the concentration is 220 µM. Peak 1 & 2 elute in the same position and with the same absorbance spectrum as AMP and ADP and their concentrations were 165 µM and 37.8 µM, respectively. In (B), 217 µM ATP was added to the protein sample prior HPLC analysis to calibrate the system. The areas under the AMP, ADP and ATP peaks were measured. These results imply that AMPK co-purifies, with AMP in a 1:1 stoichiometry.

4.2 Fluorescence studies

4.2.1 Overview

The crystal structure of truncated mammalian AMPK shows that three adenine nucleotide molecules bind to the γ subunit of AMPK. One binding site (site-3) has been shown to contain non-exchangeable AMP (site-3) as just described. The other two binding sites are exchangeable in that AMP, ADP or ATP can bind competitively. Characterizing the binding properties of these two sites is likely to be important for understanding how AMPK activity is regulated. Although not a quantitative measure of binding affinity, site-1 consistently shows stronger electron density for bound nucleotide ligands than site-2 in my crystallographic studies, suggesting at least that the two sites behave differently. The main focus of this chapter is to establish the affinities of nucleotides for the two exchangeable binding sites in AMPK and whether these sites display a reduced affinity for nucleotides in WPW mutants. The binding of nucleotides to the two exchangeable sites of AMPK, as monitored by a fluorescently-labelled AMP, can be represented schematically as such.

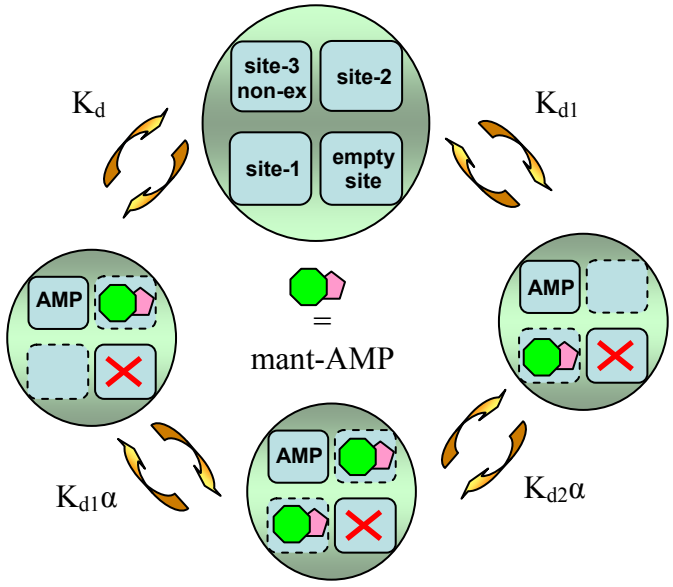

Figure 4.2: Schematic representation of nucleotide binding to AMPK: Site-3 is non-exchangeable and mostly contains AMP. The fourth potential site is always empty. Site-1 and -2 are the two exchangeable sites, where α is the cooperativity factor, if $\alpha > 1$ there is positive co-operativity between ligands binding in the two sites; if $\alpha < 1$ then there is negative co-operativity.

In general it is simplest to assume that a binding event is non-cooperative, both energetically (i.e., α =1) and spectroscopically (i.e., that the optical properties of the ligand in one site are not affected by occupancy of the other site) (discussed later in **section 5.3**). Indeed, most analysis methods work on this assumption. The fluorescence signal observed for a mixture of AMPK (P) and ligand (L) will be given by the following equation:

$$F = F_L[L] + F_{PL1}[PL_1] + F_{PL2}[PL_2] + F_{PL1,2}[PL_{1,2}]$$

where the F values are molar fluorescence coefficients, L_1 represents a ligand binding to site-1, L_2 to site-2 and $L_{1,2}$ to ligands binding to both sites. The terms in square brackets are concentrations, the values of which depend on total concentrations and on the K_d values. What will be observed in any particular fluorescent titration therefore depends not only on the individual K_d values but also on how much of the total fluorescence change is contributed by binding at a particular site. Essentially, the equation means that the fluorescent signal obtained is the sum of the fluorescence obtained from the fluorescent reporter uncomplexed, in complex with one or the other site and when bound in both sites. A successful analysis for two K_d values requires accurate determination of the F values. If the two sites have significantly different affinities it is unlikely that the F value for the complex with a single ligand molecule in the low affinity site will be determinable. The reason for this is illustrated in **Fig 4.3** which shows how concentrations of different species vary for the two possible titration 'modes': titration of the ligand with the protein (A) and titration of the protein with the ligand (B).

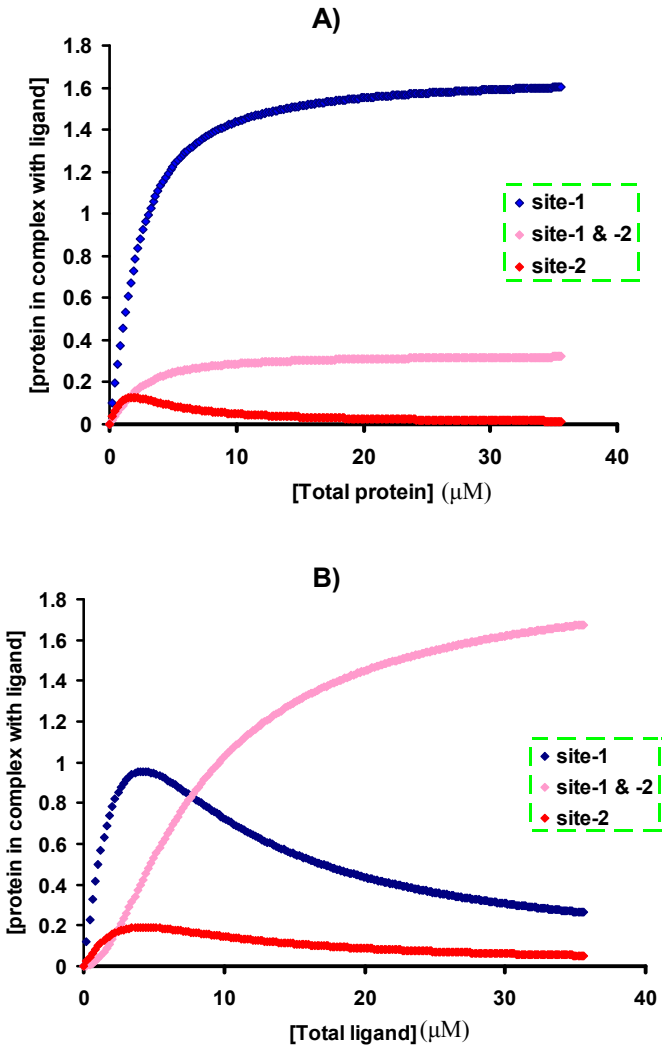

Figure 4.3: Schematic representation of how concentrations of different species vary for the two possible titration 'modes': titration of the protein with the ligand (A) and titration of the ligand with the protein (B). In this simulation the dissociation constants (K_{ds}) for sites 1 and 2 were set arbitrarily at 1 and 5 μM, respectively. The concentration of the ligand (in A) and protein (in B) were held constant at 2 μM. Interestingly, the two simulations demonstrate how approaching the experiment in different ways might show different proportions of the two species.

The key point is that in either case the fraction of total protein with a single ligand in the low affinity site remains low throughout the course of the titration and this species cannot therefore be fully characterized in terms of K_d or optical properties.

Consequently, any binding curve for AMPK obtained with a fluorescent reporter that monitors two sites with significantly different affinity it is likely to provide relatively little information about the lower affinity site.

4.2.2 Identification of NADPH as a fluorescent reporter for AMPK

Previous activity studies on AMPK showed that low micromolar concentrations of AMP cause allosteric activation of the protein [85,229]. These enzymatic assays were carried out using different techniques, but typically employed radioactively labeled [γ-^{32}P]ATP. My attempts to reproduce the effects of AMP on AMPK using the pyruvate kinase – lactate dehydrogenase coupled enzyme assay system [230] were unsuccessful in the sense that very high concentrations of AMP were required to activate AMPK. A possible explanation for this was that one of the ingredients in the coupled assay mixture was interfering with AMP binding to AMPK. Because the assay contains high concentrations of NADH and given the structure of NADH (**Fig 4.4**), I decided to investigate NADH binding to the enzyme.

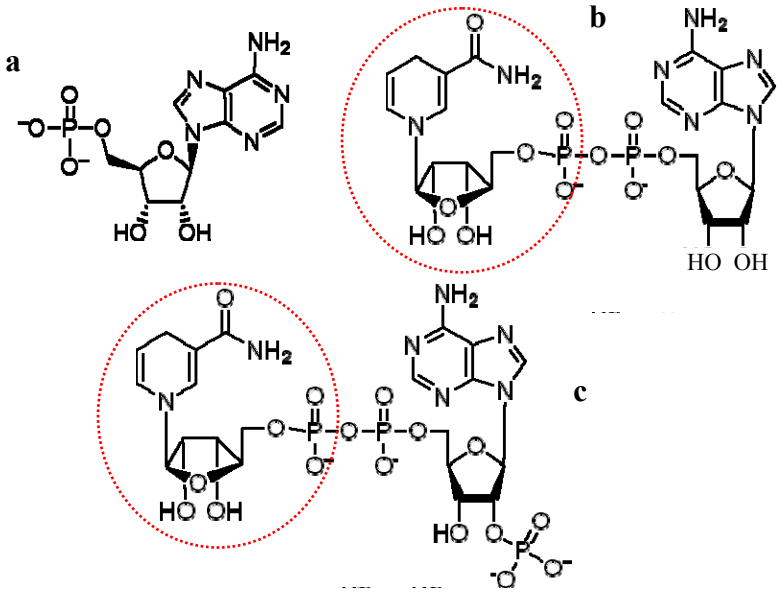

Figure 4.4: Comparison of the structures of AMP (a), NADH (b) and NADPH (c). The parts that confer fluorescence properties to the nucleotide are circled in red.

NADH is a physiologically important nucleotide whose structure is similar to AMP, but with an additional group extending from the phosphate moiety. NADPH is

similar to NADH but has an extra phosphate group linked to the 2' position of the ribose (**Fig 4.4**). The nicotinamide group is responsible for the fluorescence of these nucleotides.

The binding of NADH and NADPH to AMPK was monitored by adding protein to a solution of the nucleotide (10 μM) in Tris buffer. Free (uncomplexed) NADPH has an emission maximum at 461 nm. Addition of AMPK blue-shifts the fluorescence maximum to 428 nm and increases the signal approximately 9-fold (**Fig 4.5A**). The signal enhancement is significantly less for NADH **(Fig 4.5B)**. To determine the stoichiometry of NADPH binding to AMPK, I carried out some titrations with the nucleotide in buffers with no salt and/or at a temperature of 4˚C. These conditions were chosen with the idea of increasing the binding affinitiy and therefore making the determination of the stoichiometry clearer. Interestingly, the stoichiometry between NAD(P)H and AMPK is 1:1 (**Fig 4.5C**).

To confirm that the binding properties of the crystallized construct were similar to those of the full-length protein, both proteins were analyzed under the same conditions. Because the protein are routinely stored in a buffer containing 100mM NaCl, the majority of titrations were performed in a buffer with 100mM NaCl in order to keep the ionic strength of the solution constant. Affinities were determined from plots of fluorescent intensity at 440 nm as a function of protein concentration. The fluorescent emission was monitored at 440 nm because this is the wavelength where the difference in fluorescence intensity between free and bound NADPH is greatest. Both full-length AMPK and the truncated construct bind NADPH similarly with 1:1 stoichiometry and an affinity of 19 ± 2.5 μM (See **Appendix 1.1**). Having established the properties of NADPH binding to AMPK, I then examined the effects of AXPs as potential competitors of NADPH binding. Such competition experiments with AXPs showed that the site which is competing with NADPH binds AMP, ADP or ATP with affinities of 3.3 ± 0.6 μM, 1.3 ± 0.2 μM and 1.1 ± 0.2 μM, respectively (**Fig 4.5C; Table 4.1** & **Appendix 1.2**).

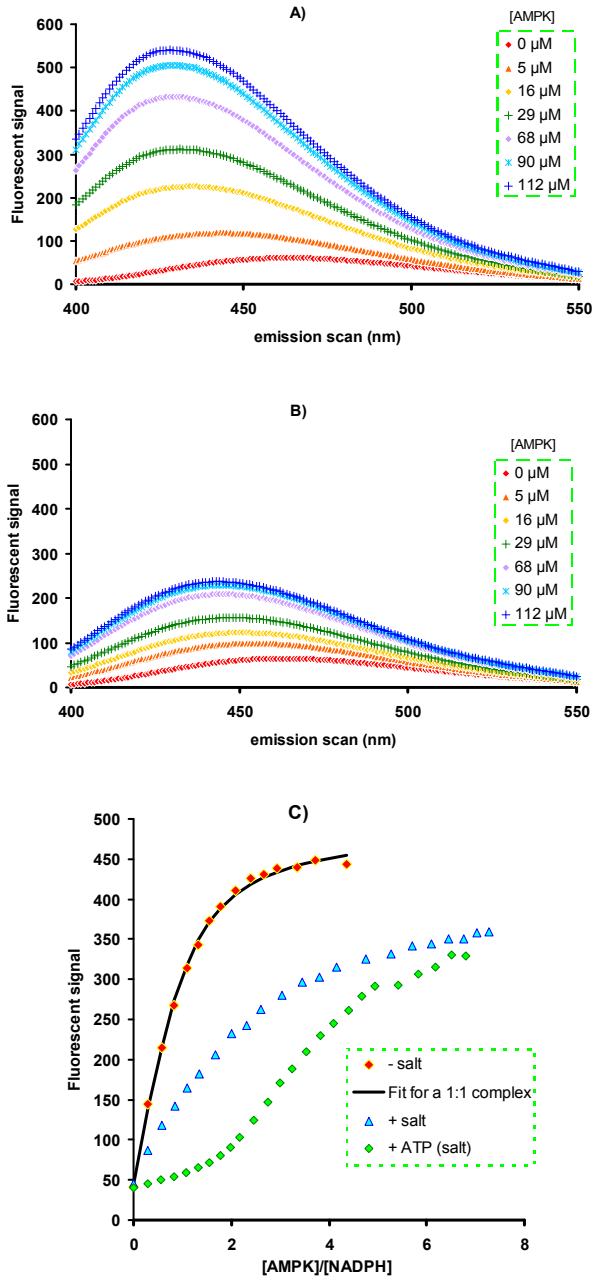

Figure 4.5: Fluorescence emission scans for the titration of NADPH (a) or NADH (b) with AMPK with an excitation wavelength of 340 nm. AMPK binding of NADPH produces a fluorescence signal change more than two-fold larger than that seen with NADH. (c) Titration of 10 µM NADPH with AMPK done at low ionic strength (red) and in 100 mM NaCl (blue); A representative competition experiment with ATP is shown in green. The solid line represents the best fit to the data for AMPK with a one-site model for NADPH. Evidently the one site model provides very good fit to the experimental data and as such there is no reason to fit the data to a two site model. This analysis does not, of course, preclude the possibility that there is a second, much weaker site, that is not significantly occupied under the experimental conditions.

A

Nucleotide	**Kd (µM)**
NADH (low salt)	7.4 ± 3.3
NADPH (low salt)	2.9 ± 0.3
NADH (100mM NaCl)	18.3 ± 2
NADPH (100mM NaCl)	19 ± 2.5

B

Nucleotide	Kd (µM)	
	Direct	Displacement
AMP	3.3 ± 0.6	2.2 ± 0.3
ADP	1.3 ± 0.2	0.8 ± 0.2
ATP	1.1 ±.0.2	1.3 ± 0.3

Table 4.1: Dissociation constants for the interaction of wild type AMPK with different NADH/NADPH (A) and AXPs (B) at the tighter site. AXP competition experiments were done in 100 mM NaCl.

NADPH and NADH bind to AMPK with similar affinities which are 5-20-fold weaker than those for AXPs. I also tested the binding of the non-fluorescent oxidized forms of the nucleotides NAD^+/$NADP^+$ in competition assays. Interestingly, NAD^+ and $NADP^+$ bind to AMPK much weakly than the reduced forms. The dissociation in 100 mM NaCl constants were estimated to be 156 ± 6.7 µM (NAD^+) and >1 mM ($NADP^+$) compared with 18.3 ± 2 µM and 19 ± 2.5 µM for the reduced forms under the same conditions.

The affinities of nucleotides can also be determined using displacement experiments (see **Appendix 1.2**). In this case a mixture of 30 µM of AMPK, 30 µM NADPH and 200 µM of AMP, ADP or ATP is titrated into a solution containing the same concentration of protein and NADPH but no AXP. With increasing concentration of AXP the NADPH is displaced from its binding site and the fluorescence signal decreases accordingly. The K_{ds} determined by displacement experiments are in good agreement with my previous competition experiments (**Table 4.1B**) (**Fig 4.6**).

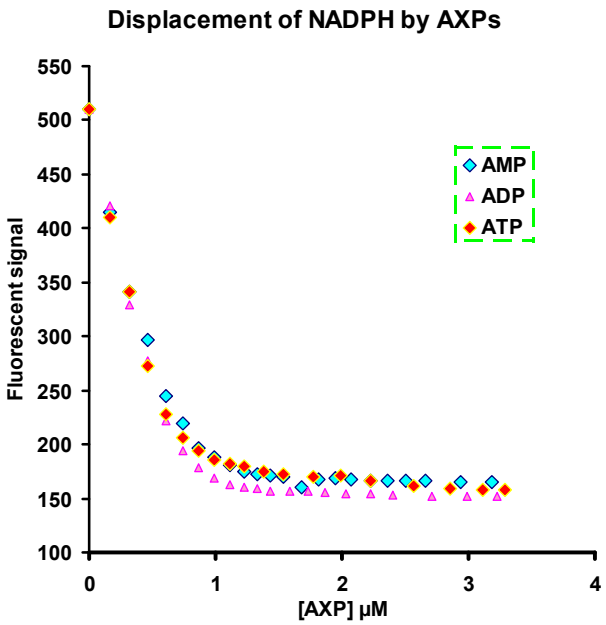

Figure 4.6: Displacement of NADPH by AXPs from AMPK. The concentration of AMPK and NADPH remained constant throughout the experiment (30 µM). Experiments were carried out using an excitation wavelength of 340 nm and the fluorescent signal at 440 nm was used to monitor the fraction of bound NADPH.

To test whether the affinities of AMPK for nucleotides change upon phosphorylation state of the enzyme, I carried out binding studies using phosphorylated full-length AMPK. Full-length AMPK was phosphorylated by incubation overnight with a constitutively active form of CaMKKβ. Constitutively active CaMKKβ is produced by expressing a truncated form of the protein missing its autoinhibitory domain. Consequently, AMPK is fully phosphorylated on Thr-172 with additional auto-phosphorylation sites. NADPH binds phosphorylated AMPK with a similar affinity to that of the un-phosphorylated form (K_d = 25 ± 3 µM). The competition and displacement experiments described above were used to determine K_d values for the binding of AXPs to the phosphorylated protein: 2.6 ± 2.1 µM for AMP, 2.5 ± 0.39 µM for ADP and 3.4 ± 2.1 µM for ATP. Thus, the affinity of AMPK for AXPs for phosphorylated protein remains essentially unchanged, compared to the un-phosphorylated form, at least for the site that is monitored by NADPH.

4.2.3 Mant-nucleotides

Having established the binding affinity of one of the two exchangeable sites, I carried out a series of experiments to determine the properties of the second site. The use of mant-labelled AMP or ATP was mainly used for this study. The structure of mant-nucleotides consists of an AXP molecule with a mant group linked to the ribose at either at the 2' or 3' position (**Fig 4.7**). The mant group gives the nucleotide fluorescent properties. One of the advantages of using this fluorophore is its relatively small size, which should minimize any perturbation of binding properties [231]. Although our crystal structure shows that there is an aspartic acid that interacts with the ribose moiety of the nucleotide in each of the three sites (γ-89, γ-244 and γ-316), it is evident from my co-crystallization structure of AMPK/mant-AMP that the modified AMP binds in much the same way as unmodified AMP (**section 3.2.4**).

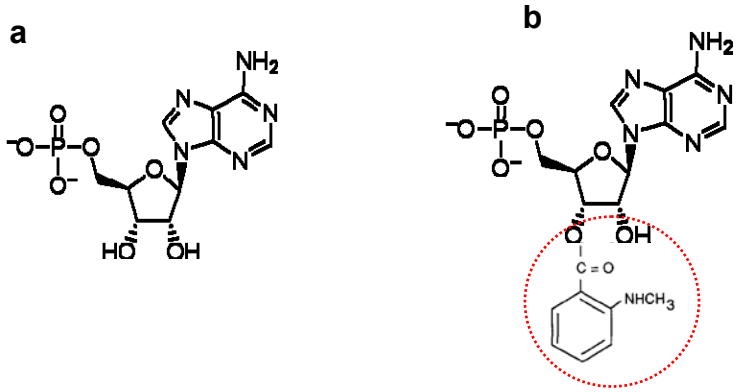

Figure 4.7: Comparison of the structures of AMP (a) and mant-AMP (b). The part that confers the fluorescence properties to the nucleotide is circled in red.

When excited at a wavelength of 380 nm, the uncomplexed mant-nucleotides have an emission maximum at 449 nm. In the presence of saturating AMPK the emission maximum is slightly blue-shifted to 441 nm and the fluorescence intensity is increased ca. 2-3 times (**Fig 4.8A**). Binding of mant-nucleotide was initially

monitored by titrating 10 µM solutions of mant-AMP or mant-ATP with AMPK in Tris buffer with and without 100 mM NaCl. Experiments performed at low ionic strength gave more definitive information on stoichiometry because of the higher affinity for the ligand under these conditions. The change in the fluorescence signal was largest at 438 nm and this wavelength was used to monitor binding. K_d values were calculated from the resulting curves (**Fig 4.8B**).

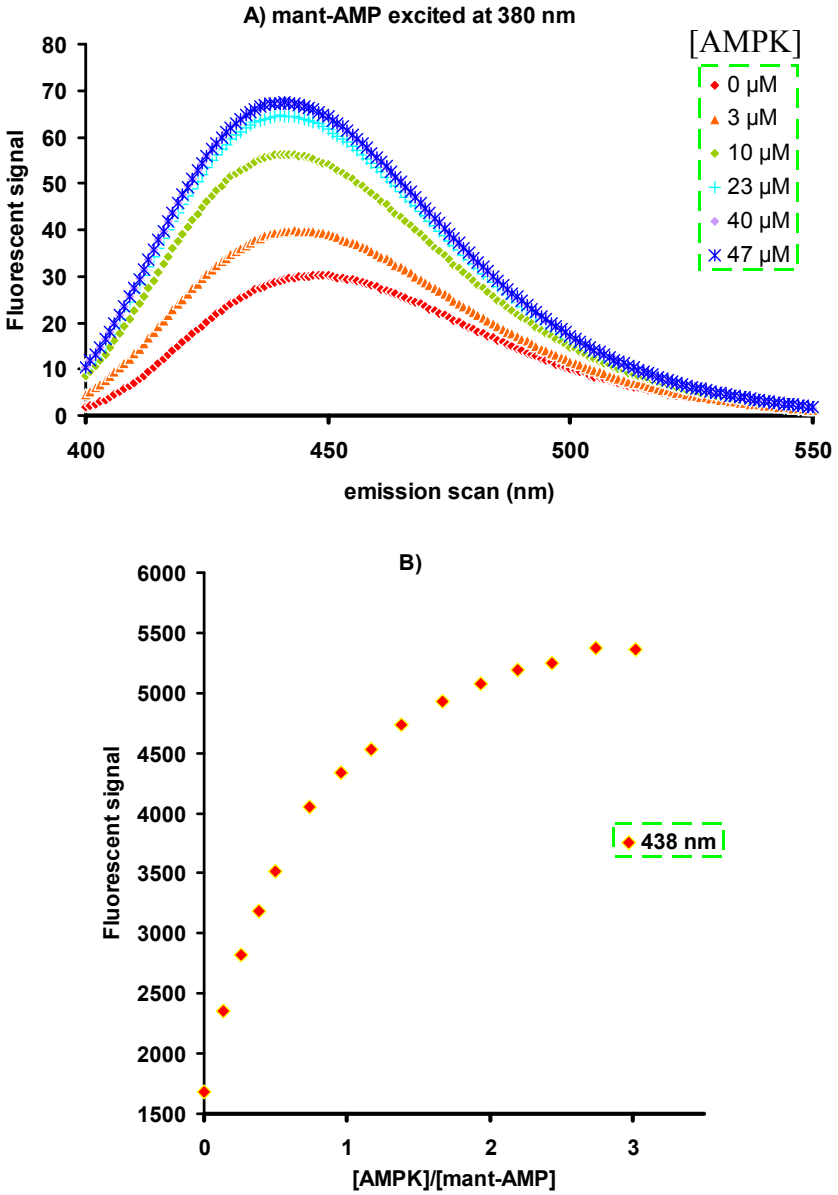

Figure 4.8: Fluorescence emission scan for a titration of mant-AMP with AMPK with an excitation wavelength of 380 nm (A). The 438 nm value from each curve was used to estimate the affinities for mant-AMP (B).

To confirm that the binding properties of the crystallized construct are similar to those of the full-length protein the two proteins were analyzed under the same conditions (**Fig 4.9**). These fluorescence titrations clearly indicate that AMPK binds two molecules of mant-nucleotide. The dissociation constants were determined using standard methods with the assumption that the two binding sites were non-interacting, both energetically (α=1) and spectroscopically. The analysis did not assume that the two sites were identical nor that binding at the two sites generates the same fluorescence change. Analysis shows that mant-AMP displays somewhat different binding at the two exchangeable sites of AMPK in 100 mM NaCl with estimated K_ds of 31 ± 8 μM and 52 ± 15 μM, respectively. In contrast, mant-ATP appears to have significantly different affinities for the two sites with K_ds of 5.8 ± 2 μM and 50 ± 12 μM. Because of the low affinity binding of mant-nucleotides for the weaker site, the resulting K_d values have large errors. The same experiments were carried out at low ionic strength (no added salt) and the affinities of mant-AMP for the two sites were 10.4 ± 3 μM and 10.8 ± 5 μM. The affinities of mant-ATP for the two sites under low salt conditions were again significantly different with K_ds of 0.7 ± 0.6 μM and 15.2 ± 5 μM. In contrast to the studies performed with NADPH, which monitors only one binding site, mant-nucleotides bind to two sites with different affinities. Unfortunately, this means that the binding constants for the unlabelled ligands are complicated to extract using either competition or displacement assays.

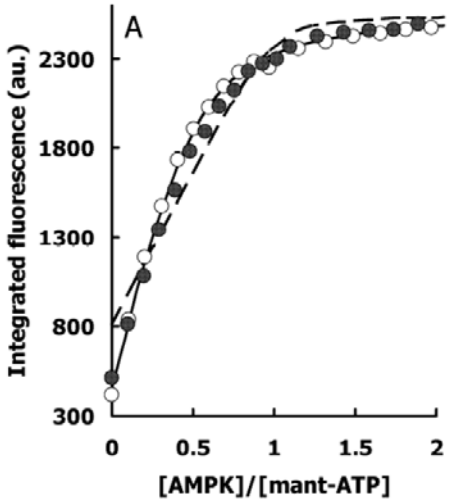

Figure 4.9: Titration of mant-AMP with AMPK at low ionic strength: full length (open circles) and truncated protein (closed circles). The dashed and solid lines represent the best fit for full length AMPK using one- and two-site binding models, respectively.

Fluorescence binding studies were also performed using FRET (Förster resonance energy transfer) based assays with mant-AMP as the reporter (see **Appendix 1.3**) [223-224]. The use of FRET provides an alternative method for estimating the K_d values for the two sites and has the added advantage of using much less protein for each experiment. In this approach, binding of nucleotides to AMPK was monitored by adding mant-AMP to a solution of AMPK, rather than *vice versa*. Salt concentration remained constant throughout the experiment at 100 mM. Fluorescence emission scans from 400 to 550 nm were recorded as described earlier except that the excitation wavelength was 290 nm to take advantage of energy transfer from AMPK's tryptophan residues to the mant group **(Fig 4.10A)**. Changes in fluorescence intensities at 440 nm were used to estimate K_d values (**Fig 4.10B**). The estimated affinities of mant-AMP for AMPK in the presence of 100 mM NaCl were 5.5 ± 3 μM and 10.5 ± 5 μM. Although the values for the two sites are similar, they are quite different from those determined using the alternative titration 'mode' (adding AMPK to mant-AMP). This is most likely to be associated with the

difficulty in extracting the molar fluorescence intensities from the previous data (see **section 4.2.1**).

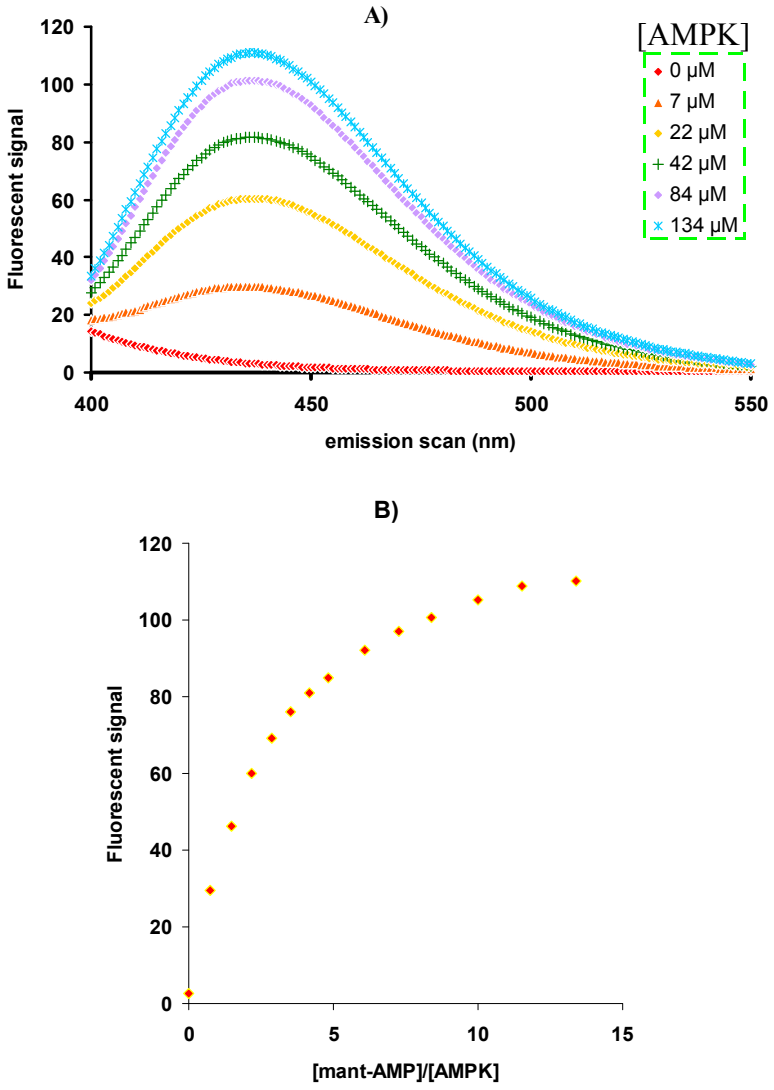

Figure 4.10: Fluorescence emission scans from 400 – 550 nm for the fluorescent titration of AMPK with mant-AMP performed using FRET. Experiments were carried out using an excitation wavelength of 290 nm (A). The 440 nm value from each curve was used to estimate the K_{ds} (B).

The FRET technique can also be applied with displacement or competition assays in order to estimate the binding constants for unlabelled nucleotides. In a typical experiment, 10 µM AMPK, 60 µM mant-AMP and 400 µM AMP, ADP or ATP were added to a solution containing 10 µM AMPK and 60 µM mant-AMP. Protein

and mant-AMP concentrations therefore remain constant throughout the experiment. The use of a large excess of mant-AMP ensures that the weaker site is also at least partially occupied and this will then be displaced when increasing amounts of AXP are added. Emission scans from 400 to 550 were performed as above **(Fig 4.11A)** and the decrease in fluorescence intensity at 440 nm was monitored.

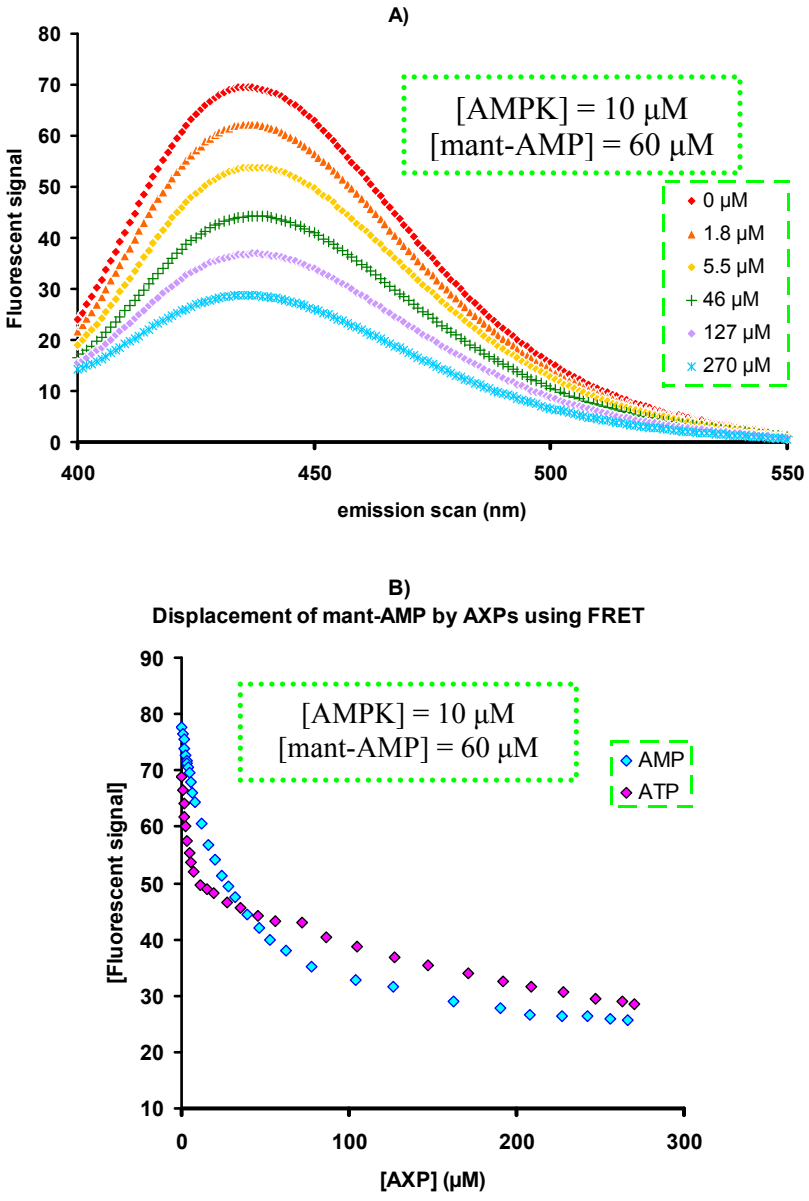

Figure 4.11: Fluorescence emission scan from 400 – 550 nm for a titration of mant-AMP/AMPK mixture with AXP. The concentrations of AMPK (10 µM) and mant-AMP (60 µM) remain constant throughout the titration. Experiments were carried out using an excitation wavelength of 290 nm (A). The 440 nm value from each curve was used to estimate the affinity of the nucleotides (B).

From the titration curve **(Fig 4.11B)** it can be seen that ATP binds more tightly than AMP to the high affinity site but somewhat more weakly than AMP to the low affinity site. Unfortunately, these displacement experiments with unlabelled nucleotides proved to be somewhat less informative than I had hoped. This is largely due to the uncertainty in the K_d values for the binding of mant-AMP to the two, particularly the weaker, sites (see above). Nonetheless, it is clear that the displacement of mant-AMP observed at low added [AXP] is consistent with AXP binding with low micromolar affinity to the higher affinity site, as also determined in the experiments with NADPH. The best that can be said about the binding of AXPs to the lower affinity site is that the K_d for AMP is probably in the range 20-40 μM and that the binding of ATP to this site is somewhat weaker, perhaps in the range 40-70 μM. What is particularly clear from these studies is that the mant-nucleotides (particularly mant-AMP) do not bind with the same affinity as the unlabelled nucleotides.

4.2.4 The magnesium effect on AMPK

Initially, in our lab the structure of AMPK with bound ATP was obtained by soaking crystals of AMPK/AMP with Mg^{2+}-free ATP. (EDTA was used as a Mg^{2+} chelator). The resulting structure showed the presence of Mg^{2+}-free ATP, as was also reported for the yeast homologue [113]. The fluorescence studies detailed below show that magnesium is not required for ATP binding by AMPK, but that both free-ATP and Mg^{2+}-ATP bind to AMPK with similar affinity. Only titrations of mant-ATP at very high Mg^{2+} concentrations (1.25, 2.5, 5 and 10 mM) somewhat reduced the affinity of the protein for the nucleotide (**Fig 4.12**). However, this effect may not be physiologically relevant because the cellular concentration of free-Mg^{2+} may be as low as 0.4mM [232]. In the presence of as much as 125 μM of the metal ion, the fluorescence titration is similar to the one observed in the absence of Mg^{2+}. This concentration of the metal ion would virtually saturate the ATP present in the binding assay (K_d around 10-50μM) [232]. These results agree with earlier studies on ATP binding to AMPK which concluded that the affinity of the enzyme for ATP is

independent of magnesium [16]. Further soaking experiments of AMPK/AMP crystals in Mg^{2+}-ATP were performed and the new electron density maps showed, in addition to the non-exchangeable AMP, the presence of two Mg^{2+}-ATP molecules in the same nucleotide binding sites where previously there were Mg^{2+}-free ATP or AMP. The structures of AMPK in complex with Mg^{2+}-ATP and the one with free-ATP are very similar and thus confirm that ATP binding to AMPK is magnesium-independent. The metal ion does not interact directly with the protein, but with the β- and γ-phosphates of the nucleotide.

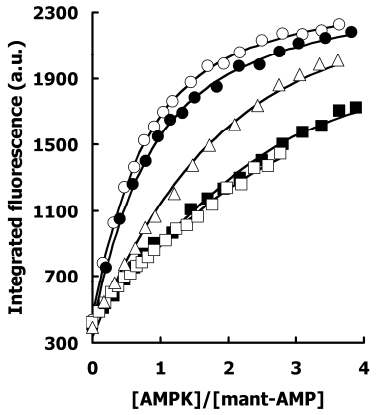

Figure 4.12: Titration of AMPK with 10 μM mantAMP with in the presence of 0 mM(open circles), 0.125 mM (closed circles), 1.25 mM (triangles), 2.5 mM (squares), 5 mM (diamonds), and 10 mM $MgCl_2$ (closed squares).

4.2.5 AMPK mutations which cause Wolff-Parkinson-White syndrome (WPW)

Fluorescence spectroscopy was also used to study naturally occurring AMPK mutations which cause WPW, a glycogen storage cardiomyopathy [186] (see **section 1.1.5.2**). It is assumed that these mutations interfere with normal activation of the enzyme by affecting the protein's affinity for regulatory nucleotides [232]. These mutations are found in the γ-subunit, mainly close to the nucleotide binding sites.

The mutations I have studied are Arg69Gln, His150Arg and Arg298Gly. These mutants were selected because they are the most common and the most widely studied. Our previous wild type AMPK structure [213] shows that these mutations are situated close to the nucleotide binding pockets and that these mutated residues interact with the phosphate groups of AMP or ATP (**Fig 4.13**). See **section 3.2.5** for the crystal structures of these mutants.

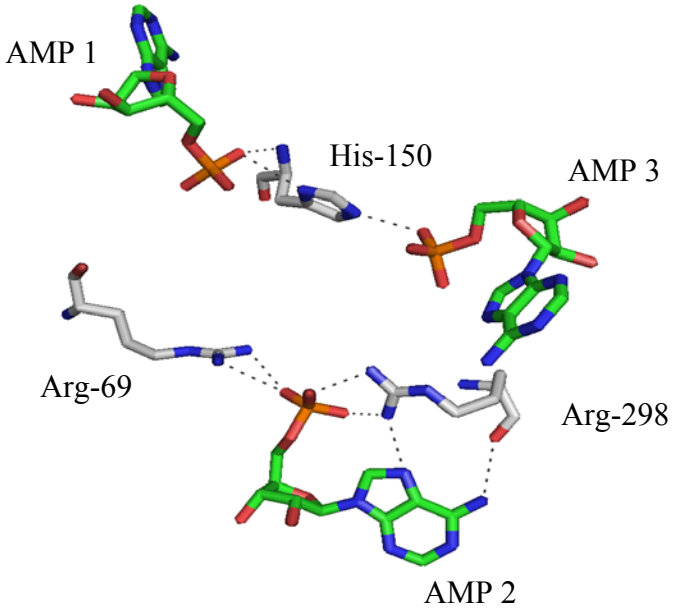

Figure 4.13: Interactions between AMP molecules and three of the basic residues which, if mutated, cause a glycogen storage cadiomyopathy.

After I made the relevant constructs, I expressed and purified the proteins with which I carried out the fluorescent binding studies. The first experiment looked at NADPH binding to the mutants. NADPH binds to Arg69Gln, His150Arg and Arg298Gly in 100 mM NaCl with estimated dissociation constants of 53 ± 6 μM, 27 ± 4 μM and 31 ± 4 μM, respectively, compared to 19 μM for wild type (see **Table 4.1**, **pag81**). Competition experiments carried out with NADPH as a reporter show that AMP, ADP and ATP have dissociation constants for the NADPH-monitored site of 7.3 ± 2.1 μM, 3.1 ± 1.0 μM and 5.2 ± 1.1 μM for the Arg69Gln mutant. The dissociation constants of AMP, ADP and ATP for His150Arg are 2.1 ± 0.4 μM, 0.9 ± 0.3 μM and 1.1 ± 0.2 μM and those for Arg298Gly are 7.5 ± 0.8 μM, 2.2 ± 0.3 μM

and 1.6 ± 0.2 μM (**Table 4.2**). Somewhat surprisingly perhaps, AXPs still bind to this site with similar affinities as the wild-type.

	AMP	ADP	ATP
wt	3.3 ± 0.6	1.3 ± 0.2	1.1 ±.0.2
R69Q	7.3 ± 2.1	3.1 ± 1.0	5.2 ± 1.1
H150R	2.1 ± 0.4	0.9 ± 0.3	1.1 ± 0.2
R298G	7.5 ± 0.8	2.2 ± 0.3	1.6 ± 0.2

Table 4.2: Kd values for the interaction of nucleotides with site-1 of wild type and mutated AMPK. The truncated construct was used for these experiments. All the units are in μM.

Measurements on WPW mutants were also performed with mant-AMP in order to address the question of the stoichiometry of binding. Titrations of mant-AMP with AMPK showed that all three mutants (Arg69Gln, His150Arg and Arg298Gly) bind two molecules of mant-AMP. Measurements using FRET based assays gave similar results (**Fig 4.14A** and **Table 4.3**).

The affinity of mant-AMP for the strong site appears to be significantly weakened for His150Arg and Arg298Gly. This observation is apparently different to the results obtained with NADPH for the effect of these mutations on the affinities for AXPs (see above). Of course it must be remembered that the effect on the binding of an AXP may be different from the effect on the fluorescently labeled analogue. It appears that the mutations also affect the affinity of mant-AMP for the weaker site, with two-fold, eight-fold and eleven-fold reduced affinity for Arg69Gln, His150Arg and Arg298Gly, respectively.

Displacement experiments of mant-AMP by AMP and ATP with mutant AMPKs display behavior similar to that observed with the wild type and it appears that ATP binds more tightly than AMP to the high affinity site but somewhat more weakly than AMP to the low affinity site (**Fig 4.14B**). As mentioned above, K_d values for unlabelled nucleotides cannot be accurately calculated from these experiments.

Nonetheless, they are consistent with K_ds in the low micromolar range for the tighter site and tens of micromolar for the weaker site.

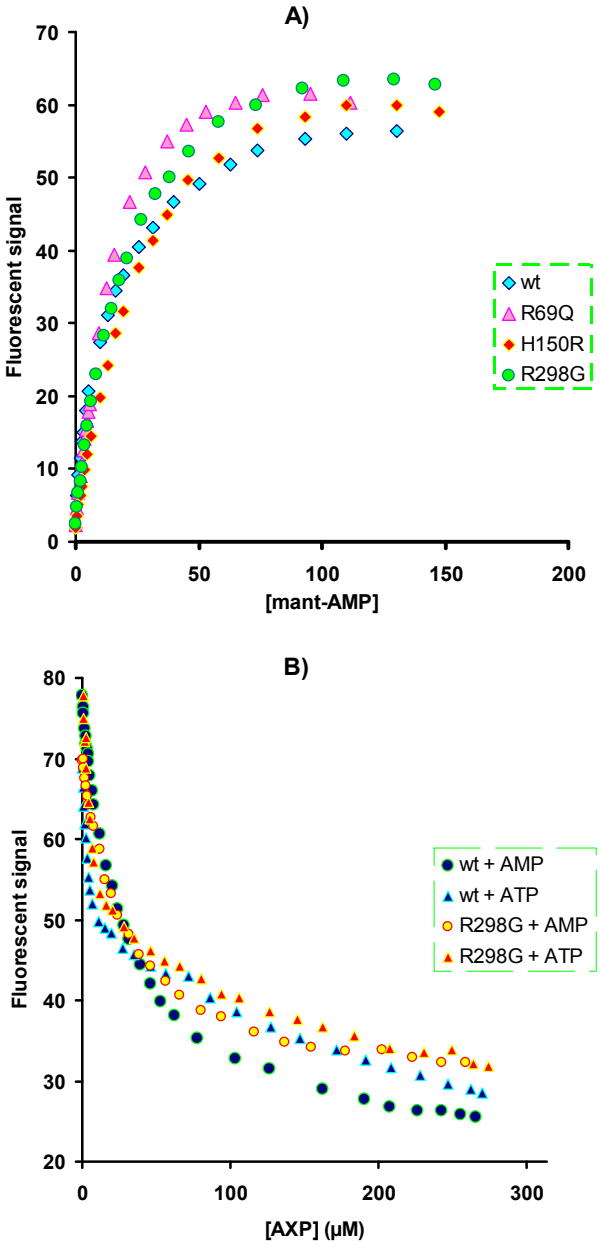

Figure 4.14: Fluorescence titrations of mant-AMP with AMPK using an excitation wavelength of 290 nm. (A) In the direct experiment increasing concentrations of mant-AMP were added to a solution of AMPK (10 µM). (B) Displacement of (60 µM) mant-AMP by AMP and ATP in wild type and mutated AMPKs (10 µM). Only data for the Arg298Gly mutant only is shown in the figure. The 440 nm value from each curve was used to estimate the affinity of mant-AMP.

	mant-AMP
wt	5.5 ± 1.3 & 10.5 ± 2.2
R69Q	2.5 ± 0.6 & 21.8 ± 3.5
H150R	15 ± 6 & 86 ± 21
R298G	9.2 ± 2.4 & 119 ± 24

Table 4.3: Kd values for the interaction of wild type and mutated AMPK with mant-AMP in the tighter and weaker sites. All the units are in μM.

The fluorescence binding studies with the two fluorescence reporters (NADPH and mant-AMP) agree to the extent that the two exchangeable nucleotide binding sites have different affinities for AXPs. Within the same binding site, AMP, ADP and ATP bind with similar affinity. The WPW mutants seem to have a reduced affinity for AMP in both exchangeable sites, but especially in the weaker site. Therefore nucleotides do bind but the preferential binding of ATP relative to AMP in both sites and the reduced affinity of AMP for the weak site will eventually help to explain the phenotype of WPW syndrome (see **section 5.8**).

4.2.6 Phosphopeptide

Under cellular homeostasis the concentration of Mg^{2+}-ATP is around 2-5mM. AMP and ADP, which are largely magnesium-free because they bind magnesium with lower affinity, are around 2-5 μM and 200-500 μM, respectively [232]. Given the binding constants described above, the γ-subunit of AMPK would be mostly bound to Mg^{2+}-ATP and the majority of the enzyme would therefore be inactive; only a tiny proportion of AMPK (<<1%) would be in the AMP-bound form. When cells are subject to stresses, such as physical exercise, there is a small rise in AMP levels [87]. It is thought that AMP concentrations increase by perhaps 2-3-fold at most. This increase in AMP would cause a similar fold increase in the AMP-bound form of the kinase. When the enzyme is AMP-bound there is an increase in the amount of phosphorylation at Thr-172 of the α-subunit [38], probably due to reduced rates of

dephosphorylation [232]. Phosphorylation of Thr-172, which is within the activation loop of the kinase domain, activates AMPK. At present, the mechanism of propagating signals from ATP/AMP binding at the regulatory γ subunit to the kinase domain is unclear. Given that the nucleotide binding sites on the γ subunit are markedly basic, it occurred to me that the phosphorylated activation loop of the kinase might, under some circumstances, interact with it. In order to test this idea, a phosphopeptide of 20 residues (NMMSDGEFLR**T**$_{(P)}$SCGSPNYAA) from the activation loop of the kinase domain was studied using the crystallized construct. The peptide has a phosphothreonine at the position corresponding to the physiological phosphorylation site at Thr-172. Titrations of labeled nucleotides (either mant-AMP or NADPH) with AMPK were essentially identical in the presence and absence of this phosphopeptide (**Fig 4.15**). This was the case even when the peptide concentration was as high as 1 mM, suggesting that the phosphopeptide does not bind at the nucleotide binding sites in the γ subunit. The recent crystal structure from our lab of an AMPK construct that includes the kinase domain shows that the phosphorylated Threonine forms a strong interaction with the kinase domain that orders the otherwise disordered activation loop. In the light of this result, and given what is known about the effects of phosphorylation of kinase activation loops of this sort of kinase, the idea behind my peptide experiment seems naïve in retrospect.

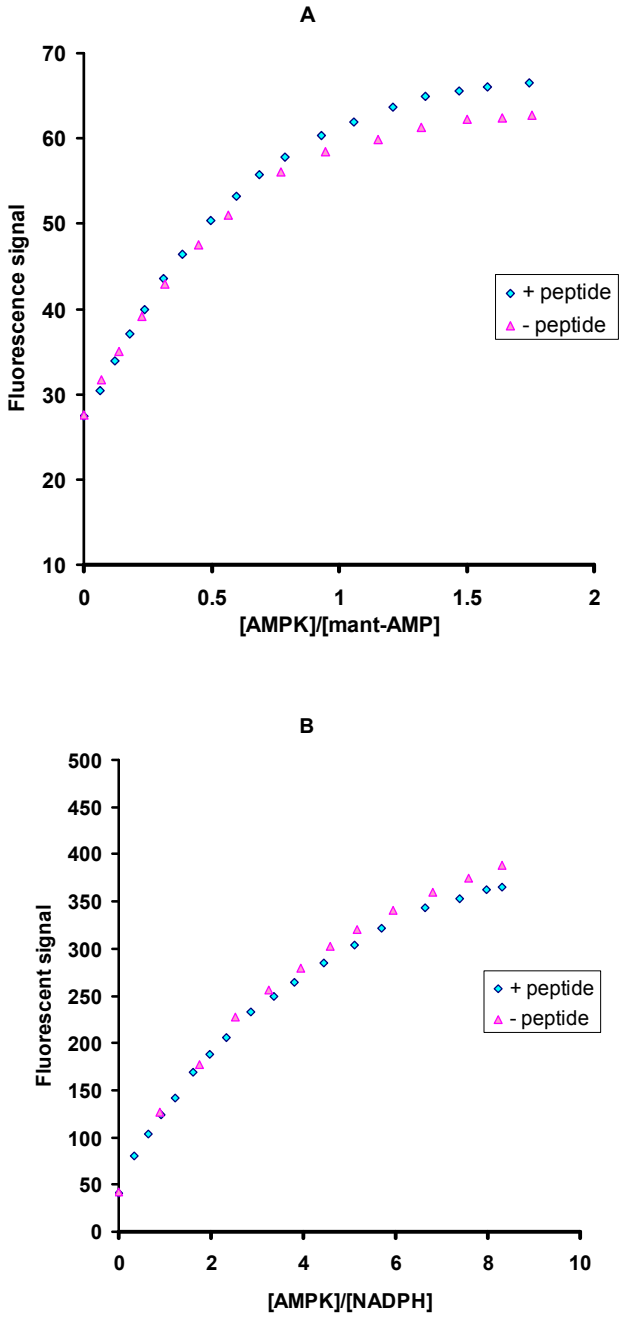

Figure 4.15: Fluorescence titrations of mantAMP (A) and NADPH (B) with AMPK in the presence and absence of the phosphopeptide. Each point represents the 438 nm value from the emission scan. There is no competition detectable at either of the exchangeable binding sites.

4.2.7 Binding characterization of C05-1 and ZMP compounds

In the next section of this chapter I will describe how I identified a novel small molecule compound that binds to AMPK – C05-1 (see **section 4.3.4**). Fluorescence studies were also undertaken to provide insight into how C05-1 might interact with AMPK. Titration experiments with AMPK and mant-AMP both in the presence of 50 μM C05-1 did not work because the fluorescence signal was variable and unstable, probably due to aggregation caused by the compound. Titrations of AMPK with NADPH in the presence and absence of C05-1 were essentially identical (**Fig 4.16**) and suggest therefore that C05-1 does not compete with AXP binding at the tighter site.

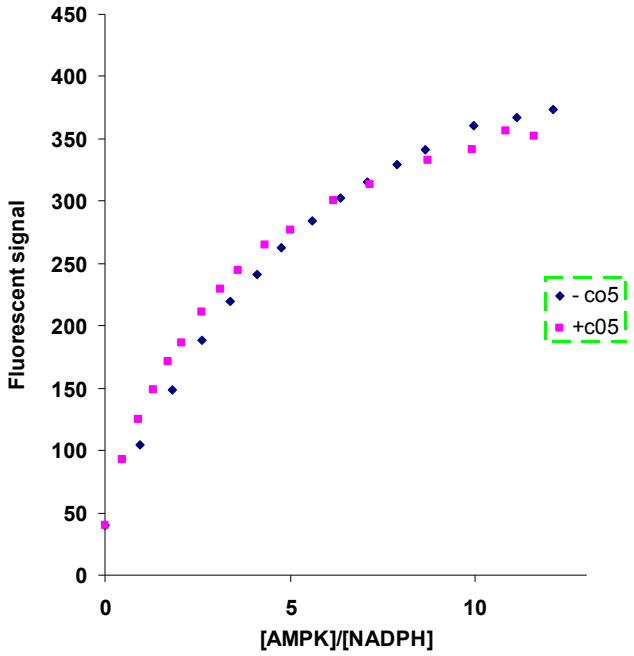

Figure 4.16: Titration of NADPH with AMPK in the presence and absence of C05-1.

ZMP has been a valuable tool to investigate AMPK regulation as it mimics the effects of AMP (i.e. allosteric activation and reduced dephosphorylation) (see **section 1.3.2**) (**Fig 3.6**). However, this compound is not completely specific for AMPK, as ZMP interacts with other AMP-sensitive enzymes. Titration experiments with ZMP in competition assays with NADPH, which monitors the tighter of the two

exchangeable sites, suggest a K_d of 18 ± 1.2 µM (**Fig 4.17).** Interestingly, the affinity of this activator is therefore about five-fold weaker than that of AMP for site-1. Displacement experiments with mant-AMP were performed in an attempt to assess the affinity of ZMP for site-2. However, binding of ZMP at this site is evidently very weak and a K_d value could not be determined, suggesting that the affinity is weaker than 200-300 µM. The low affinity of ZMP for AMPK compared with that of AMP limits the physiological utility of this compound as a drug. It remains however a useful tool for biochemical studies. See **section 3.2.3** for the crystal structure of AMPK in complex with ZMP.

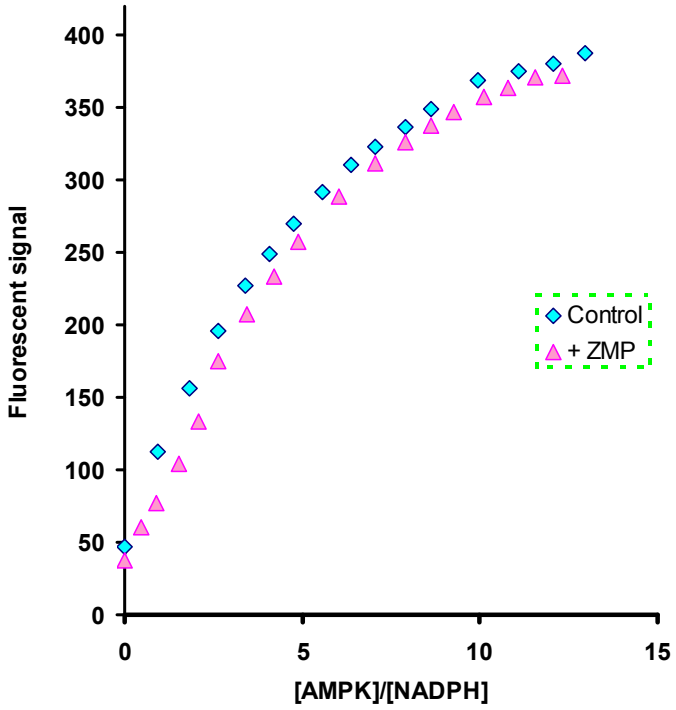

Figure 4.17: Titration of NADPH with AMPK in the presence and absence of ZMP. ZMP shows a significantly reduced affinity compared with AXPs.

4.3 Thermal stability shift measurements

4.3.1 Overview

This section describes how I tested a list of compounds, selected from an *in silico* screen, carried out by our colleagues at MRCT, for binding to the regulatory subunit of AMPK. Fluorimetry is a time-consuming technique that requires larges amount of highly concentrated protein for each experiment, therefore it would not have been practical to test >400 compounds with a fluorimeter. In contrast, thermally induced unfolding is a technique that requires small quantities of protein per experiment. This technique can be useful for the study of protein stability, and since the stability of a protein is altered when ligands bind, such studies can be used to screen for novel ligands [233]**.** Therefore I monitored AMPK unfolding by detecting the increase in turbidity as the protein aggregates following unfolding at high temperatures. It is not ideal to monitor turbidity but given that it is what happens on heating a protein sample I did not have any choice. Solution turbidity can be monitored at sufficiently high wavelength to avoid interference in the measurements from nucleotide/compound absorption. The binding of these ligands is compared to the natural ligands, AMP & ATP and a known AMPK activator, A-769662.

The shape of the thermal unfolding curve for AMPK is sigmoidal (**Fig 4.18**). The absorbance remains unchanged until the sample reaches the temperature at which the protein starts to unfold (~51 ºC for AMPK). The turbidity then increases and eventually reaches a plateau when most of the protein present has unfolded and precipitated. The midpoint of the curve is used as a reference point for comparing the stability of different protein samples because, when a protein is rendered more stable, there is a shift of the curve to the right (i.e. to a higher temperature) and the T_m value is increased (See **Appendix 2.1**).

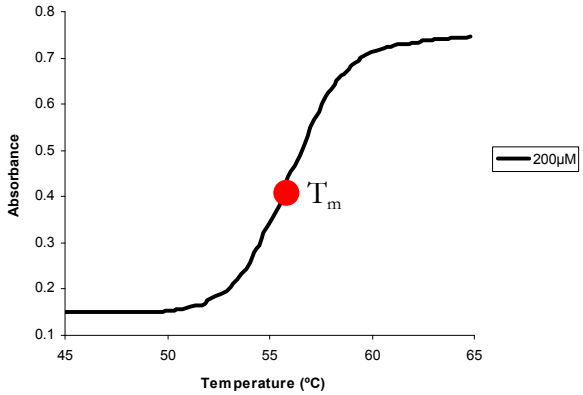

Figure 4.18: Typical sigmoidal curve for the thermal unfolding of AMPK. The midpoint is indicated in red.

4.3.2 Natural ligand stabilization

Thermal denaturation was measured at different AMP and ATP concentrations (25 µM, 50 µM, 100 µM, 200 µM, 400 µM, 800 µM, 1.7 mM and 4.5 mM). The results show that ATP and AMP stabilize the AMPK to a similar extent, confirming that these nucleotides bind to AMPK with similar affinities (**Fig 4.19**). At higher nucleotide concentrations, there is a larger the shift of the midpoint of the unfolding curve (**Table 4.4**). The average T_m of the unliganded AMPK is 53.1ºC, but this value can increase up to 62ºC with 4.5 mM AMP. The affinity of ligands at the melting point can be estimated if the unfolding constant is known, but this K_d is very different from the one at room temperature, as binding affinities of ligands for proteins get substantially weaker with increasing temperatures (see **Appendix 2.2**).

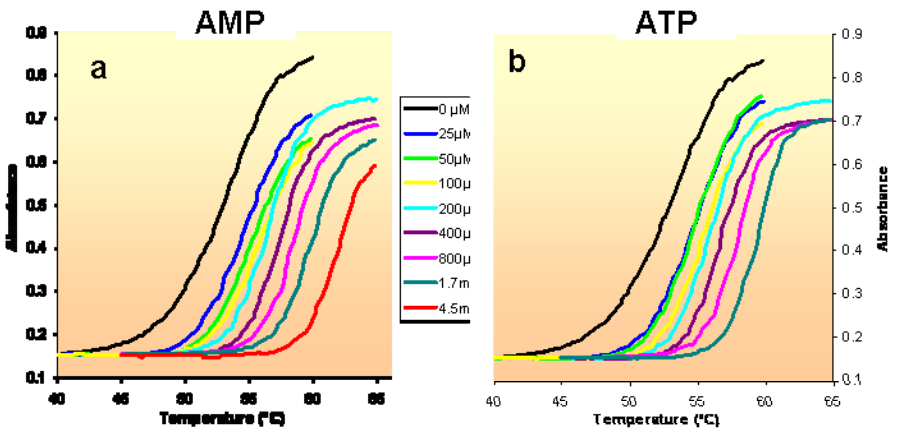

Figure 4.19: Thermal shift assay result for truncated AMPK in the presence of AMP (a) and ATP (b). The control curve (protein sample without nucleotide) is in black. A significant shift in the curves to the right is observed as nucleotides are added to the protein sample. The higher the ligand concentration, the bigger the shift of the curve. The protein sample with 4.5 mM ATP (not shown) is unstable and precipitates before the control sample.

	T_m (°C)	
Concentration (mM)	AMP	ATP
0	53.1	53.1
0.025	54.8	55.2
0.05	55.7	55.6
0.1	56.1	56
0.2	56.6	56.2
0.4	57.4	57.1
0.8	58.8	58.2
1.7	60.6	60.2
4.5	62	ND

Table 4.4: Midpoint temperatures of the protein-unfolding transition (T_m) for AMPK in the presence of nucleotides.

4.3.3 Drug-induced stabilization

The stabilizing effect of the activator drug A-769662 was also examined at different concentrations (125 µM, 250 µM, 370 µM and 490 µM) (**Fig 4.20**). The behavior was similar to that observed with AMP and ATP (**Table 4.5**). Interestingly, the drug

stabilizes AMPK to a smaller extent than nucleotides since 250 µM A-769662 produces approximately the same shift as that induced by 50 µM AMP. It is difficult to interpret why AMP and A-769662 stabilize AMPK so differently, because the melting point of a protein is influenced by many factors such as the affinity for the ligand and the number of binding sites. At time of writing, the specific binding site for A-769662 has not been published. It is possible that A-769662 binds in one or more sites other than the nucleotide binding sites given its generally hydrophobic nature.

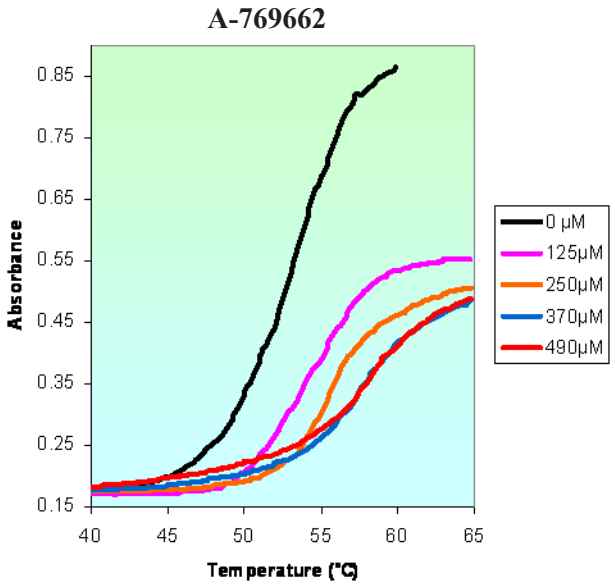

Figure 4.20: Stability measurement of AMPK in the presence of A-769662 compound. The control curve is indicated in black.

Concentration (µM)	T_m (°C)
0	53.1
125	54.8
250	55.7
370	56.1
490	56.6

Table 4.5: Midpoint temperatures of the unfolding curve (Tm) of AMPK in the presence of varying concentrations of A-769662.

4.3.4 Discovery of a new binding compound: C05-1

Once the crystal structure of the trimeric complex used for these stability assays was solved in our laboratory, our collaborators at MRCT used the atomic coordinates of the nucleotide-binding sites of AMPK in a virtual screen to identify potential ligands. More than 2 million compounds were analyzed in the virtual screen and this resulted in a good drug docking-site score for 413 compounds. The compounds thus identified from the virtual screen were bought in to be assessed with our thermal stability assay. To minimize experimental time and the amount of the protein used, compounds were screened in pools of four. The concentration of each of the four compounds in the assay was 50 μM. Because the compounds were dissolved in 100% DMSO the control was an AMPK sample with the same final DMSO concentration. When a mixture of four compounds gave a T_m shift of >1˚C relative to the control each of the four compounds was assayed individually.

Among these 413 compounds I discovered one (C05-1) that produced a significant shift in the unfolding curve to a higher temperature. 50 μM of this compound give a T_m value of 56.7˚C, which is significantly above the average T_m of the other compounds [53.2 (± 0.3)˚C] (**Fig 4.21**). This ligand is more effective in stabilizing AMPK than AMP as concentrations as low as 50 μM gives a T_m shift comparable to that produced by ~ 210 μM AMP, meaning that C05-1 could be binding stronger than AXPs. However, this compound does not appear to bind in the exchangeable binding sites, as monitored by fluorescence binding assays (**section 4.2.7**). Also, our collaborators tested whether C05-1 mimics the effects of AMP (i.e. allosteric activation and reduced dephosphorylation) but neither of the two effects was detected (**Matt Sanders, personal communication**). In conclusion, the novel C05-1 compound is going to be employed for co-crystallization trials with the full-length protein, for which no structure is yet available. Hopefully the stabilizing properties of the compound will facilitate crystallization trials.

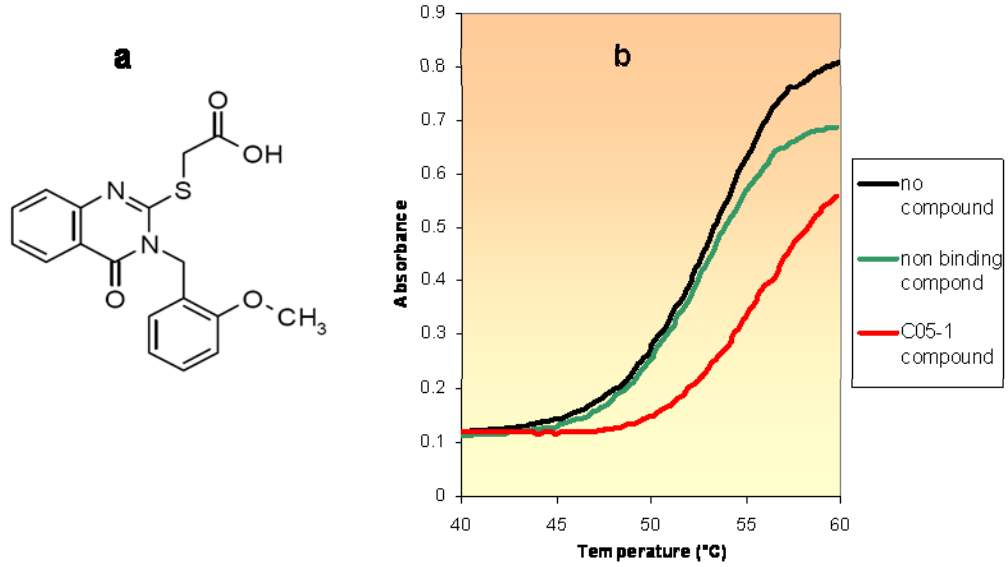

Figure 4.21: Structure and effect of C05-1. (a) Chemical structure of C05-1. (b) Thermal shift assay results for AMPK in the absence, and presence of tested compounds. The control curve is in black. Compound concentration is 50 µM. The green line represents an average curve for the 412 non-binding compounds. The 53.2˚C T_m value for this curve does not differ significantly from that of the control (53.1˚C). C05-1 compound (red) instead seems to stabilize the protein and causes a positive shift of 3.5˚C.

DISCUSSION

5. Discussion

5.1 Overview

The aim of my thesis was to characterize, through structural and binding studies, the mechanism of regulatory nucleotide binding to mammalian AMPK. The crystal structure of truncated AMPK shows how the heterotrimeric complex is formed and that there are three nucleotides binding sites on the γ regulatory subunit. I used mant-AMP as a fluorescent reporter to determine, by competition experiments, the affinity of AMP & ATP for the two exchangeable ones. HPLC experiments explained the observation of three bound AMPs in the crystal structure because the third site is non-exchangeable. Crystal soaking experiments with ATP helped to assign site-1 & site-2 as the exchangeable binding sites and site-3 as the non-exchangeable AMP site. Interestingly, I also discovered that NADH and NADPH bind to one of the two exchangeable sites. Given its intrinsic fluorescent properties I used it as a reporter for further binding studies.

The reason why a pseudo-symmetric 'fourth site' in γ remains empty in mammalian AMPK is discussed and compared to the structure of a yeast homologue of AMPK, SNF-like protein. I carried out further structural and binding studies on AMPK with the activator ZMP to better understand why it binds with reduced affinity to AMPK, and thus its poor potency compared to physiological ligands such as AMP. Crystal structures and binding affinities for nucleotides were determined for three naturally occurring AMPK mutants. Arg-69→Gln, His-150→Arg and Arg-298→Gly, represent three of the most common mutations that appear in Wolff-Parkinson-White syndrome. I suggest that the phenotype of this disease arises because the binding of nucleotides to site-2 is diminished.

5.2 The AMP binding site

The ability of AMPK to monitor cellular energy status comes from its capacity to competitively bind adenyl-containing nucleotides (AXPs) at its regulatory γ subunit [16]. The γ subunit of AMPK is made up of two Bateman domains, each being composed of a pair of CBS motifs [16-17]. A CBS motif is a conserved domain of about 60 amino acids. The crystal structure of truncated AMPK shows how each one of the four CBS motifs consists of a conserved α1-β2-β3-α4 pattern in an anti-parallel arrangement [213] (**Fig 5.1**). The packing of these four pseudo-symmetric motifs generates four potential adenyl binding sites. Interestingly, in the truncated wild type AMPK structure only three of these sites are seen to bind AXPs bind. One nucleotide binds between CBS 1-2 (site-1) and two nucleotides between CBS 3-4 (site-2 and site-3) (**Fig 5.1**). Each of the three nucleotides sits in a partially basic pocket formed at the interface between a pair of CBS domains (**Fig 5.2 A&B**). Between CBS 1-2 there is a potential fourth nucleotide binding site, but in mammalian AMPK no nucleotide has been observed at this site (discussed in more detail in **section 5.6**).

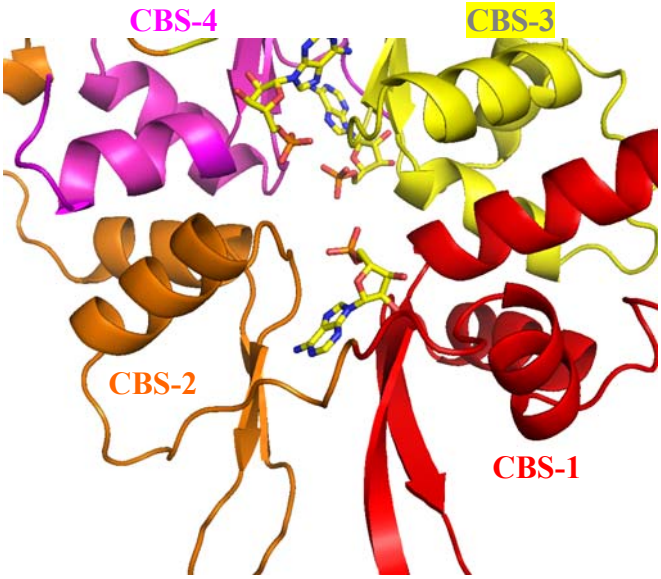

Figure 5.1: Ribbon representation of AMPK in complex with three AMP molecules. A face-on view of Bateman 1 is shown. CBS 1-2 (Bateman 1) are colored in red and orange, whereas CBS 3-4 (Bateman 2) are in yellow and magenta, respectively.

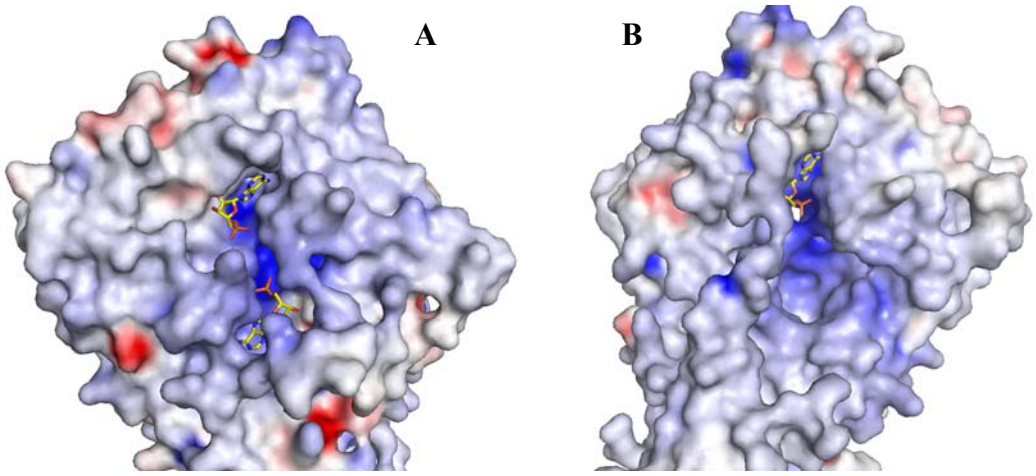

Figure 5.2: Surface representation of AMPK in complex with three AMP molecules. (A) Face-on view with site-1 and site-3; (B) View after rotating the molecule 180˚ around vertical axis showing site-2. The surface is colored according to the electrostatic potential [blue, positive (contour level +30.0 K_bT / e_c); red, negative (-30.0 K_bT / e_c)]. AMP molecules are in stick representation with carbon atoms in yellow.

Bateman domains occur in over a thousand other known proteins such as metabolic enzymes, kinases, and membrane channels and are responsible, in some of these cases, for binding adenosine-containing ligands such as AMP, ATP or SAM between a pair of CBS motifs [16,21]. What makes AMPK apparently unique is that although AXPs bind at the interface of two CBS motifs within a Bateman domain, there are additional interactions of the nucleotides with amino acids from the distal Bateman domain; for example, AMP-2 interacts with residues predominantly from CBS3-4, but also with Arg-69 and Lys-169 (which belong to CBS-1 and -2, respectively); AMP-3 interacts with residues from CBS3-4 but also with His150 (CBS-2) (**Fig 5.3**).

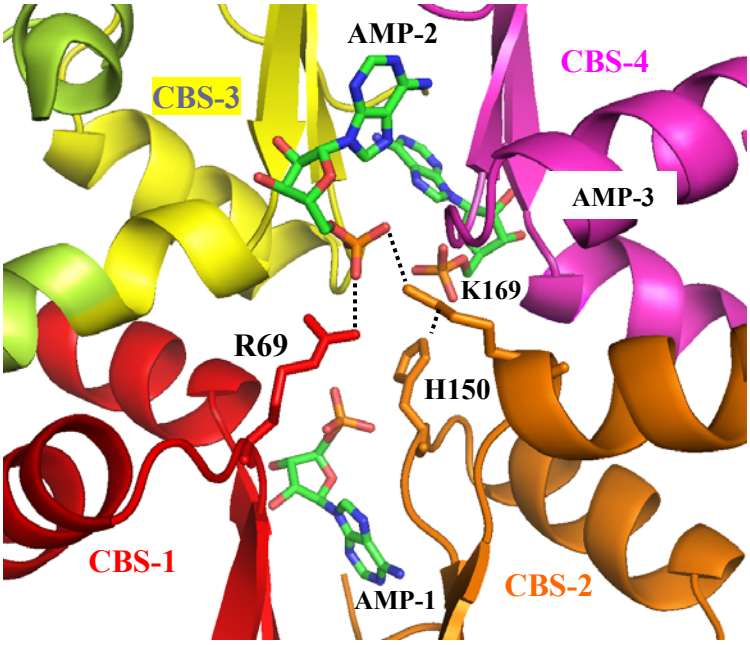

Figure 5.3: Ribbon representation of AMPK in complex with three AMP molecules. CBS 1-2 (Bateman 1) are colored in red and orange, whereas CBS 3-4 (Bateman 2) are in yellow and magenta, respectively. AMP molecules are in stick representation with carbon atoms in green.

5.3 Characterizing the three binding sites

Binding studies using a fluorescent-labelled analogue of AMP, mant-AMP, gave a stoichiometry of 2:1 (nucleotide/protein). The finding that the crystal structure contains three bound AMP molecules is rationalized by bound-nucleotide studies which show that AMPK contains one permanently bound AMP moiety (see **section 4.1**). Competition assays, using mant-AMP as a reporter, demonstrate that AMP, ADP and ATP can all bind at the two exchangeable nucleotide binding sites.

Initially, I assumed that both exchangeable sites had equal affinities, but with more experiments and re-examination of the original data I realized that the two exchangeable sites have significantly different affinities for nucleotides. I was able to determine the affinity of mant-AMP and AXPs for the stronger of the two sites

reasonably accurately, but somewhat less so for the weaker site. This is explained in more detail in **section 4.2.3** but, in brief, in a system where a fluorescent reporter binds to two sites with different affinities, the consequent fluorescent signal is mainly due to the contribution from the high affinity site and less information can be extracted for the weaker site. The K_d of AMP and ATP for the tight site of wild type AMPK are in the range 1-3 μM. In contrast, the affinities of AMP and ATP at the weaker site are in the range of 20-40 μM and 40-70 μM, respectively. The difference in affinities between the two sites suggests that it is likely that the tight site is responsible for the enzyme's sensitivity to cellular AMP changes and therefore important for regulating kinase activity.

The complementary use of structural and binding studies enabled the identification of the non-exchangeable site and the likely assignment of the tight and weak exchangeable sites. Crystal soaking experiments using either ATP, or ZMP, suggest that site-3 is non-exchangeable whereas site-1 & -2 can bind nucleotides other than AMP (**Fig 5.4**). Although not a quantitative measure of binding affinity, site-1 consistently shows stronger electron density for bound nucleotide ligands than site-2. One has to be very cautious when correlating occupancy of binding sites in a crystal with binding affinities in solution, but the best guess would be that site-1 is the tight site and site-2 the weak site. Additional reasons for these assignments are discussed in **section 5.8**.

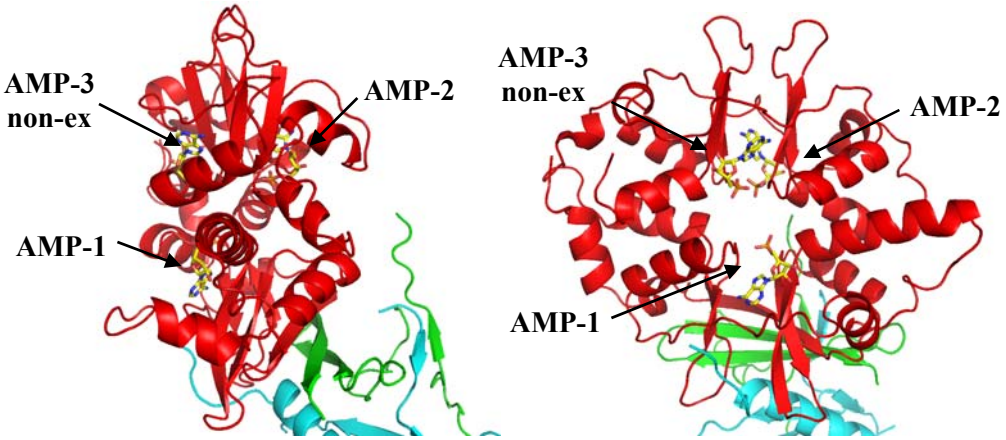

Figure 5.4: Ribbon representation of the crystallized complex with three bound AMPs in two orthogonal views. The α, β and γ subunits are colored in cyan, green and red, respectively.

5.3.1 Specificity of mant-AMP for AMPK

The availability of fluorescent-labelled nucleotides opens up a very useful way of measuring binding of unlabelled nucleotides by competition experiments. However, the generation of fluorescently labelled nucleotides often involves the introduction of an additional hydrophobic group. This new substituent may lead to additional, adventitious, interactions with the protein that do not occur with unlabelled nucleotides. For example, the julolidine derivative of ATP shows an increase in fluorescence signal upon addition to myosin subfragment-1, but this effect is not reversed upon addition of ATP, indicating that it binds to sites other than the active site [221]. Mant-nucleotides have been shown to bind specifically to proteins such as ATPases and GTPases [221]. However, mant-AMP has not previously been used in the study of nucleotide binding to AMPK.

In order to confirm, and visualize, how mant-AMP binds at the exchangeable nucleotide binding sites of AMPK, I solved the crystal structure of AMPK in complex with mant-AMP by soaking crystals with 0.5 mM mant-AMP overnight. The structure shows mant-AMP moieties bound at site-1 & site-2, while the third non-exchangeable site remains occupied by AMP (**Fig 3.9A**). In the AMPK/AMP

complex, the ribose of AMPs makes a bidentate interaction between the 2' and 3' hydroxyl groups of the nucleotide with the negatively charged side chain of an aspartate residue. In the AMPK/mant-AMP complex, the mant-group, which is linked via the ribose, does not significantly alter the binding of the adenyl moiety even though one of the hydrogen bonds between the aspartate and the ribose is lost (**Fig 5.5**). The mant moiety extends away from the adenyl binding pocket onto the surface of γ. In site-1, the mant group hydrogen bonds with the side chain of Asn-92 and makes hydrophobic contacts with Tyr-120, Leu-121, Gln-122 and Lys-126. In site-2, the mant moiety makes hydrophobic interactions with Phe-243, Arg-268, Ser-269, His-270 and Tyr-271 (**Fig 5.5**) (see **details in 3.2.4**).

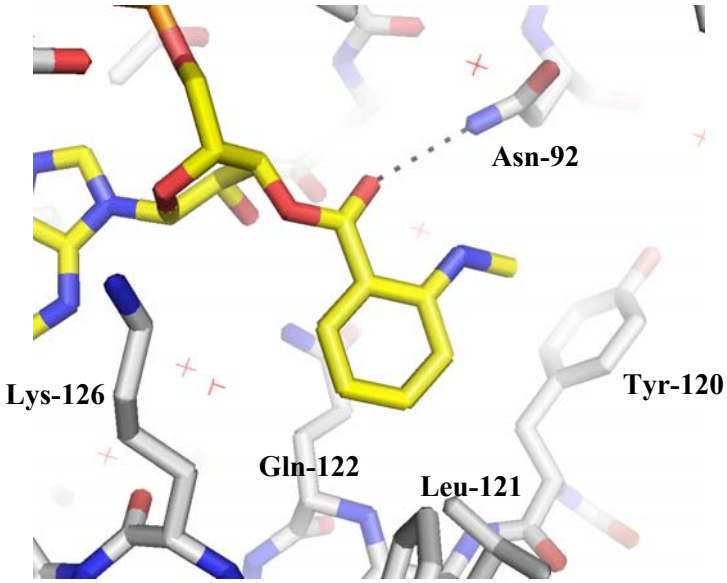

Figure 5.5: Atomic model of mant moiety. The binding pocket shown is site-1. Carbon atoms of AMPK and of the mant-AMP are in grey and yellow sticks, respectively.

5.4 Cooperativity

Cooperativity refers to the enhanced binding of a ligand to a protein due to the prior binding of the same ligand at another site. The best known example of a multimer displaying cooperative binding is the binding of four oxygen molecules to

haemoglobin. It is composed of four separate globin chains ($\alpha_2\beta_2$), each capable of carrying one molecule of oxygen. On the other hand, an example of proven cooperativity within a single polypeptide chain is calmodulin. The crystal structure of calmodulin resembles a dumbbell with two globular domains separated by a central helix and each one of these domains contains two Ca^{2+}-binding sites [234]. Positive cooperativity for calcium binding to calmodulin takes place within each globular domain, whereas cooperativity is not observed between the globular domains.

The cooperativity factor, α, is commonly used as a measure of the cooperativity displayed by a system. If $\alpha > 1$ there is positive co-operativity between ligands binding at different sites; if $\alpha < 1$ then there is negative co-operativity. The value of α depends on the free energy change for binding at a site when the other is occupied. α can only be properly calculated in cases where one has two identical sites, which is unlikely to be the case in systems other than those containing multiple subunits, e.g. haemoglobin. The Hill equation is also used as a measure of cooperativity in systems in where multiple ligand molecules bind to a protein. The Hill equation provides a useful means of assessing cooperativity but it has clear limitations. For example, the equation can provide evidence for positive cooperativity; however, it can not be used to definitely show negative cooperativity or non-cooperative binding without also knowing the relative affinities of the different sites on the protein for the ligand. In addition, the Hill equation can not provide accurate measurements of the K_d values for the interaction of a nucleotide at any site on the protein, or a quantitative assessment of the level of cooperativity (i.e. it is not obvious how to convert the Hill constant to α). The Hill equation can be useful for determining whether there is positive cooperativity in systems where two or more molecules of one type bind to a single target. The limitations in the Hill equation analysis result from the primary assumption that intermediate complexes with AXP bound only to one site do not exist. Clearly, this is not the case for AMPK.

A previous study by Scott *et al* [16] has suggested that AMP binding to AMPK is cooperative. In my binding studies, the data can readily be fitted assuming that there is no cooperativity between the two exchangeable sites. The difference in interpretation between my work and that described previously could be due to the use of significantly different constructs. Scott *et al.* used a full-length γ subunit, or part of it, with a GST tag. My construct does not have a GST-tag but is a complex of the three subunits. The hydrophobic interaction between the carboxyl terminal of the β subunit and the γ subunit seems to be important for the stable association of the subunits and the ability of the complex to remain monodisperse. However, to investigate the potential impact of cooperativity on AMP binding to AMPK, a cooperativity parameter was added to the fitting equation I used. A simulation of this binding model is shown graphically in **Fig 5.6** and in **Table 5.1**.

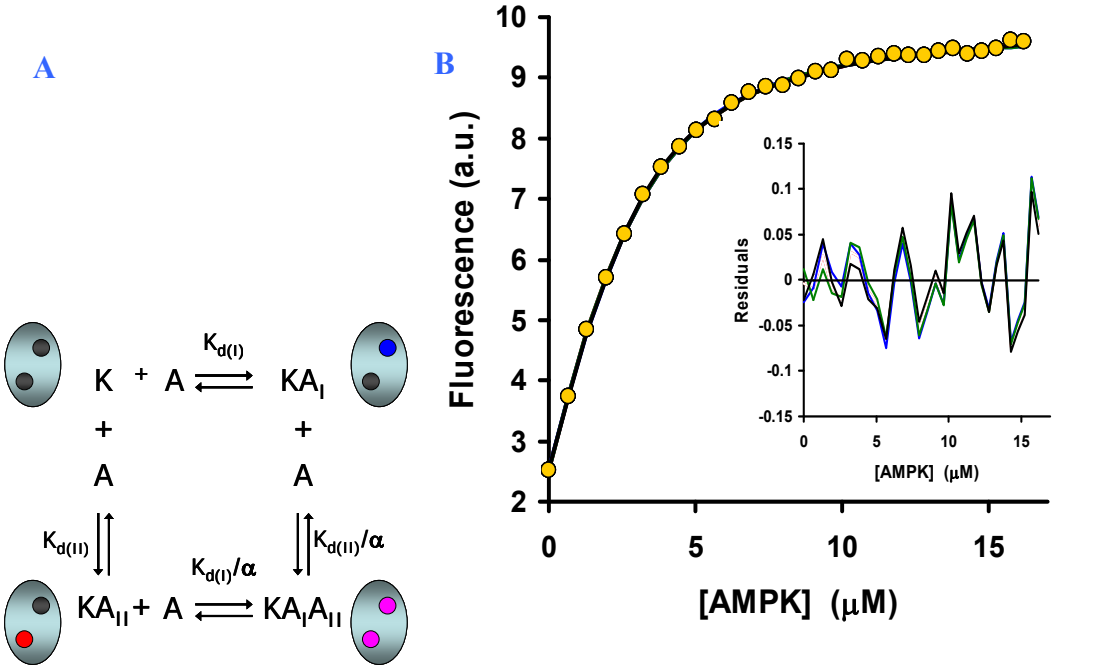

Figure 5.6: (A) Schematic representation of two nucleotides binding to AMPK: where K = kinase; A = AMP; In (B), $K_{d(I)}$ and $K_{d(II)}$ (affinity of AMP for site I & II) are simulated to be 1 μM & 5 μM, respectively; the fluorescence derived from site I & II is identical ($F_{(I)}=F_{(II)}$ therefore $F_{(I)}/F_{(II)}=1$ and $F_{(I,\,II)}= F_{(I)}+F_{(II)}$). The black line is the best fit for a 2:1 non-cooperative complex (α =1). Two other lines (green & blue) represent the fit for a cooperative complex (α =0.5 & α =5, respectively) and are completely overlapping. The residual plot demonstrate that the curves with or without including an α term fit just as well, although the K_d values change (**Table 5.1**).

F(II)/F(I)	α	K_d/(I) (μM)	K_d/(II) (μM)	χ^2
1	1	0.91	5.7	1.09
1	5.0	0.81	32.5	1.09
1	0.4	1.15	1.5	1.12
2	1	1.18	11.2	1.07
0.5	1	0.73	3.1	1.16

Table 5.1: Insertion of cooperativity as an additional fitting parameter: if α = 5 then the affinity of AMP for site I & II become respectively 0.8 μM and 32.5 μM; if α = 0.4 (negative cooperativity) then the affinity of AMP for site I & II become respectively 1.1 μM and 1.5 μM. In fits where a new parameter is added, the chi^2 (χ^2) should change if the term is meaningful. In simulations both with and without a cooperativity factor the chi^2 remains unchanged suggesting that there is no mathematical justification to adding this term as an additional parameter in the fitting equation.

What the simulations demonstrate is that the only effect of including a positive cooperativity term is to make the binding constant for the weaker site lower than it otherwise appears. It does not improve the quality of the fit. As far as I can understand, my interpretations of AMPK regulation do not change whether I assume a weak-binding second site or a very weak binding second site that becomes tighter upon prior occupation of the tighter site.

Cooperativity can only be properly determined in a binding assay where the degree of saturation ([bound ligand]/[total protein] can be determined as a function of free ligand concentration [234]. This can be done with techniques such as equilibrium dialysis or by radioactive-labelled nucleotides in a filter-based binding assay [235]. I did not have the facility to handle radioactive-labelled nucleotides and so I did not investigate this issue [16]. It is not easy to understand structurally, in the case of AMPK, how the addition of a negative charge from the phosphate of a nucleotide can help the binding of another negatively charged phosphate relatively close by. In

the final analysis my studies do not disprove positive cooperativity, but my data can be fit perfectly well without it.

5.5 Potential role of NAD(P)H as a down-regulator of AMPK

The non-equivalence of the two exchangeable binding sites is also evident from the fact that NAD(P)H binds to one of them but not the other. NADH/NAD^+ and NADPH/$NADP^+$ are essential cofactors in a range of biological processes, including the regulation of cellular energy metabolism [236]. None of these species have been considered to be involved in AMPK regulation as they do not allosterically activate the enzyme. However, my fluorescent titrations show that NADPH has an affinity of about 19 μM for AMPK, whereas the oxidized form, $NADP^+$, binds much weaker with a K_d of over 1 mM. My experiments show that both NADPH and NADH compete with AMP, ADP and ATP for binding to one of the two exchangeable sites on AMPK. Competition experiments with NADPH suggest K_d values around 1-3 μM for AXPs, in good agreement with the data obtained for the tighter of the two sites by mant-AMP. The fact that NADPH monitors AXPs binding at low micromolar affinity suggests that the cofactor binds to the higher affinity exchangeable site. As mentioned above (**section 5.3**), in the context of the truncated construct, I cautiously attribute the higher affinity binding to site-1 (**Fig 5.7**).

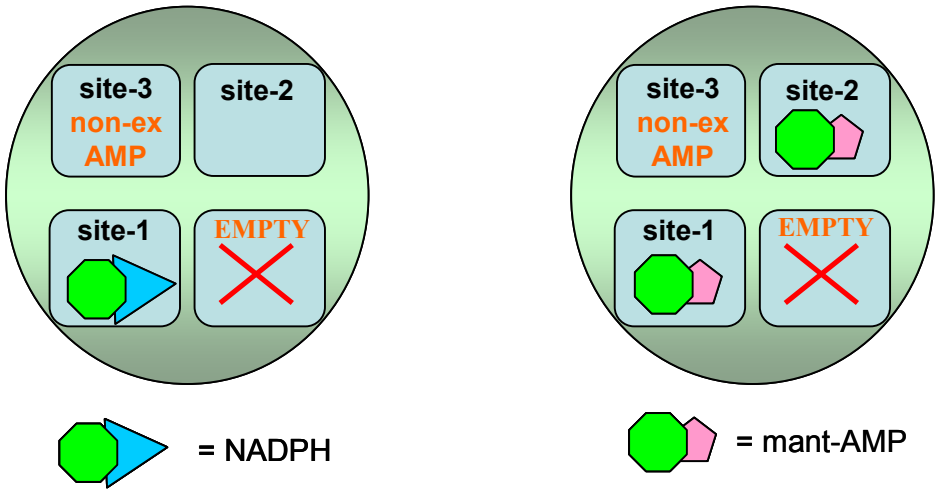

Figure 5.7: Schematic representation of the binding mode of NADPH and mant-AMP. NADPH binds to the tighter of the two exchangeable sites whereas mant-AMP binds to both.

In order to confirm that NADPH binds at site-1 of AMPK I carried out a series of soaking and co-crystallization experiments. Co-crystallization trials were unsuccessful as the resulting 2.6Å structure resulted in a map with poor density near the nucleotide binding sites that could not be interpreted. It is possible that the cofactor oxidized during the course of my crystal soaking experiments. However, from very recent crystallization work carried out in the lab by other workers, it seems that one NADH molecule binds to site-1 of the truncated mammalian AMPK construct (**Richard Heath, personal communication**). While I am disappointed that I did not achieve this result, it is gratifying to see that it supports my general conclusions.

This NADH/AMPK complex also offers a molecular explanation of why the protein binds the reduced, but not oxidized, forms. The nicotine group of NADH interacts with four basic residues (Arg-69, Lys-169, His-297 and Arg-298) (**Richard Heath, personal communication**), suggesting that there would be considerable electrostatic repulsion with the positively charged oxidized form of the cofactor.

As well as ATP, NADPH and NADH represent biochemical energy reserves. The large difference in affinity between the reduced and oxidized form of NADPH and NADH suggests that the binding of these nucleotides could be physiologically relevant. I propose that NADPH and NADH, like ATP, are physiological competitors for AMP binding to AMPK, and act to down-regulate AMPK by reducing its allosteric activation and its phosphorylation level. Therefore in the cell, in homeostasis, AMPK is mostly bound to ATP, NADPH or NADH, competing out AMP binding to the two exchangeable sites (**Fig 5.8**). Under these conditions the enzyme is more likely to be de-phosphorylated. When the cell is subject to metabolic stress, ATP is converted into ADP & AMP and NADPH and NADH are oxidized to $NADP^+$ and NAD^+. Thus, a higher proportion of the enzyme will be bound to AMP and in turn it will be more active. Thus, my suggestion is that AMPK may be down-regulated by ATP, NADH or NADPH but up-regulated by AMP.

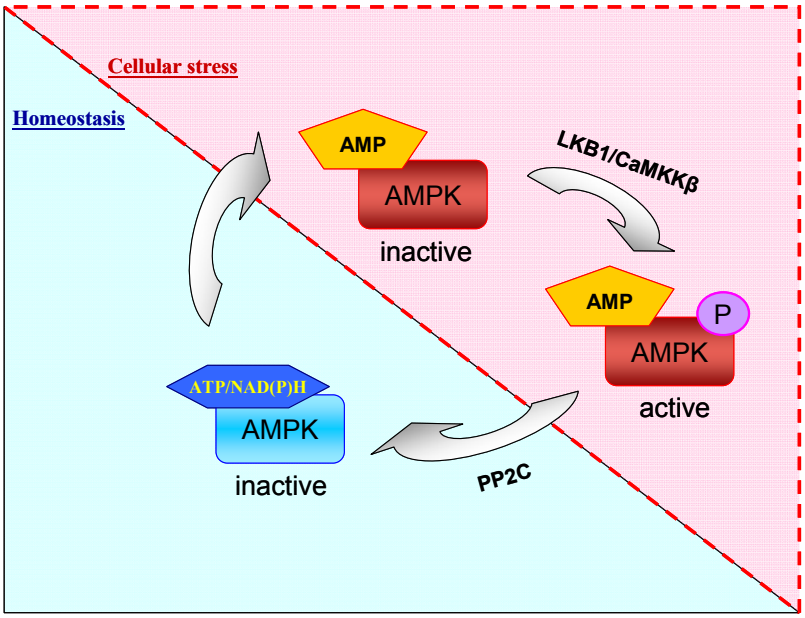

Figure 5.8: Diagram representing AMPK during energy homeostasis and during cellular stress. In homeostasis AMP levels are low; therefore AMPK is in the ATP-bound or NAD(P)H-bound state. In this state AMPK is kept de-phosphorylated by phosphatases (PP2C/PPM) and is therefore largely inactive. Cellular stress increase AMP concentration which competes off ATP and NAD(P)H binding to the γ subunit of AMPK. When upstream kinases (LKB1 and CaMKKβ) phosphorylate AMPK at Thr 172, AMP protects the activation loop from dephosphorylation and AMPK retains more activity.

5.6 The empty 'fourth' site

The approximate symmetry relating the four CBS motifs of AMPK generates four basic pockets. In mammalian AMPK, three of these pockets are occupied by nucleotides, whereas the fourth remains empty. The crystal structure of the AMPK homologue from *S. Pombe*, suggest that site-3 can bind either AMP or ATP (PDB coords: 200X, 200Y; [113]). A later publication by the same group involved soaking ADP into these crystals which then showed ADP bound in site-4 and either AMP or ATP in site-3 (2QRC; 2QRD [237]). Inspection of the mammalian AMPK structure suggests that nucleotides do not bind at site-4 because there is no aspartate from the γ subunit which can form a bi-dentate hydrogen bond with the 2' and 3' hydroxyl groups of the ribose (as there is for the other three sites). Interestingly, in the SNF-like protein, an aspartate from the β subunit, Asp-250, interacts with the ribose

of ADP-4. This aspartate residue is conserved across species and is the equivalent of Asp-226 in the β subunit of the mammalian structure (**Fig 5.9A**). The super-position of the two structures suggests that nucleotides could, theoretically, bind in site-4 of mammalian AMPK (**Fig 5.9B & 5.10**). However, in our AMPK structure, the loop from β-223 to β-232 is disordered in all the complexes we have looked at. Moreover, my binding studies on AMPK always show two, and not three, exchangeable sites. Since I do not have access to detailed binding data for SNF-like protein, it is difficult to know whether this 'fourth' site is really occupied in solution or if it is the result of soaking a crystal in very high concentrations of ligand.

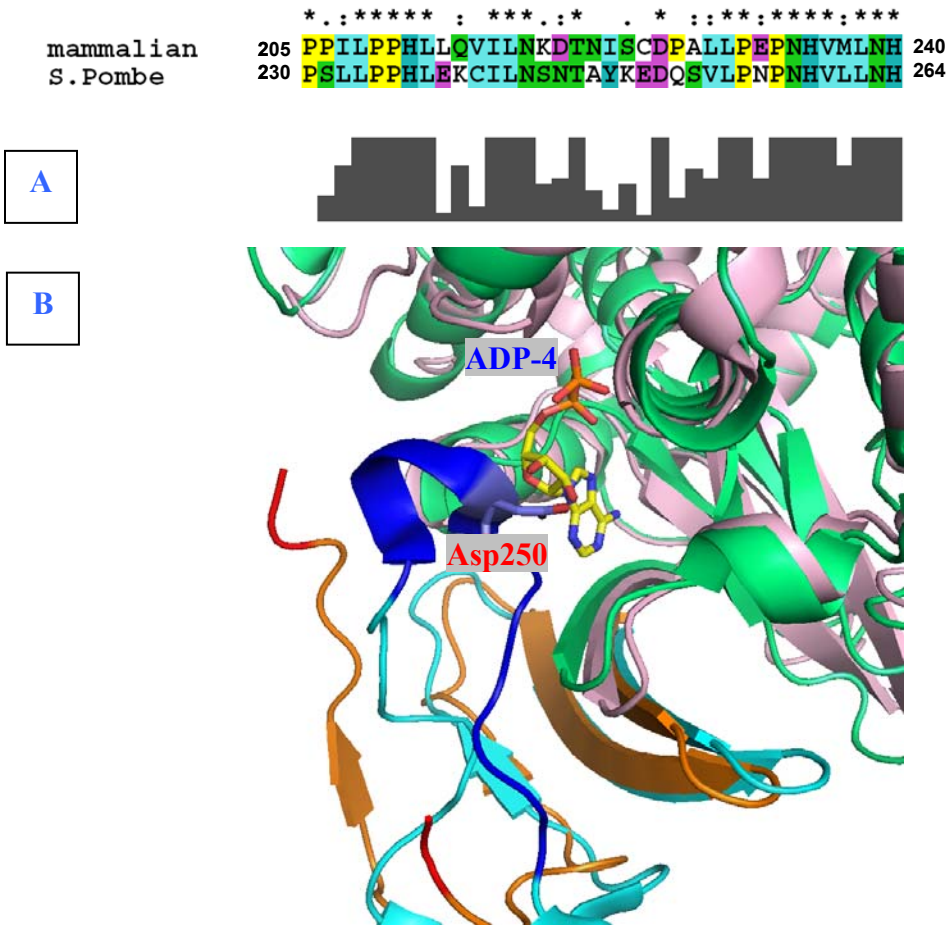

Figure 5.9: (A) Sequence alignment (Clustlax) of a fragment of β subunit of mammalian AMPK with SNF-like protein (*S. Pombe*) which, in yeast, appears to interact with nucleotides at site-4. (B) Superposition of mammalian AMPK with SNF-like protein. The γ subunits of AMPK and SNF-like are in green and pink, respectively. The β subunit of AMPK is in orange with the two edges of the missing loops in red. The β subunit of SNF-like is in cyan with the equivalent loop in blue. The ADP is in sticks with carbon atoms in yellow.

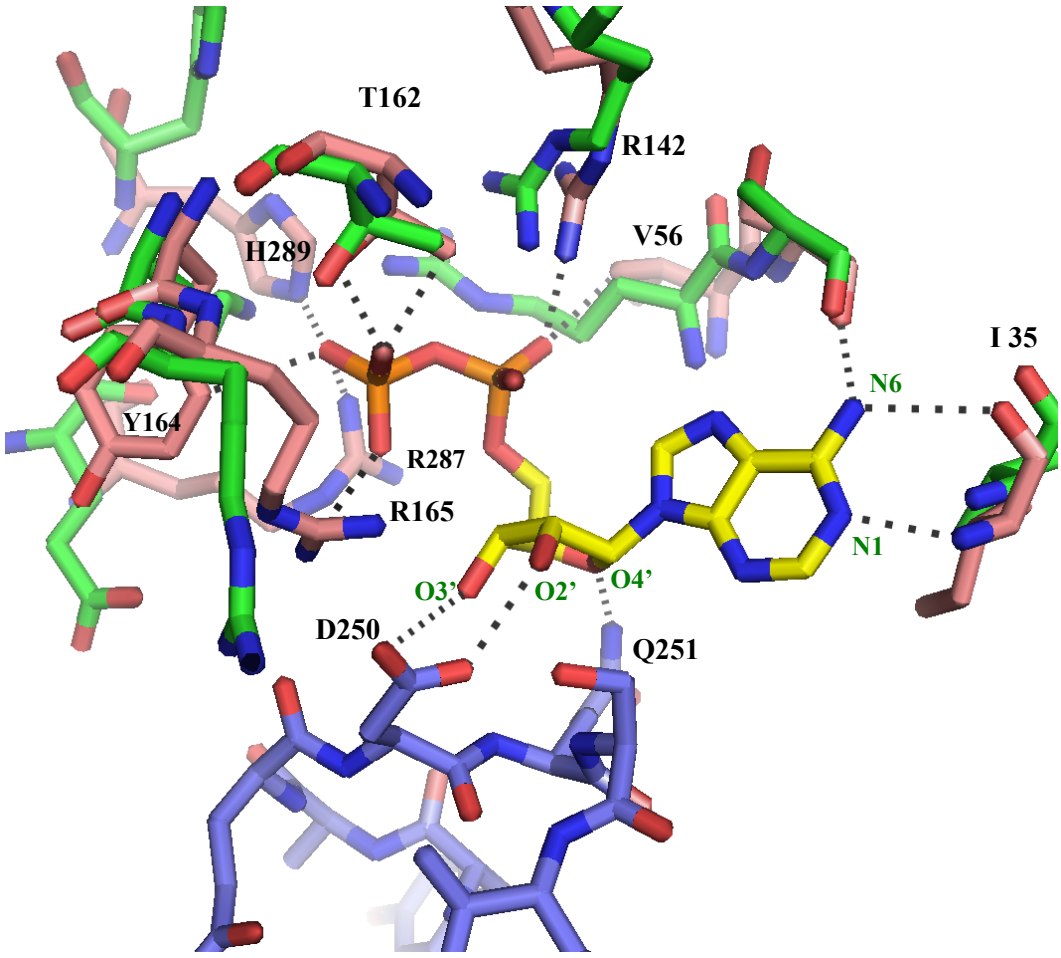

Figure 5.10: ADP-4 site: Superposition of mammalian AMPK with SNF-like protein. In the yeast structure, ADP binding is apparently facilitated by the hydrogen bonding between the 2' and 3' hydroxyl groups of the ribose with Asp-250 and the 4' oxygen of the ribose and the amino group of the side chain of Gln-251 in β. In the adenosine part, the NH_2 at position 6 hydrogen bonds with carbonyl group of the main chain of Ser-57 and Ile-35 (the corresponding residues in mammalian AMPK are in parenthesis: Ala-70, Val-48). The N1 atom interacts with amino group of the main chain of Ile-35. The α phosphate of ADP interacts with Val-56 (Arg-69), Arg-142 (Arg-151), Arg-287 (Glu-295); the β phosphate with Thr-162 (Thr-167), Tyr-164 (Lys-169), Arg-165 (Arg-170) and His-289 (His-297). Proteins and the ADP are in sticks representation. The γ subunits of AMPK and SNF-like are in green and pink, respectively. The extra loop from the β subunit of SNF-like is in blue sticks. The ADP is colored with carbon atoms in yellow. Residues from SNF-like protein have been labelled.

Interestingly, in the crystal structure of SNF1, the AMPK homologue in *S. Cerevisiae* [112], no nucleotide has been reported in any of the four potential binding sites, although the crystals were grown in the presence of 1 mM AMP. By fluorescence binding assays I was able to show that one AXP nucleotide binds to SNF1. Crystal soaking experiments with SNF1 recently enabled a member of our lab to solve the crystal structure of SNF1 in the presence of AMP in site-3 (**Richard Heath, personal communication**). Thus, nucleotides bind to the *S. Cerevisiae* homologues of AMPKs in site-3 which corresponds to the non-exchangeable site of mammalian AMPK. This single site binding is in agreement with my binding studies on SNF1.

5.7 Binding of ZMP to AMPK

AICAR is metabolized to ZMP within cells by phosphorylation at the 5′ position. Since, to some extent, it mimics the effects of AMP on AMPK, it has been widely used as an activator in AMPK biochemical studies. Unfortunately, its potency is significantly less than for AMP [59,90]. I determined that the affinity of ZMP for the tight exchangeable site of AMPK is about 18 μM and over a hundred micromolar for the weak site (see **section 4.2.7**). The crystal structure of a fragment of the γ-domain of mammalian AMPK in complex with ZMP has previously been reported [238]. In that case the construct comprised just one Bateman domain (CBS3-4) and the single ZMP was bound at a site that corresponds to our non-exchangeable AMP-3 site. Although the crystal soaking experiments reported with the γ fragment construct involved incubating crystals for 1-2 days with 20 mM ZMP, neither an AMP nor ZMP were seen in the AMP-2 site. My structural and binding studies lead me to speculate that the AMP-2 site is the weaker of the two exchangeable AXP sites on AMPK (see **section 5.3**). I used X-ray crystallography to understand the structural basis for the poorer binding and potency of ZMP relative to AMP. The 2.1 Å resolution electron density map shows that, in my construct, 2mM ZMP leads to

good occupancy at both the exchangeable sites (corresponding to AMP-1 and AMP-2 sites of the AMPK/AMP complex [**Fig 3.6B**]). The presence of ZMP in site-1 and -2 in my construct, but not in the truncated γ construct, probably occurs because nucleotide binding involves additional interactions of the nucleotides with residues from the other Bateman domains.

ZMP-1 adopts a very similar binding mode to the corresponding nucleotide in the AMP complex. In contrast, ZMP-2 does not superimpose that well with the corresponding AMP-2 of the wild type structure (**Fig 3.8A**). Binding of ZMP-2 to AMPK, in my construct, involves a conformational change in the side chain of His 297 relative to the AMP-bound enzyme. In its new orientation, the side chain of the histidine is oriented away from AMP-3 and interacts with ZMP-2. The re-oriented His-297 does not clash with the α phosphate of ZMP-2, as I see with WPW mutants, because of the change in conformation of the nucleotide just mentioned (**section 5.8**).

Additionally, the structure suggests that ZMP-2 binds weakly because of the loss of interaction between the phosphate group of the nucleotide and the side chain of a couple of basic residues from the protein (**section 3.2.3**). This probably accounts for the reduced potency of this drug.

Adenosine-like nucleotides activate AMPK, whereas other nucleotide monophosphates such as GMP, CMP, IMP, UMP and 6-SH-PMP (6-mercaptopurine riboside 5'-monophosphate) do not [90,239]. All these compounds have a similar monophosphate riboside moiety but they differ in the nucleobase (adenosine, cytidine, guanine, thymine, uracil and 6-mercaptopurine riboside) (**Fig 5.11**). Interestingly, compounds like ZMP, tubercidin 5'-monophosphate (Tu-MP) and 5'-deoxy-AMP (dAMP) (**Fig 5.11**) do activate AMPK, thus leading *Henin et al.* to suggest that a free 6-NH2 group in the nucleobase may be critical for ligand binding to γ. My crystal structure shows how ZMP mimics AMP binding by retaining the hydrogen bonds between the free-NH2 atom at position N2 and two main chain

carbonyl groups from the protein, and thus confirms this earlier suggestion (**Fig 3.8B**) [90].

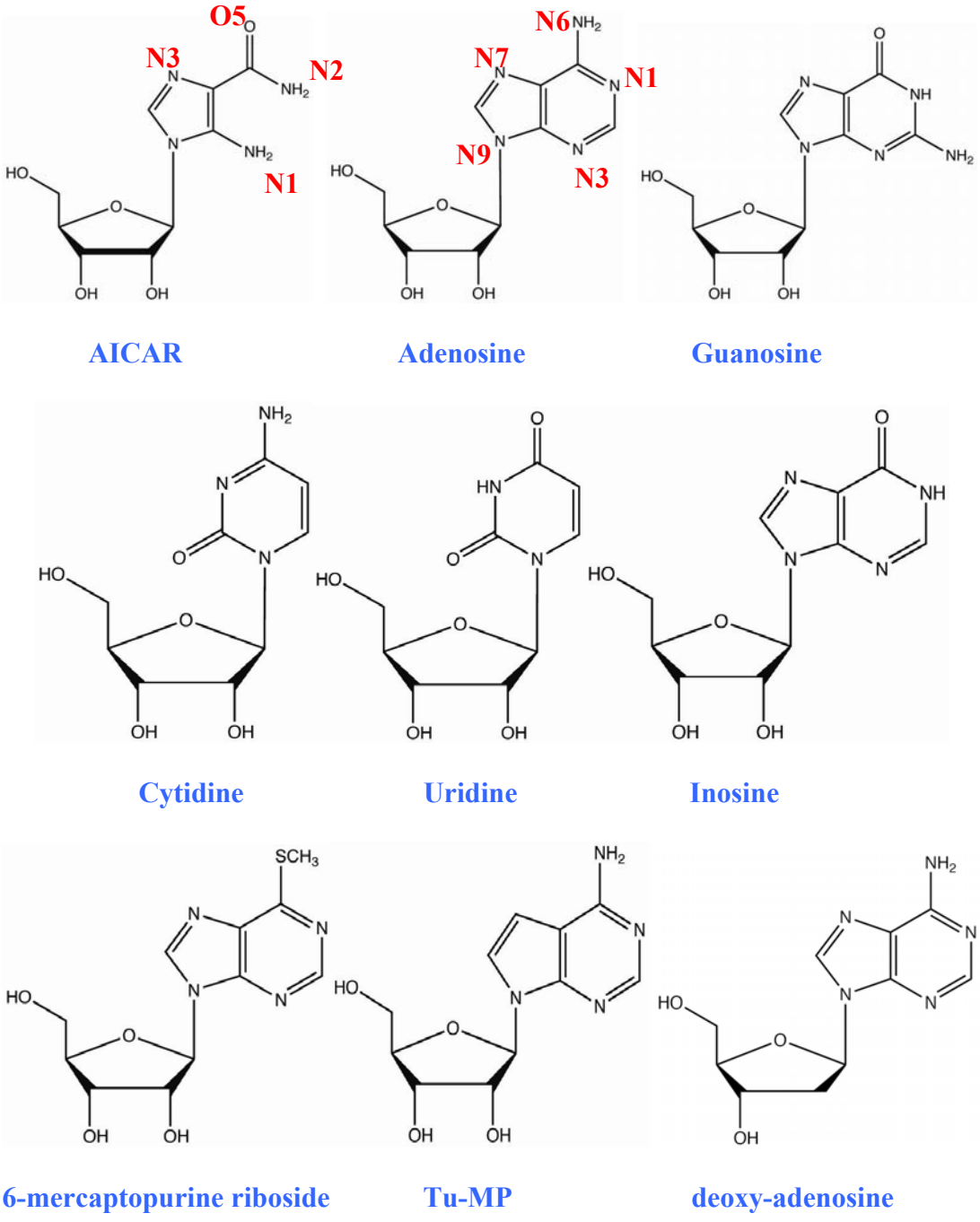

Figure 5.11: Comparison of the structures of AICAR with other nucleosides. When AICAR is phosphorylated it becomes ZMP. In this figure, selected atoms positioning of AICAR and adenosine are numbered in red.

5.8 WPW structures and implications for AMPK activation

Naturally occurring mutations in mainly basic residues of the γ2 isoform of AMPK cause WPW syndrome, which is a glycogen storage cardiomyopathy associated with electro-physiological abnormalities. Mapping of the corresponding residues onto the γ1 component of the crystal structure shows that most of the mutations involve the side chains of amino acids found close to the nucleotide binding sites [213]. I looked at three of the most common mutations involving Arg-69, His-150 and Arg-298. Arg-298 and Arg-69 interact with nucleotide in binding site-2, whereas His-150 interacts with the non-exchangeable AMP-3 and with the AXP in site-1 (**Fig 5.12**).

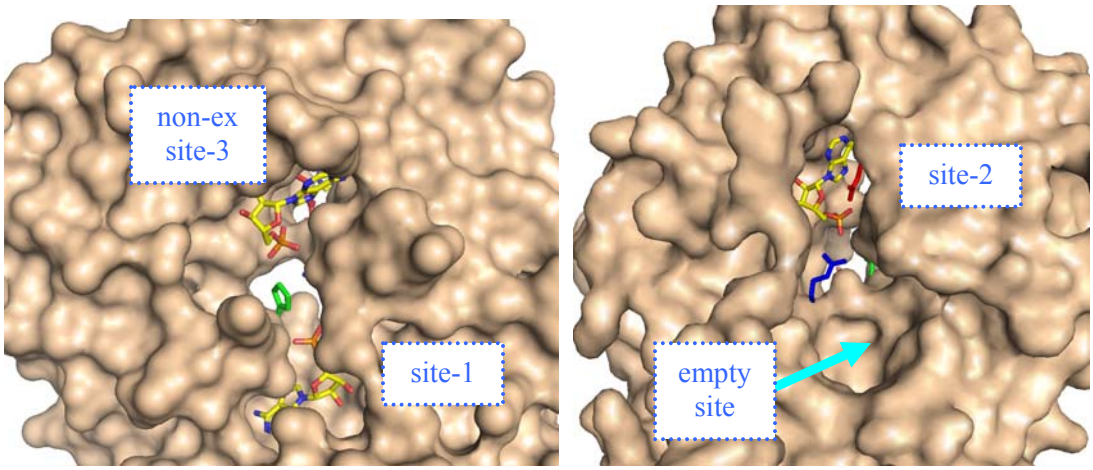

Figure 5.12: Surface representation of wild type AMPK. The front view (left) shows site-1 & site-3 and the back view (right) shows site-2. Residues His-150 (green), Arg-69 (blue) and Arg-298 (red) are shown in stick representation, AMP molecules are also in stick representation with carbon atoms colored in yellow.

To study the role of these three mutations, I made the relevant constructs, expressed and purified the proteins, and carried out binding and structural studies. Using NADPH competition I determined that wild type AMPK binds AMP, ADP and ATP at 3.3 μM, 1.3 μM and 1.1 μM at the tighter site. Interestingly, the three mutants Arg-69→ Gln, His-150→Arg and Arg-298→Gly show similar values for this tighter

site (**section 4.2.5**). Consistent with these results, the competition of mant-AMP with AXPs appears largely unchanged at the tighter site but is reduced to different extents, at the weak site. Arg-69→Gln is reduced about two-fold while His-150→Arg and Arg-298→Gly are down about 8-fold and 11-fold, respectively.

To test whether the non-exchangeable site-3 is conserved in the Arg-69→Gln, His-150→Arg and Arg-298→Gly mutants, I examined the over-expressed and purified mutant proteins by high-performance liquid-chromatography for bound nucleotides. All three mutant protein samples showed approximately one AMP molecule bound for every AMPK. Interestingly, when His-150, which interacts with the non-exchangeable AMP, is mutated, the resulting protein still co-purifies with one AMP moiety (**Fig 4.1**). These results indicate that WPW mutations affect only the binding at the weaker site of the two exchangeable sites.

I also used X-ray crystallography to examine nucleotide binding to these three WPW mutants. Crystals of the mutant proteins in complex with AXPs diffracted to reasonably high resolution (2.0 Å to 2.6 Å) and produced clearly defined electron density for bound AMP in site-1 and the non-exchangeable site-3. There was no electron density for nucleotides in site-2 in either His-150→Arg or Arg-298→Gly, but there was for the Arg-69→Gln mutant. This result is consistent with Arg-69→Gln being the mutant that is least affected in the binding studies, with only a two-fold decrease in affinity for nucleotides in the weak site compared to wild type AMPK.

The situation was somewhat different when I carried out ADP and ATP soaks on these crystals. Interestingly, in the R298G/ATP complex there is some electron density for nucleotide in site-2. I was able to model ATP into this site and refine it with an occupancy of 0.5 which indicates that ATP binding to site-2, at least in the crystal, is more favorable than for AMP or ADP. This data is consistent with the fluorescence binding experiments on WPW mutants described in **section 4.2.5**, where mant-AMP is more strongly displaced in the weak site by ATP than AMP

(**Fig 4.14B**). This suggests that in WPW mutants, site-2 preferentially binds ATP rather than AMP. These observations may explain why kinase activation in WPW proteins is compromised. A weaker affinity for AMP, and with unchanged K_d for ATP, would lead, presumably, to a less active, and less activatable enzyme.

As stated above, the overall structure of the WPW mutant proteins is similar to wild type. The main differences occur in the occupancies of nucleotides in the weaker of the two exchangeable sites and in the rearrangement of the side chain of residue His-297. The side chain of this residue is rotated 120º about the Cα-Cβ bond in the His-150→Arg and the Arg-298→Gly structures (**Fig 5.13**). In the wild type structure the imidazole group of the histidine hydrogen bonds or salt bridges with the phosphate of AMP-3; in the His-150→Arg and Arg-298→Gly mutants, the new orientation of the side chain of the histidine would clash with the α phosphate of AMPs in site-2 - if it were occupied. This could account for the reduced affinity of one of the two exchangeable AMP sites. It is possible that ATP binding to site-2 is less affected because of the extra interactions of the γ phosphate of the ATP with the side chains of Arg 151, an interaction which is not possible when either AMP or ADP are bound. This interpretation is consistent with the Arg-298→Gly structure in complex with ATP which displays partial occupancy for ATP in site-2.

The complementary use of binding and structural studies with WPW mutants consistently show that site-1 remains unchanged, confirming the suggestion (see **section 5.3**) that, at least in the construct I am working with, site-1 is the tight site and site-2 is the weaker site.

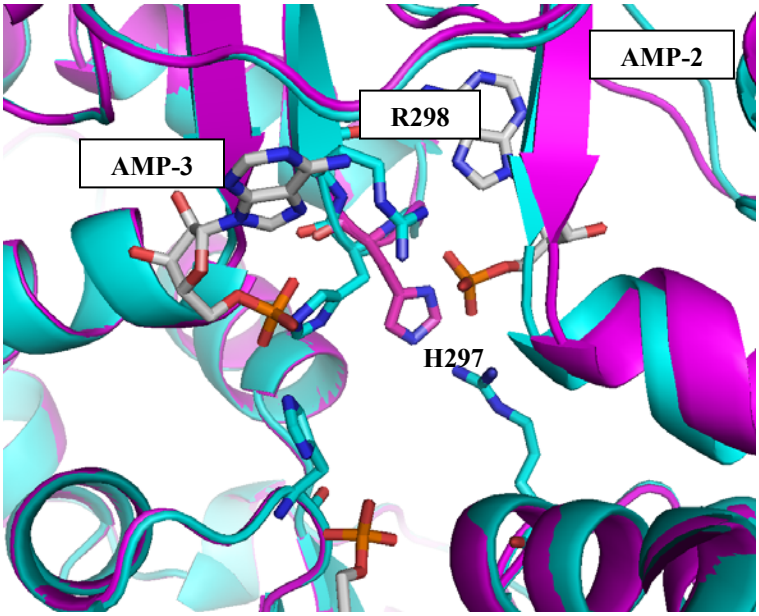

Figure 5.13: Ribbon representation of the superposition between wild type and mutant mammalian AMPK structures: wild type protein is in cyan and the WPW mutant Arg298→Gly is in purple. AMP molecules are shown in stick representation together with selected residues important in nucleotide binding.

Yeast AMPKs (SNF1 in *S. Cerevisiae* and SNF-like protein in *S. Pombe*) are not regulated by AMP as far as I am aware. Interestingly, if I overlap my AMPK structure with the two yeasts structures (SNF1 [112] and SNF-like protein [113]) the position of the side chain of the histidine (corresponding to mammalian AMPK His-297) is different. In yeast AMPKs, the rotamer adopted by the histidine is similar to the one selected by WPW mutants in mammalian AMPK. These two yeast structures do not have nucleotides bound at site-2, possibly because the α phosphate of the nucleotide in site-2 clashes with His 297 in the same way seen with the mammalian WPW mutants. As a consequence I speculate that the affinity for AMP in site-2 of yeast AMPKs is too weak to be measured or to be physiologically relevant (**Fig 5.14**).

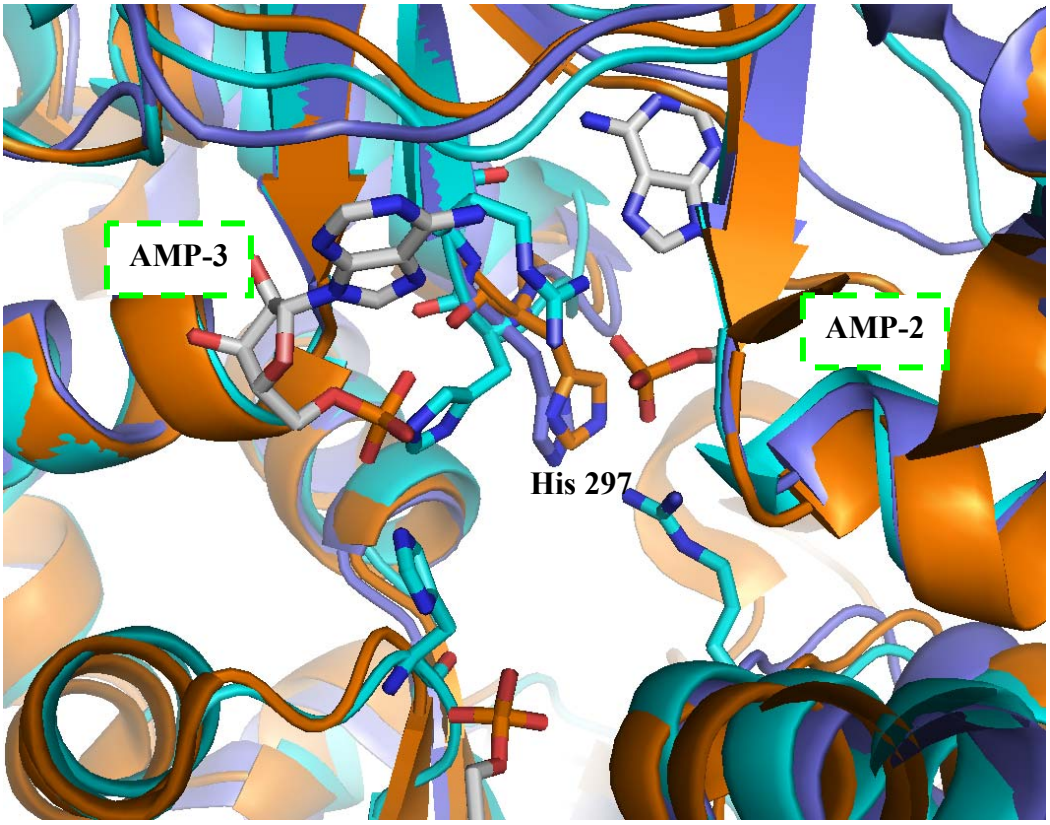

Figure 5.14: Ribbon representation of the superposition between wild type AMPK and yeast homologues: AMPK is in cyan, SNF1 in Violet and SNF-like is in orange. AMP molecules are from the AMPK complex only. AMP molecules with carbon atoms in grey are shown in stick representation together with residues important in nucleotide binding.

5.9 Concluding remarks

AMPK functions as a master regulator of cellular energy metabolism. The aim of this thesis was to understand, via structural and binding studies, the regulation of AMPK by nucleotides which may help the design of sensitive and potent activators of this protein kinase. My work on AMPK demonstrates that the two exchangeable nucleotide binding sites have different affinities. It is likely that the tighter of the two is the site important in mediating allosteric activation and the protection from dephosphorylation of the kinase domain.

The affinity of nucleotides for site-2 is difficult to establish accurately, but finding a specific fluorescent reporter for site-2 might help determining the K_d of ligands for this site. We are still missing the crystal structure of full-length protein showing the GBD and the kinase domain interacting with the rest of the protein and such a structure is probably necessary to further enhance our understanding of the regulation of the kinase. Much work still needs to be done in order to elucidate the molecular mechanisms of AMPK. Given the tempo of discoveries in this field it may well be that we will not have to wait too long before such data are available. These may well inform the development of new drugs and AMPK activators as promising leads for the treatment of disorders such as the metabolic disorder, obesity, diabetes and perhaps some forms of cancer [129].

Epilogue

After submission of my thesis, several additional pieces of work were finished in the lab which gives additional confidence to the interpretation of my data. Firstly, as I have described, the binding of NADH to AMPK occurs at the tighter of the two exchangeable sites. Recent work from Carling's lab has shown that NADH, even at high concentrations, does not compete with AMP for protection against de-phosphorylation. Secondly, also from Carling's lab, the dose response of the protection from de-phosphorylation by AMP also correlates closely with binding at the weaker, but not the stronger of the two exchangeable sites. Finally, recently completed work in the Gamblin lab has revealed the crystal structure of an active AMPK complex (**Bing Xiao, personal communication**). One of the notable features of this structure is that a part of the α chain, that links the kinase domain to the regulatory fragment, is ordered and interacts with the AMP-2 binding site. Taken together, these data argue strongly that it is AMP binding at the weaker of the two exchangeable sites that is responsible for mediating protection against de-phosphorylation.

If AMP binding at site-2 is the site that is important for protection against de-phosphorylation, the reduced affinity of AMP for site-2 would explain the reduced levels of AMPK activity seen in WPW mutants. *Sanders et al.* have shown that the effect of AMP on protection of AMPK against de-phosphorylation is lost in the Arg298→Gly mutant and reduced in the His150→Arg and the Arg69→Gln mutants **[10]**. In this light, my results on WPW mutants, both in solution, and by crystallography make good sense. I find that these mutations reduce the affinity for nucleotide binding to site-2 – the weak site. Therefore, my conclusion is that WPW mutants exert their effect because they alter nucleotide binding at the weaker exchangeable site and this results in reduced protection against de-phosphorylation thus leading to lower enzyme activity.

Appendix 1: Analysis of fluorescence binding studies

1.1 Titration of mant-nucleotide or NADPH with AMPK

The K_d values of the titration assays where determined according to the following model: Assuming that there are two similar and separate AXP binding sites and that each one does not necessarily produce the same fluorescent signal at the binding of the labeled nucleotide, the nucleotides mant-AXP or NADPH (N) bind to AMP-Kinase (K) according to the following scheme:

$N + K \leftrightarrow NK$ with $K_d = ([N][K])/[NK]$ (1)

Total concentrations of AMPK and nucleotide (K_T and N_T) are given by:

$K_T = [K] + [NK]$ (2)

$M_T = [N] + [NK]$ (3)

Then $K_d = [(K_T - (KN))(N_T - (NK)]/[NK]$ (4)

$K_d\,[NK] = N_T K_T - [NK](K_T + N_T) + [NK]^2$

$[NK]^2 - [NK](K_d + K_T + N_T) + K_T N_T = 0$ (5)

The remaining concentrations are calculated using:

$[N] = N_T - [NK]$ and $[K] = K_T - [NK]$ (6)

The fluorescence signal (S) measure is:

$S = S_K[K] + S_N[N] + S_{NK}[NK]$ (7)

where S_K, S_N, and S_{NK} are the specific fluorescence intensities of K, N and NK, respectively.

The data were fitted to the above equation with the specific fluorescence intensities and K_d as variables. A standard non linear least squares fitting procedure written by Dr. Stephen Martin (N.I.M.R.) was used.

1.2 Competition and displacement Assays

The values for the competition and displacement assays where determined according to the alternative model: A mixture of two competing nucleotide ligands,

mantATP/AMP or NADPH (N) and ATP/AMP (A), is titrated with the protein AMP-Kinase (K). If either K_d is known then the other can be determined.

The AMP-Kinase (K) should interact with two ligands (N and A) according to the following scheme:

$K + N \leftrightarrow KN$ with $K_{dB} = ([K][N]/[KN]$ (1)

$K + A \leftrightarrow KA$ with $K_{dA} = ([K][A]/[KA]$ (2)

Total concentration of protein, ligand M and A (K_T, N_T, and A_T) are given by:

$K_T = [K] + [KN] + [KA]$ (3)

$N_T = [N] + [KN]$ (4)

$A_T = [A] + [KA]$ (5)

Then

$[N] = K_{dN}[KN]/[K]$ and $N_T = K_{dN}[KN]/[K] + [KN]$ (6)

Then $N_T = [KN](K_{dN}/[K] + 1)$ (7)

$[KN] = N_T/(K_{dN}/[K] + 1) = N_T[K]/(K_{dN} + [K])$ (8)

In the same way one can show that

$[KA] = A_T[K]/(K_{dA} + [K])$ (9)

Substituting these expressions for [KN] and [KA] in the equation for K_T gives:

$K_T = [K] + B_T[K]/(K_{dN} + [K]) + A_T[K]/(K_{dA} + [K])$ (10)

Expanding this equation gives:

$[K]^3 + [K]^2(- K_T + K_{dN} + K_{dA} + N_T + A_T) + [K](- K_TK_{dN} – K_TK_{dA} + K_{dN}K_{dA} + N_TK_{dA} + A_TK_{dN}) – K_TK_{dN}K_{dA} = 0$ (11)

The remaining concentrations are calculated using

$[KN] = N_T[K]/(K_{dN} + [K])$ (12)

$[KA] = A_T[K]/(K_{dA} + [K])$ (13)

$[N] = K_{dN}[KN]/[K]$ (14)

$[A] = K_{dA}[KA]/[K]$ (15)

The fluorescence intensity (S) is given by:

$S = S_K[K] + S_N[N] + S_A[A] + S_{KN}[KN] + S_{KA}[KA]$ (16)

where S_K, S_N, S_A, S_{KN} and S_{KA} are the specific fluorescence intensities of K, N, A, KN, and KA, respectively. The experimental data were fitted to the above equation

with the specific fluorescence intensities and the unknown association constant K_{dA} as variables and K_{dN} instead was held constant at the value measured with the direct fluorescence titration. A standard non linear least square procedure written by Dr Stephen Martin (N.I.M.R.) was used in the analysis.

1.3 Fluorescent resonance energy transfer (FRET)

Performing titrations in which the mant nucleotides are added to the AMPK (rather than adding the AMPK to the mant nucleotide) can, in principle give additional useful information. However, such experiments cannot easily be performed using direct excitation of the mant fluorophore because the change in fluorescence associated with the binding event(s) will be small compared with the fluorescence coming from the high concentration of free nucleotide reached at the end of the titration. However, because the emission spectrum of tryptophan overlaps the excitation spectrum of mant nucleotides it is possible to make use of resonance energy transfer [223-224] by exciting AMPKs tryptophans at 290nm and monitoring the mant emission that derives from the energy transfer. Because the excitation of the free nucleotide is almost zero at 290 nm, the contribution from binding event(s) then becomes large relative to the contribution from the free nucleotide.

Appendix 2: *Analysis of thermal shift data*

2.1 Basic theory for two-state transitions

Despite the irreversible nature of protein unfolding for many large proteins at high protein concentrations, it has been suggested that irreversible unfolding may be treated as two discrete steps where a relatively fast folded to unfolded reaction is uncoupled from a much slower aggregation step [226]. Under this condition, an apparently irreversible process may be treated as a reversible unfolding transition. Protein unfolding is therefore described by the following:

Consider the following simple two-state equilibrium between the folded (F) and unfolded (U) forms of a protein:

$$F \underset{k_f}{\overset{k_u}{\rightleftharpoons}} U$$

The unfolding constant is defined as:

$$K_u = \frac{[U]}{[F]} = \frac{F_u}{F_f} = \frac{1 - F_f}{F_f} = e^{-\Delta G/RT} \quad (1)$$

K_u is related to the Gibbs free energy change (ΔG) by the following equations:

$$\Delta G = -RT\ln K \quad (2)$$

where T is the absolute temperature and R is the Universal Gas Constant (0.0019872 kcal/mol).

the Gibbs-Helmholtz equation states:

$$\Delta G = \Delta H - T\Delta S \quad (3)$$

Where ΔH and ΔS are, respectively, the enthalpy and entropy of binding. For proteins, ΔH and ΔS are known to vary with temperature according to the following equations:

$$\Delta H_T = \Delta H_{T_R} + \Delta C_P (T - T_R) \quad (4)$$

$$\Delta S_T = \Delta S_{T_R} + \Delta C_P \ln\left(\frac{T}{T_R}\right) \quad (5)$$

where T_R is any convenient reference temperature and ΔC_P is the heat capacity change.

Substituting equations (4) and (5) in equation (3) gives

and $$\Delta G_T = \Delta H_{T_R} - T\Delta S_{T_R} + \Delta C_P\left\{\left(T - T_R\right) - T\mathrm{Ln}\left(\frac{T}{T_R}\right)\right\} \quad (6)$$

This is known as the modified Gibbs-Helmholtz equation.

The equation can be simplified further by letting the reference temperature be the midpoint of the unfolding transition (i.e., where the protein is, by definition, 50% unfolded and $F_u = F_f = 0.5$). By convention, the midpoint of the unfolding transition is designated as T_m. By definition:

$$\Delta G_{T_m} = -RT_m\mathrm{Ln}K_{T_m} = 0$$

$$\Delta S_{T_m} = \frac{\Delta H_{T_m}}{T_m} \quad (7)$$

Substituting equation (7) in equation (6) and substitution of T_m for T_R in equation (3) gives:

$$\Delta G_T = \Delta H_{T_m}\left(1 - \frac{T}{T_m}\right) + \Delta C_P\left\{\left(T - T_m\right) - T\mathrm{Ln}\left(\frac{T}{T_m}\right)\right\} \quad (8)$$

The optical signal at a given temperature in a thermal denaturation experiment can be related to the fractions of folded and unfolded protein present by:

$$F_u = \frac{S_{OBS} - S_f}{S_u - S_f} \quad (9)$$

Substituting in equation (1), gives:

$$S_{OBS} = \frac{S_f + S_u e^{-\Delta G/RT}}{1 + e^{-\Delta G/RT}} \quad (10)$$

Knowing that the optical signals characteristic of the folded and unfolded states (S_f and S_u respectively) depended linearly on temperature according to:

$$S_f = S_{f(0)} + \beta_f T_C \quad (11)$$

$$S_u = S_{u(0)} + \beta_u T_C \quad (12)$$

And by substituting for ΔG from equation (8)

$$S_{OBS} = \frac{S_{f(0)} + \beta_f T_C + (S_{u(0)} + \beta_u T_C)\exp\left(-\frac{\Delta H_{T_m}}{RT}\left(1 - \frac{T}{T_m}\right) - \frac{\Delta C_P}{RT}\left\{(T - T_m) - T\mathrm{Ln}\left(\frac{T}{T_m}\right)\right\}\right)}{1 + \exp\left(-\frac{\Delta H_{T_m}}{RT}\left(1 - \frac{T}{T_m}\right) - \frac{\Delta C_P}{RT}\left\{(T - T_m) - T\mathrm{Ln}\left(\frac{T}{T_m}\right)\right\}\right)} \qquad (13)$$

Where $S_{f(0)}$ and $S_{u(0)}$ are the optical signals of the folded and unfolded states at 0^oC, T_C is the temperature in ^oC, and Δ_f and Δ_u are the coefficients describing the linear temperature dependence of S_f and S_u respectively.

Data for the variation of S_{OBS} with temperature can then be analyzed using non-linear least-squares methods to give the thermodynamic parameters ΔH, T_m, and ΔC_p, plus S_f and S_u. In practice, ΔC_p is frequently set to a constant (or, more often, zero) because it is generally a small contribution to the unfolding and because it enables difficult transition curves to be solved more readily.

2.2 Temperature dependence of association and dissociation constants

Consider a protein (P) that binds a ligand (L) to form a simple 1:1 complex (PL) according to the following scheme:

$$F \rightleftharpoons U \qquad F + L \rightleftharpoons FL$$

$$K_a = \frac{[FL]}{[F][L]} \qquad (14) \qquad \text{and} \qquad K_u = \frac{[U]}{[F]} \qquad (1)$$

where K_a is the association constant

The unfolding constant in the presence of ligand, defined as $K_{u,APP}$, is given by:

$$K_{u,APP} = \frac{[U]}{[F] + [FL]} = K_{u,APP} = \frac{K_u}{1 + K_a[L]} \qquad (15)$$

At the midpoint of the thermal unfolding transition observed in the presence of the ligand, $T_{m(L)}$, the concentrations of folded and unfolded forms must, by definition, be the same and one has from equation (15):

$$K_{u,APP} = 1 = \frac{K_{u,Tm(L)}}{1 + K_{a,Tm(L)}[L]} \tag{16}$$

Where $K_{u,Tm(L)}$ is the unfolding constant at $T_{m(L)}$ and $K_{a,Tm(L)}$ is the association constant for the binding of the ligand to the folded protein at $T_{m(L)}$. The relationship between ligand binding and total free ligand, $[L_{Tm}]$, at the T_m point is

$$K_{a,Tm(L)} = \frac{K_{u,Tm(L)} - 1}{[L]} \tag{17}$$

Therefore the association constant $K_{a,Tm(L)}$ can be calculated when $K_{u,Tm(L)}$ is known. Analysis of the unfolding curve recorded in the absence of the ligand using equation (13) should yield ΔH_{Tm} , T_m, and (perhaps) ΔC_p. Note: T_m is the mid-point for unfolding observed in the absence of ligand.

$$K_{u,Tm(L)} = \exp\left(-\frac{\Delta H_{T_m}}{RT_{m(L)}}\left(1 - \frac{T_{m(L)}}{T_m}\right) - \frac{\Delta C_P}{RT_{m(L)}}\left\{\left(T_{m(L)} - T_m\right) - TLn\left(\frac{T_{m(L)}}{T_m}\right)\right\}\right) \tag{18}$$

and substitution of this value in equation (17) gives $K_{a,Tm(L)}$.

If one has estimates for both the enthalpy of binding, ΔH_L, and binding heat capacity, ΔC_{pL}, then the association constant, K_a, can therefore be calculated at any temperature from:

$$K_a(T) = \exp\left(\frac{-\Delta G_T}{RT}\right) = \exp\left(-\frac{\Delta H_{T_m}}{RT}\left(1 - \frac{T}{T_m}\right) - \frac{\Delta C_P}{RT}\left\{\left(T - T_m\right) - TLn\left(\frac{T}{T_m}\right)\right\}\right) \tag{19}$$

6. References

1 Berg, J., Tymoczko, J. & Stryer, L. *Biochemistry* 5th edition edn, (W.H. Freeman & company, 2002).

2 Kahn, B. B., Alquier, T., Carling, D. & Hardie, D. G. AMP-activated protein kinase: Ancient energy gauge provides clues to modern understanding of metabolism. *Cell Metabolism* **1**, 15-25, doi:10.1016/j.cmet.2004.12.003 (2005).

3 Veech, R. L., Lawson, J. W., Cornell, N. W. & Krebs, H. A. Cytosolic phosphorylation potential. *J. Biol. Chem.* **254**, 6538-6547 (1979).

4 Corton, J. M., Gillespie, J. G., Hawley, S. A. & Hardie, D. G. 5-aminoimidazole-4-carboxamide ribonucleoside. A specific method for activating AMP-activated protein kinase in intact cells? *Eur. J. Biochem.* **229**, 558-565 (1995).

5 Hardie, D. G., Salt, I. P., Hawley, S. A. & Davies, S. P. AMP-activated protein kinase: an ultrasensitive system for monitoring cellular energy charge. *Biochem. J.* **338 (Pt 3)**, 717-722 (1999).

6 Hedbacker, K. & Carlson, M. SNF1/AMPK pathways in yeast. *Front. Biosci.* **13**, 2408-2420 (2008).

7 Rubenstein, E. M. & Schmidt, M. C. Mechanisms regulating the protein kinases of Saccharomyces cerevisiae. *Eukaryot. Cell* **6**, 571-583 (2007).

8 Hardie, D. G., Hawley, S. A. & Scott, J. W. AMP-activated protein kinase--development of the energy sensor concept. *J. Physiol.* **574**, 7-15 (2006).

9 Davies, S. P. *et al.* Purification of the AMP-activated protein kinase on ATP-gamma-sepharose and analysis of its subunit structure. *Eur. J. Biochem.* **223**, 351-357 (1994).

10 Carling, D. The AMP-activated protein kinase cascade - a unifying system for energy control. *Trends in Biochemical Sciences* **29**, 18-24, doi:10.1016/j.tibs.2003.11.005 (2004).

11 Polekhina, G. *et al.* AMPK beta subunit targets metabolic stress sensing to glycogen. *Curr. Biol.* **13**, 867-871 (2003).

12 Littler, D. R. *et al.* A conserved mechanism of autoinhibition for the AMPK kinase domain: ATP-binding site and catalytic loop refolding as a means of regulation. *Acta Crystallogr. Sect. F Struct. Biol. Cryst. Commun.* **66**, 143-151 (2010).

13 Hudson, E. R. *et al.* A novel domain in AMP-activated protein kinase causes glycogen storage bodies similar to those seen in hereditary cardiac arrhythmias. *Curr. Biol.* **13**, 861-866 (2003).

14 Polekhina, G. *et al.* Crystallization of the glycogen-binding domain of the AMP-activated protein kinase beta subunit and preliminary X-ray analysis. *Acta Crystallogr. Sect. F Struct. Biol. Cryst. Commun.* **61**, 39-42 (2005).

15 Polekhina, G. *et al.* Structural basis for glycogen recognition by AMP-activated protein kinase. *Structure* **13**, 1453-1462 (2005).

16 Scott, J. W. *et al.* CBS domains form energy-sensing modules whose binding of adenosine ligands is disrupted by disease mutations. *J. Clin. Invest.* **113**, 274-284 (2004).

17 Bateman, A. The structure of a domain common to archaebacteria and the homocystinuria disease protein. *Trends in Biochemical Sciences* **22**, 12-13 (1997).
18 Meyer, S., Savaresi, S., Forster, I. C. & Dutzler, R. Nucleotide recognition by the cytoplasmic domain of the human chloride transporter ClC-5. *Nat. Struct. Mol. Biol.* **14**, 60-67 (2007).
19 Sharpe, M. L., Gao, C., Kendall, S. L., Baker, E. N. & Lott, J. S. The structure and unusual protein chemistry of hypoxic response protein 1, a latency antigen and highly expressed member of the DosR regulon in Mycobacterium tuberculosis. *J. Mol. Biol.* **383**, 822-836 (2008).
20 Sintchak, M. D. *et al.* Structure and mechanism of inosine monophosphate dehydrogenase in complex with the immunosuppressant mycophenolic acid. *Cell* **85**, 921-930 (1996).
21 Ignoul, S. & Eggermont, J. CBS domains: structure, function, and pathology in human proteins. *Am. J. Physiol. Cell Physiol.* **289**, C1369-1378 (2005).
22 Kemp, B. E. Bateman domains and adenosine derivatives form a binding contract. *J. Clin. Invest.* **113**, 182-184 (2004).
23 Marsin, A. S., Bouzin, C., Bertrand, L. & Hue, L. The stimulation of glycolysis by hypoxia in activated monocytes is mediated by AMP-activated protein kinase and inducible 6-phosphofructo-2-kinase. *J. Biol. Chem.* **277**, 30778-30783 (2002).
24 Choi, S. L. *et al.* The regulation of AMP-activated protein kinase by H(2)O(2). *Biochem. Biophys. Res. Commun.* **287**, 92-97 (2001).
25 Salt, I. P., Johnson, G., Ashcroft, S. J. & Hardie, D. G. AMP-activated protein kinase is activated by low glucose in cell lines derived from pancreatic beta cells, and may regulate insulin release. *Biochem. J.* **335 (Pt 3)**, 533-539 (1998).
26 Kudo, N., Barr, A. J., Barr, R. L., Desai, S. & Lopaschuk, G. D. High rates of fatty acid oxidation during reperfusion of ischemic hearts are associated with a decrease in malonyl-CoA levels due to an increase in 5'-AMP-activated protein kinase inhibition of acetyl-CoA carboxylase. *J. Biol. Chem.* **270**, 17513-17520 (1995).
27 Marsin, A. S. *et al.* Phosphorylation and activation of heart PFK-2 by AMPK has a role in the stimulation of glycolysis during ischaemia. *Curr. Biol.* **10**, 1247-1255 (2000).
28 Hutber, C. A., Hardie, D. G. & Winder, W. W. Electrical stimulation inactivates muscle acetyl-CoA carboxylase and increases AMP-activated protein kinase. *Am. J. Physiol.* **272**, E262-266 (1997).
29 Winder, W. W. & Hardie, D. G. Inactivation of acetyl-CoA carboxylase and activation of AMP-activated protein kinase in muscle during exercise. *Am. J. Physiol.* **270**, E299-304 (1996).
30 Steinberg, G. R. & Kemp, B. E. AMPK in Health and Disease. *Physiol. Rev.* **89**, 1025-1078 (2009).
31 Cohen, P. Signal integration at the level of protein kinases, protein phosphatases and their substrates. *Trends Biochem. Sci.* **17**, 408-413 (1992).

32 Klumpp, S. & Krieglstein, J. Reversible phosphorylation of histidine residues in proteins from vertebrates. *Sci. Signal* **2**, pe13, doi:scisignal.261pe13 [pii] 10.1126/scisignal.261pe13 (2009).
33 Hardie, D. G. Protein phosphorylation and dephosphorylation. *Curr. Opin. Cell Biol.* **1**, 220-226 (1989).
34 Cohen, P. The role of protein phosphorylation in the hormonal control of enzyme activity. *Eur. J. Biochem.* **151**, 439-448 (1985).
35 Cohen, P. Protein kinases--the major drug targets of the twenty-first century? *Nat. Rev. Drug Discov.* **1**, 309-315 (2002).
36 Nolen, B., Taylor, S. & Ghosh, G. Regulation of protein kinases; controlling activity through activation segment conformation. *Mol. Cell.* **15**, 661-675 (2004).
37 Hawley, S. A. *et al.* Complexes between the LKB1 tumor suppressor, STRAD alpha/beta and MO25 alpha/beta are upstream kinases in the AMP-activated protein kinase cascade. *J. Biol.* **2**, 28 (2003).
38 Hawley, S. A. *et al.* Characterization of the AMP-activated protein kinase kinase from rat liver and identification of threonine 172 as the major site at which it phosphorylates AMP-activated protein kinase. *J. Biol. Chem.* **271**, 27879-27887 (1996).
39 Hawley, S. A. *et al.* Calmodulin-dependent protein kinase kinase-beta is an alternative upstream kinase for AMP-activated protein kinase. *Cell Metab.* **2**, 9-19 (2005).
40 Woods, A. *et al.* LKB1 is the upstream kinase in the AMP-activated protein kinase cascade. *Curr. Biol.* **13**, 2004-2008 (2003).
41 Denison, F. C., Hiscock, N. J., Carling, D. & Woods, A. Characterization of an alternative splice variant of LKB1. *J. Biol. Chem.* **284**, 67-76 (2009).
42 Baas, A. F. *et al.* Activation of the tumour suppressor kinase LKB1 by the STE20-like pseudokinase STRAD. *Embo J.* **22**, 3062-3072 (2003).
43 Boudeau, J., Sapkota, G. & Alessi, D. R. LKB1, a protein kinase regulating cell proliferation and polarity. *FEBS Lett.* **546**, 159-165 (2003).
44 Sakamoto, K. *et al.* Deficiency of LKB1 in skeletal muscle prevents AMPK activation and glucose uptake during contraction. *Embo J.* **24**, 1810-1820 (2005).
45 Sakamoto, K. *et al.* Deficiency of LKB1 in heart prevents ischemia-mediated activation of AMPKalpha2 but not AMPKalpha1. *Am. J. Physiol. Endocrinol. Metab.* **290**, E780-788 (2006).
46 Shaw, R. J. *et al.* The tumor suppressor LKB1 kinase directly activates AMP-activated kinase and regulates apoptosis in response to energy stress. *Proc. Natl. Acad. Sci. U S A* **101**, 3329-3335 (2004).
47 Hawley, S. A. *et al.* 5'-AMP activates the AMP-activated protein kinase cascade, and Ca2+/calmodulin activates the calmodulin-dependent protein kinase I cascade, via three independent mechanisms. *J. Biol. Chem.* **270**, 27186-27191 (1995).
48 Hurley, R. L. *et al.* The Ca2+/calmodulin-dependent protein kinase kinases are AMP-activated protein kinase kinases. *J. Biol. Chem.* **280**, 29060-29066, (2005).

49 Woods, A. *et al.* Ca2+/calmodulin-dependent protein kinase kinase-beta acts upstream of AMP-activated protein kinase in mammalian cells. *Cell Metabolism* **2**, 21-33 (2005).
50 Momcilovic, M., Hong, S. P. & Carlson, M. Mammalian TAK1 activates Snf1 protein kinase in yeast and phosphorylates AMP-activated protein kinase in vitro. *J. Biol. Chem.* **281**, 25336-25343 (2006).
51 Xie, M. *et al.* A pivotal role for endogenous TGF-beta-activated kinase-1 in the LKB1/AMP-activated protein kinase energy-sensor pathway. *Proc. Natl. Acad. Sci. U S A* **103**, 17378-17383 (2006).
52 Warden, S. M. *et al.* Post-translational modifications of the beta-1 subunit of AMP-activated protein kinase affect enzyme activity and cellular localization. *Biochem. J.* **354**, 275-283 (2001).
53 Woods, A. *et al.* Identification of phosphorylation sites in AMP-activated protein kinase (AMPK) for upstream AMPK kinases and study of their roles by site-directed mutagenesis. *Journal of Biological Chemistry* **278**, 28434-28442 (2003).
54 Davies, S. P., Helps, N. R., Cohen, P. T. & Hardie, D. G. 5'-AMP inhibits dephosphorylation, as well as promoting phosphorylation, of the AMP-activated protein kinase. Studies using bacterially expressed human protein phosphatase-2C alpha and native bovine protein phosphatase-2AC. *FEBS Lett.* **377**, 421-425 (1995).
55 Ludin, K., Jiang, R. & Carlson, M. Glucose-regulated interaction of a regulatory subunit of protein phosphatase 1 with the Snf1 protein kinase in Saccharomyces cerevisiae. *Proc. Natl. Acad. Sci. U S A* **95**, 6245-6250 (1998).
56 Feng, Z. H. *et al.* The yeast GLC7 gene required for glycogen accumulation encodes a type 1 protein phosphatase. *J. Biol. Chem.* **266**, 23796-23801 (1991).
57 Stein, S. C., Woods, A., Jones, N. A., Davison, M. D. & Carling, D. The regulation of AMP-activated protein kinase by phosphorylation. *Biochem. J.* **345 Pt 3**, 437-443 (2000).
58 Carling, D. & Hardie, D. G. The substrate and sequence specificity of the AMP-activated protein kinase - phosphorylation of glycogen-synthase and phosphorylase kinase. *Biochimica et Biophysica Acta* **1012**, 81-86 (1989).
59 Henin, N., Vincent, M. F., Gruber, H. E. & Van den Berghe, G. Inhibition of fatty acid and cholesterol synthesis by stimulation of AMP-activated protein kinase. *Faseb J.* **9**, 541-546 (1995).
60 Jorgensen, S. B. *et al.* The alpha2-5'AMP-activated protein kinase is a site 2 glycogen synthase kinase in skeletal muscle and is responsive to glucose loading. *Diabetes* **53**, 3074-3081 (2004).
61 Chan, A. Y. & Dyck, J. R. Activation of AMP-activated protein kinase (AMPK) inhibits protein synthesis: a potential strategy to prevent the development of cardiac hypertrophy. *Can. J. Physiol. Pharmacol.* **83**, 24-28 (2005).
62 Bolster, D. R., Crozier, S. J., Kimball, S. R. & Jefferson, L. S. AMP-activated protein kinase suppresses protein synthesis in rat skeletal muscle

through down-regulated mammalian target of rapamycin (mTOR) signaling. *J. Biol. Chem.* **277**, 23977-23980 (2002).
63 Gwinn, D. M. *et al.* AMPK phosphorylation of raptor mediates a metabolic checkpoint. *Mol. Cell* **30**, 214-226 (2008).
64 Inoki, K., Zhu, T. & Guan, K. L. TSC2 mediates cellular energy response to control cell growth and survival. *Cell* **115**, 577-590 (2003).
65 Kimura, N. *et al.* A possible linkage between AMP-activated protein kinase (AMPK) and mammalian target of rapamycin (mTOR) signalling pathway. *Genes Cells* **8**, 65-79 (2003).
66 Cho, Y. S. *et al.* Molecular mechanism for the regulation of human ACC2 through phosphorylation by AMPK. *Biochem. Biophys. Res. Commun.* **391**, 187-192 (2010).
67 Garton, A. J. *et al.* Phosphorylation of bovine hormone-sensitive lipase by the AMP-activated protein kinase. A possible antilipolytic mechanism. *Eur. J. Biochem.* **179**, 249-254 (1989).
68 Haemmerle, G. *et al.* Hormone-sensitive lipase deficiency in mice causes diglyceride accumulation in adipose tissue, muscle, and testis. *J Biol Chem* **277**, 4806-4815 (2002).
69 Luiken, J. J. *et al.* Contraction-induced fatty acid translocase/CD36 translocation in rat cardiac myocytes is mediated through AMP-activated protein kinase signaling. *Diabetes* **52**, 1627-1634 (2003).
70 Merrill, G. F., Kurth, E. J., Hardie, D. G. & Winder, W. W. AICA riboside increases AMP-activated protein kinase, fatty acid oxidation, and glucose uptake in rat muscle. *Am. J. Physiol.* **273**, E1107-1112 (1997).
71 Treebak, J. T. *et al.* AMPK-mediated AS160 phosphorylation in skeletal muscle is dependent on AMPK catalytic and regulatory subunits. *Diabetes* **55**, 2051-2058 (2006).
72 Velasco, G., Geelen, M. J. & Guzman, M. Control of hepatic fatty acid oxidation by 5'-AMP-activated protein kinase involves a malonyl-CoA-dependent and a malonyl-CoA-independent mechanism. *Arch. Biochem. Biophys.* **337**, 169-175 (1997).
73 Chavez, J. A., Roach, W. G., Keller, S. R., Lane, W. S. & Lienhard, G. E. Inhibition of GLUT4 translocation by Tbc1d1, a Rab GTPase-activating protein abundant in skeletal muscle, is partially relieved by AMP-activated protein kinase activation. *J. Biol. Chem.* **283**, 9187-9195 (2008).
74 Chen, S. *et al.* Complementary regulation of TBC1D1 and AS160 by growth factors, insulin and AMPK activators. *Biochem. J.* **409**, 449-459 (2008).
75 Taylor, E. B. *et al.* Discovery of TBC1D1 as an insulin-, AICAR-, and contraction-stimulated signaling nexus in mouse skeletal muscle. *J. Biol. Chem.* **283**, 9787-9796 (2008).
76 Foretz, M., Carling, D., Guichard, C., Ferre, P. & Foufelle, F. AMP-activated protein kinase inhibits the glucose-activated expression of fatty acid synthase gene in rat hepatocytes. *J. Biol. Chem.* **273**, 14767-14771 (1998).
77 Leclerc, I., Kahn, A. & Doiron, B. The 5'-AMP-activated protein kinase inhibits the transcriptional stimulation by glucose in liver cells, acting through the glucose response complex. *FEBS Lett.* **431**, 180-184 (1998).

78 Lochhead, P. A., Salt, I. P., Walker, K. S., Hardie, D. G. & Sutherland, C. 5-aminoimidazole-4-carboxamide riboside mimics the effects of insulin on the expression of the 2 key gluconeogenic genes PEPCK and glucose-6-phosphatase. *Diabetes* **49**, 896-903 (2000).
79 Leclerc, I. *et al.* Hepatocyte nuclear factor-4alpha involved in type 1 maturity-onset diabetes of the young is a novel target of AMP-activated protein kinase. *Diabetes* **50**, 1515-1521 (2001).
80 Zheng, D. *et al.* Regulation of muscle GLUT-4 transcription by AMP-activated protein kinase. *J. Appl. Physiol.* **91**, 1073-1083 (2001).
81 McGee, S. L. *et al.* AMP-activated protein kinase regulates GLUT4 transcription by phosphorylating histone deacetylase 5. *Diabetes* **57**, 860-867 (2008).
82 Koo, S. H. *et al.* The CREB coactivator TORC2 is a key regulator of fasting glucose metabolism. *Nature* **437**, 1109-1111 (2005).
83 Lin, J., Handschin, C. & Spiegelman, B. M. Metabolic control through the PGC-1 family of transcription coactivators. *Cell Metab.* **1**, 361-370 (2005).
84 Monod, J., Changeux, J. P. & Jacob, F. Allosteric proteins and cellular control systems. *J. Mol. Biol.* **6**, 306-329 (1963).
85 Carling, D., Zammit, V. A. & Hardie, D. G. A common bicyclic protein kinase cascade inactivates the regulatory enzymes of fatty acid and cholesterol biosynthesis. *FEBS Lett.* **223**, 217-222 (1987).
86 Cheung, P. C. F., Salt, I. P., Davies, S. P., Hardie, D. G. & Carling, D. Characterization of AMP-activated protein kinase gamma-subunit isoforms and their role in AMP binding. *Biochemical Journal* **346**, 659-669 (2000).
87 Sanders, M. J., Grondin, P. O., Hegarty, B. D., Snowden, M. A. & Carling, D. Investigating the mechanism for AMP activation of the AMP-activated protein kinase cascade. *Biochemical Journal* **403**, 139-148 (2007).
88 Gadalla, A. E. *et al.* AICA riboside both activates AMP-activated protein kinase and competes with adenosine for the nucleoside transporter in the CA1 region of the rat hippocampus. *J. Neurochem.* **88**, 1272-1282 (2004).
89 Vincent, M. F., Marangos, P., Gruber, H. E. & Van den Berghe, G. AICAriboside inhibits gluconeogenesis in isolated rat hepatocytes. *Adv. Exp. Med. Biol.* **309B**, 359-362 (1991).
90 Henin, N., Vincent, M. F. & Van den Berghe, G. Stimulation of rat liver AMP-activated protein kinase by AMP analogues. *Biochim. Biophys. Acta* **1290**, 197-203 (1996).
91 Longnus, S. L., Wambolt, R. B., Parsons, H. L., Brownsey, R. W. & Allard, M. F. 5-Aminoimidazole-4-carboxamide 1-beta -D-ribofuranoside (AICAR) stimulates myocardial glycogenolysis by allosteric mechanisms. *Am. J. Physiol. Regul. Integr. Comp. Physiol.* **284**, R936-944 (2003).
92 Wojtaszewski, J. F., Jorgensen, S. B., Hellsten, Y., Hardie, D. G. & Richter, E. A. Glycogen-dependent effects of 5-aminoimidazole-4-carboxamide (AICA)-riboside on AMP-activated protein kinase and glycogen synthase activities in rat skeletal muscle. *Diabetes* **51**, 284-292 (2002).

93 Derave, W. *et al.* Dissociation of AMP-activated protein kinase activation and glucose transport in contracting slow-twitch muscle. *Diabetes* **49**, 1281-1287 (2000).
94 McBride, A. & Hardie, D. G. AMP-activated protein kinase--a sensor of glycogen as well as AMP and ATP? *Acta Physiol. (Oxf)* **196**, 99-113 (2009).
95 Dzamko, N. L. & Steinberg, G. R. AMPK-dependent hormonal regulation of whole-body energy metabolism. *Acta Physiol. (Oxf)* **196**, 115-127 (2009).
96 Minokoshi, Y. *et al.* Leptin stimulates fatty-acid oxidation by activating AMP-activated protein kinase. *Nature* **415**, 339-343 (2002).
97 Yamauchi, T. *et al.* Adiponectin stimulates glucose utilization and fatty-acid oxidation by activating AMP-activated protein kinase. *Nat. Med.* **8**, 1288-1295 (2002).
98 Andreelli, F. *et al.* Liver adenosine monophosphate-activated kinase-alpha2 catalytic subunit is a key target for the control of hepatic glucose production by adiponectin and leptin but not insulin. *Endocrinology* **147**, 2432-2441 (2006).
99 Becker, D. J., Ongemba, L. N., Brichard, V., Henquin, J. C. & Brichard, S. M. Diet- and diabetes-induced changes of ob gene expression in rat adipose tissue. *FEBS Lett.* **371**, 324-328 (1995).
100 Campfield, L. A., Smith, F. J., Guisez, Y., Devos, R. & Burn, P. Recombinant mouse OB protein: evidence for a peripheral signal linking adiposity and central neural networks. *Science* **269**, 546-549 (1995).
101 Cusin, I., Sainsbury, A., Doyle, P., Rohner-Jeanrenaud, F. & Jeanrenaud, B. The ob gene and insulin. A relationship leading to clues to the understanding of obesity. *Diabetes* **44**, 1467-1470 (1995).
102 Frederich, R. C. *et al.* Expression of ob mRNA and its encoded protein in rodents. Impact of nutrition and obesity. *J. Clin. Invest.* **96**, 1658-1663 (1995).
103 Banerjee, R. R. *et al.* Regulation of fasted blood glucose by resistin. *Science* **303**, 1195-1198 (2004).
104 Manning, G., Whyte, D. B., Martinez, R., Hunter, T. & Sudarsanam, S. The protein kinase complement of the human genome. *Science* **298**, 1912-1934 (2002).
105 Lizcano, J. M. *et al.* LKB1 is a master kinase that activates 13 kinases of the AMPK subfamily, including MARK/PAR-1. *Embo J.* **23**, 833-843 (2004).
106 Jaleel, M. *et al.* Identification of the sucrose non-fermenting related kinase SNRK, as a novel LKB1 substrate. *FEBS Lett.* **579**, 1417-1423 (2005).
107 Jaleel, M. *et al.* The ubiquitin-associated domain of AMPK-related kinases regulates conformation and LKB1-mediated phosphorylation and activation. *Biochem. J.* **394**, 545-555 (2006).
108 Bright, N. J., Thornton, C. & Carling, D. The regulation and function of mammalian AMPK-related kinases. *Acta Physiol. (Oxf)* **196**, 15-26 (2009).
109 Gao, G. *et al.* Non-catalytic beta- and gamma-subunit isoforms of the 5'-AMP-activated protein kinase. *J. Biol. Chem.* **271**, 8675-8681 (1996).
110 Carlson, M. Glucose repression in yeast. *Curr. Opin. Microbiol.* **2**, 202-207 (1999).

111 Rudolph, M. J., Amodeo, G. A., Bai, Y. & Tong, L. Crystal structure of the protein kinase domain of yeast AMP-activated protein kinase Snf1. *Biochemical and Biophysical Research Communications* **337**, 1224-1228 (2005).
112 Amodeo, G. A., Rudolph, M. J. & Tong, L. Crystal structure of the heterotrimer core of Saccharomyces cerevisiae AMPK homologue SNF1. *Nature* **449**, 492-495 (2007).
113 Townley, R. & Shapiro, L. Crystal structures of the adenylate sensor from fission yeast AMP-activated protein kinase. *Science* **315**, 1726-1729 (2007).
114 Guigas, B. *et al.* 5-Aminoimidazole-4-carboxamide-1-beta-D-ribofuranoside and metformin inhibit hepatic glucose phosphorylation by an AMP-activated protein kinase-independent effect on glucokinase translocation. *Diabetes* **55**, 865-874 (2006).
115 Guigas, B. *et al.* AMP-activated protein kinase-independent inhibition of hepatic mitochondrial oxidative phosphorylation by AICA riboside. *Biochem. J.* **404**, 499-507 (2007).
116 Javaux, F., Vincent, M. F., Wagner, D. R. & van den Berghe, G. Cell-type specificity of inhibition of glycolysis by 5-amino-4-imidazolecarboxamide riboside. Lack of effect in rabbit cardiomyocytes and human erythrocytes, and inhibition in FTO-2B rat hepatoma cells. *Biochem. J.* **305 (Pt 3)**, 913-919 (1995).
117 Shang, J. & Lehrman, M. A. Activation of glycogen phosphorylase with 5-aminoimidazole-4-carboxamide riboside (AICAR). Assessment of glycogen as a precursor of mannosyl residues in glycoconjugates. *J. Biol. Chem.* **279**, 12076-12080 (2004).
118 Vincent, M. F., Bontemps, F. & Van den Berghe, G. Inhibition of glycolysis by 5-amino-4-imidazolecarboxamide riboside in isolated rat hepatocytes. *Biochem. J.* **281 (Pt 1)**, 267-272 (1992).
119 Barford, D., Hu, S. H. & Johnson, L. N. Structural mechanism for glycogen phosphorylase control by phosphorylation and AMP. *J. Mol. Biol.* **218**, 233-260 (1991).
120 Johnson, L. N. The regulation of protein phosphorylation. *Biochem. Soc. Trans.* **37**, 627-641 (2009).
121 Lorek, A. *et al.* Allosteric interactions of glycogen phosphorylase b. A crystallographic study of glucose 6-phosphate and inorganic phosphate binding to di-imidate-cross-linked phosphorylase b. *Biochem. J.* **218**, 45-60 (1984).
122 Lin, K., Hwang, P. K. & Fletterick, R. J. Distinct phosphorylation signals converge at the catalytic center in glycogen phosphorylases. *Structure* **5**, 1511-1523 (1997).
123 Benkovic, S. J. & deMaine, M. M. Mechanism of action of fructose 1,6-bisphosphatase. *Adv. Enzymol. Relat. Areas Mol. Biol.* **53**, 45-82 (1982).
124 Dzugaj, A. Localization and regulation of muscle fructose-1,6-bisphosphatase, the key enzyme of glyconeogenesis. *Adv. Enzyme Regul.* **46**, 51-71 (2006).

125 Rakus, D. & Dzugaj, A. Muscle aldolase decreases muscle FBPase sensitivity toward AMP inhibition. *Biochem. Biophys. Res. Commun.* **275**, 611-616 (2000).
126 el-Maghrabi, M. R., Gidh-Jain, M., Austin, L. R. & Pilkis, S. J. Isolation of a human liver fructose-1,6-bisphosphatase cDNA and expression of the protein in Escherichia coli. Role of ASP-118 and ASP-121 in catalysis. *J. Biol. Chem.* **268**, 9466-9472 (1993).
127 Bhattacharya, K. *et al.* A novel starch for the treatment of glycogen storage diseases. *J. Inherit. Metab. Dis.* **30**, 350-357 (2007).
128 Lizcano, J. M. & Alessi, D. R. The insulin signalling pathway. *Curr. Biol.* **12**, R236-238 (2002).
129 Hardie, D. G. AMP-activated protein kinase as a drug target. *Annu Rev Pharmacol. Toxicol.* **47**, 185-210 (2007).
130 Thorens, B. Glucose transporters in the regulation of intestinal, renal, and liver glucose fluxes. *Am. J. Physiol.* **270**, G541-553 (1996).
131 Marieb, E. & Hoehn, K. *Human Anatomy & Physiology* 7th ed edn, (Pearson Benjamin Cummings, 2007).
132 Gonzalez-Sanchez, J. L. & Serrano-Rios, M. Molecular basis of insulin action. *Drug News Perspect.* **20**, 527-531 (2007).
133 Lund, S., Holman, G. D., Schmitz, O. & Pedersen, O. Contraction stimulates translocation of glucose transporter GLUT4 in skeletal muscle through a mechanism distinct from that of insulin. *Proc. Natl. Acad. Sci. U S A* **92**, 5817-5821 (1995).
134 Kurth-Kraczek, E. J., Hirshman, M. F., Goodyear, L. J. & Winder, W. W. 5' AMP-activated protein kinase activation causes GLUT4 translocation in skeletal muscle. *Diabetes* **48**, 1667-1671 (1999).
135 Musi, N. *et al.* AMP-activated protein kinase (AMPK) is activated in muscle of subjects with type 2 diabetes during exercise. *Diabetes* **50**, 921-927 (2001).
136 Goodyear, L. J. & Kahn, B. B. Exercise, glucose transport, and insulin sensitivity. *Annu. Rev. Med.* **49**, 235-261 (1998).
137 Hayashi, T., Hirshman, M. F., Kurth, E. J., Winder, W. W. & Goodyear, L. J. Evidence for 5' AMP-activated protein kinase mediation of the effect of muscle contraction on glucose transport. *Diabetes* **47**, 1369-1373 (1998).
138 Kramer, H. F. *et al.* Distinct signals regulate AS160 phosphorylation in response to insulin, AICAR, and contraction in mouse skeletal muscle. *Diabetes* **55**, 2067-2076 (2006).
139 Towler, M. C. & Hardie, D. G. AMP-activated protein kinase in metabolic control and insulin signaling. *Circ. Res.* **100**, 328-341 (2007).
140 Fryer, L. G., Parbu-Patel, A. & Carling, D. The Anti-diabetic drugs rosiglitazone and metformin stimulate AMP-activated protein kinase through distinct signaling pathways. *J. Biol. Chem.* **277**, 25226-25232 (2002).
141 Hawley, S. A., Gadalla, A. E., Olsen, G. S. & Hardie, D. G. The antidiabetic drug metformin activates the AMP-activated protein kinase cascade via an adenine nucleotide-independent mechanism. *Diabetes* **51**, 2420-2425 (2002).

142 King, T. D., Song, L. & Jope, R. S. AMP-activated protein kinase (AMPK) activating agents cause dephosphorylation of Akt and glycogen synthase kinase-3. *Biochem. Pharmacol.* **71**, 1637-1647 (2006).
143 Saha, A. K. *et al.* Pioglitazone treatment activates AMP-activated protein kinase in rat liver and adipose tissue in vivo. *Biochem. Biophys. Res. Commun.* **314**, 580-585 (2004).
144 Zhou, G. *et al.* Role of AMP-activated protein kinase in mechanism of metformin action. *J. Clin. Invest.* **108**, 1167-1174 (2001).
145 Bolen, S. *et al.* Systematic review: comparative effectiveness and safety of oral medications for type 2 diabetes mellitus. *Ann. Intern. Med.* **147**, 386-399 (2007).
146 Fogarty, S. & Hardie, D. G. Development of protein kinase activators: AMPK as a target in metabolic disorders and cancer. *Biochim. Biophys. Acta* **1804**, 581-591.
147 Harris, G. in *New York Times* (New York, 2010).
148 Misbin, R. I. Phenformin-associated lactic acidosis: pathogenesis and treatment. *Ann. Intern. Med.* **87**, 591-595 (1977).
149 Galuska, D. *et al.* Effects of non-esterified fatty acids on insulin-stimulated glucose transport in isolated skeletal muscle from patients with type 2 (non-insulin-dependent) diabetes mellitus. *Acta Diabetol.* **31**, 169-172 (1994).
150 Stumvoll, M., Nurjhan, N., Perriello, G., Dailey, G. & Gerich, J. E. Metabolic effects of metformin in non-insulin-dependent diabetes mellitus. *N Engl. J. Med.* **333**, 550-554 (1995).
151 El-Mir, M. Y. *et al.* Dimethylbiguanide inhibits cell respiration via an indirect effect targeted on the respiratory chain complex I. *J. Biol. Chem.* **275**, 223-228 (2000).
152 Owen, M. R., Doran, E. & Halestrap, A. P. Evidence that metformin exerts its anti-diabetic effects through inhibition of complex 1 of the mitochondrial respiratory chain. *Biochem. J.* **348 Pt 3**, 607-614 (2000).
153 Zou, M. H. *et al.* Activation of the AMP-activated protein kinase by the anti-diabetic drug metformin in vivo. Role of mitochondrial reactive nitrogen species. *J. Biol. Chem.* **279**, 43940-43951 (2004).
154 Cool, B. *et al.* Identification and characterization of a small molecule AMPK activator that treats key components of type 2 diabetes and the metabolic syndrome. *Cell. Metab.* **3**, 403-416 (2006).
155 Moreno, D., Knecht, E., Viollet, B. & Sanz, P. A769662, a novel activator of AMP-activated protein kinase, inhibits non-proteolytic components of the 26S proteasome by an AMPK-independent mechanism. *FEBS Lett.* **582**, 2650-2654 (2008).
156 Evans, J. M., Donnelly, L. A., Emslie-Smith, A. M., Alessi, D. R. & Morris, A. D. Metformin and reduced risk of cancer in diabetic patients. *BMJ* **330**, 1304-1305 (2005).
157 Dowling, R. J., Zakikhani, M., Fantus, I. G., Pollak, M. & Sonenberg, N. Metformin inhibits mammalian target of rapamycin-dependent translation initiation in breast cancer cells. *Cancer Res.* **67**, 10804-10812 (2007).

158 Zakikhani, M., Dowling, R., Fantus, I. G., Sonenberg, N. & Pollak, M. Metformin is an AMP kinase-dependent growth inhibitor for breast cancer cells. *Cancer Res.* **66**, 10269-10273 (2006).
159 Schmelzle, T. & Hall, M. N. TOR, a central controller of cell growth. *Cell* **103**, 253-262 (2000).
160 Tee, A. R. & Blenis, J. mTOR, translational control and human disease. *Semin. Cell Dev. Biol.* **16**, 29-37 (2005).
161 Wang, W. & Guan, K. L. AMP-activated protein kinase and cancer. *Acta Physiol. (Oxf)* **196**, 55-63 (2009).
162 Inoki, K., Li, Y., Xu, T. & Guan, K. L. Rheb GTPase is a direct target of TSC2 GAP activity and regulates mTOR signaling. *Genes Dev.* **17**, 1829-1834 (2003).
163 Giardiello, F. M. *et al.* Increased risk of cancer in the Peutz-Jeghers syndrome. *N. Engl. J. Med.* **316**, 1511-1514 (1987).
164 Guldberg, P. *et al.* Somatic mutation of the Peutz-Jeghers syndrome gene, LKB1/STK11, in malignant melanoma. *Oncogene* **18**, 1777-1780 (1999).
165 Hearle, N. *et al.* Frequency and spectrum of cancers in the Peutz-Jeghers syndrome. *Clin. Cancer Res.* **12**, 3209-3215 (2006).
166 Sanchez-Cespedes, M. *et al.* Inactivation of LKB1/STK11 is a common event in adenocarcinomas of the lung. *Cancer Res.* **62**, 3659-3662 (2002).
167 Su, G. H. *et al.* Germline and somatic mutations of the STK11/LKB1 Peutz-Jeghers gene in pancreatic and biliary cancers. *Am. J. Pathol.* **154**, 1835-1840 (1999).
168 Lee, J. H. *et al.* Energy-dependent regulation of cell structure by AMP-activated protein kinase. *Nature* **447**, 1017-U1019 (2007).
169 Mirouse, V., Swick, L. L., Kazgan, N., St Johnston, D. & Brenman, J. E. LKB1 and AMPK maintain epithelial cell polarity under energetic stress. *J. Cell Biol.* **177**, 387-392 (2007).
170 Zhang, L., Li, J., Young, L. H. & Caplan, M. J. AMP-activated protein kinase regulates the assembly of epithelial tight junctions. *Proc. Natl. Acad. Sci. U S A* **103**, 17272-17277 (2006).
171 Zheng, B. & Cantley, L. C. Regulation of epithelial tight junction assembly and disassembly by AMP-activated protein kinase. *Proc. Natl. Acad. Sci. U S A* **104**, 819-822 (2007).
172 Milan, D. *et al.* A mutation in PRKAG3 associated with excess glycogen content in pig skeletal muscle. *Science* **288**, 1248-1251 (2000).
173 Hardie, D. G. AMP-activated/SNF1 protein kinases: conserved guardians of cellular energy. *Nat. Rev. Mol. Cell. Biol.* **8**, 774-785 (2007).
174 Akman, H. O. *et al.* Fatal infantile cardiac glycogenosis with phosphorylase kinase deficiency and a mutation in the gamma2-subunit of AMP-activated protein kinase. *Pediatr. Res.* **62**, 499-504 (2007).
175 Arad, M. *et al.* Constitutively active AMP kinase mutations cause glycogen storage disease mimicking hypertrophic cardiomyopathy. *J. Clin. Invest.* **109**, 357-362 (2002).
176 Arad, M. *et al.* Glycogen storage diseases presenting as hypertrophic cardiomyopathy. *N. Engl. J. Med.* **352**, 362-372 (2005).

177 Bayrak, F. *et al.* Ventricular pre-excitation and cardiac hypertrophy mimicking hypertrophic cardiomyopathy in a Turkish family with a novel PRKAG2 mutation. *Eur. J. Heart Fail.* **8**, 712-715 (2006).
178 Blair, E. *et al.* Mutations in the gamma(2) subunit of AMP-activated protein kinase cause familial hypertrophic cardiomyopathy: evidence for the central role of energy compromise in disease pathogenesis. *Hum. Mol. Genet.* **10**, 1215-1220 (2001).
179 Burwinkel, B. *et al.* Fatal congenital heart glycogenosis caused by a recurrent activating R531Q mutation in the gamma 2-subunit of AMP-activated protein kinase (PRKAG2), not by phosphorylase kinase deficiency. *Am. J. Hum. Genet.* **76**, 1034-1049 (2005).
180 Gollob, M. H. *et al.* Identification of a gene responsible for familial Wolff-Parkinson-White syndrome. *N. Engl. J. Med.* **344**, 1823-1831 (2001).
181 Gollob, M. H. *et al.* Novel PRKAG2 mutation responsible for the genetic syndrome of ventricular preexcitation and conduction system disease with childhood onset and absence of cardiac hypertrophy. *Circulation* **104**, 3030-3033 (2001).
182 Laforet, P. *et al.* A new mutation in PRKAG2 gene causing hypertrophic cardiomyopathy with conduction system disease and muscular glycogenosis. *Neuromuscul. Disord.* **16**, 178-182 (2006).
183 Murphy, R. T. *et al.* Adenosine monophosphate-activated protein kinase disease mimicks hypertrophic cardiomyopathy and Wolff-Parkinson-White syndrome: natural history. *J. Am. Coll. Cardiol.* **45**, 922-930 (2005).
184 Barnes, B. R. *et al.* The 5'-AMP-activated protein kinase gamma3 isoform has a key role in carbohydrate and lipid metabolism in glycolytic skeletal muscle. *J. Biol. Chem.* **279**, 38441-38447 (2004).
185 Hamilton, S. R. *et al.* An activating mutation in the gamma1 subunit of the AMP-activated protein kinase. *FEBS Lett.* **500**, 163-168 (2001).
186 Daniel, T. & Carling, D. Functional analysis of mutations in the gamma 2 subunit of AMP-activated protein kinase associated with cardiac hypertrophy and Wolff-Parkinson-White syndrome. *J. Biol. Chem.* **277**, 51017-51024 (2002).
187 Hawley, S. A. *et al.* Use of cells expressing gamma subunit variants to identify diverse mechanisms of AMPK activation. *Cell Metab.* **11**, 554-565 (2010).
188 Barre, L. *et al.* Genetic model for the chronic activation of skeletal muscle AMP-activated protein kinase leads to glycogen accumulation. *Am. J. Physiol. Endocrinol. Metab.* **292**, E802-811 (2007).
189 Nilsson, E. C. *et al.* Opposite transcriptional regulation in skeletal muscle of AMP-activated protein kinase gamma3 R225Q transgenic versus knock-out mice. *J. Biol. Chem.* **281**, 7244-7252 (2006).
190 Arad, M. *et al.* Transgenic mice overexpressing mutant PRKAG2 define the cause of Wolff-Parkinson-White syndrome in glycogen storage cardiomyopathy. *Circulation* **107**, 2850-2856 (2003).

191 Banerjee, S. K. *et al.* A PRKAG2 mutation causes biphasic changes in myocardial AMPK activity and does not protect against ischemia. *Biochem. Biophys. Res. Commun.* **360**, 381-387 (2007).
192 Davies, J. K. *et al.* Characterization of the role of gamma2 R531G mutation in AMP-activated protein kinase in cardiac hypertrophy and Wolff-Parkinson-White syndrome. *Am. J. Physiol. Heart Circ. Physiol.* **290**, H1942-1951 (2006).
193 Sidhu, J. S. *et al.* Transgenic mouse model of ventricular preexcitation and atrioventricular reentrant tachycardia induced by an AMP-activated protein kinase loss-of-function mutation responsible for Wolff-Parkinson-White syndrome. *Circulation* **111**, 21-29 (2005).
194 Arad, M., Seidman, C. E. & Seidman, J. G. AMP-activated protein kinase in the heart: role during health and disease. *Circ. Res.* **100**, 474-488 (2007).
195 Ahmad, F. *et al.* Increased alpha2 subunit-associated AMPK activity and PRKAG2 cardiomyopathy. *Circulation* **112**, 3140-3148 (2005).
196 Kennan, A. *et al.* Identification of an IMPDH1 mutation in autosomal dominant retinitis pigmentosa (RP10) revealed following comparative microarray analysis of transcripts derived from retinas of wild-type and Rho(-/-) mice. *Hum. Mol. Genet.* **11**, 547-557 (2002).
197 Kluijtmans, L. A. *et al.* Defective cystathionine beta-synthase regulation by S-adenosylmethionine in a partially pyridoxine responsive homocystinuria patient. *J. Clin. Invest.* **98**, 285-289 (1996).
198 Cleiren, E. *et al.* Albers-Schonberg disease (autosomal dominant osteopetrosis, type II) results from mutations in the ClCN7 chloride channel gene. *Hum. Mol. Genet.* **10**, 2861-2867 (2001).
199 Haug, K. *et al.* Mutations in CLCN2 encoding a voltage-gated chloride channel are associated with idiopathic generalized epilepsies. *Nat. Genet.* **33**, 527-532 (2003).
200 Konrad, M. *et al.* Mutations in the chloride channel gene CLCNKB as a cause of classic Bartter syndrome. *J. Am. Soc. Nephrol.* **11**, 1449-1459 (2000).
201 Lloyd, S. E. *et al.* Characterisation of renal chloride channel, CLCN5, mutations in hypercalciuric nephrolithiasis (kidney stones) disorders. *Hum. Mol. Genet.* **6**, 1233-1239 (1997).
202 Pusch, M. Myotonia caused by mutations in the muscle chloride channel gene CLCN1. *Hum. Mutat.* **19**, 423-434 (2002).
203 Goodstadt, L. & Ponting, C. P. CHROMA: consensus-based colouring of multiple alignments for publication. *Bioinformatics* **17**, 845-846 (2001).
204 Schmaier, A. H., Meloni, F. J., Nawarawong, W. & Jiang, Y. P. PPACK-thrombin is a noncompetitive inhibitor of alpha-thrombin binding to human platelets. *Thromb. Res.* **67**, 479-489 (1992).
205 Laemmli, U. K. Cleavage of structural proteins during the assembly of the head of bacteriophage T4. *Nature* **227**, 680-685 (1970).
206
207 Gill, S. C. & von Hippel, P. H. Calculation of protein extinction coefficients from amino acid sequence data. *Anal. Biochem.* **182**, 319-326 (1989).

208 Wilson, W. W. Light scattering as a diagnostic for protein crystal growth--a practical approach. *J. Struct. Biol.* **142**, 56-65 (2003).
209 Zulauf, M. & D'Arcy, A. Light scattering of proteins as a criterion for crystallization. *Journal of Crystal Growth* **122** 102-106 (2002).
210 Otwinowski, Z. & Minor, W. Sawyer, L.,Isaacs, N. & Bailey, S. edn 556-562
211 Navaza, J. AMoRe: an Automated Package for Molecular Replacement. *Acta Crystallogr.* **A 50** 157-163 (1994).
212 McCoy, A. J. *et al.* Phaser crystallographic software. *J. Appl. Crystallogr.* **40**, 658-674 (2007).
213 Xiao, B. *et al.* Structural basis for AMP binding to mammalian AMP-activated protein kinase. *Nature* **449**, 496-U414 (2007).
214 CCP4. The CCP4 suite: programs for protein crystallography. *Acta Crystallographica Section D* **50** 760-763 (1994).
215 Emsley, P. & Cowtan, K. Coot: model-building tools for molecular graphics. *Acta Crystallogr. D Biol. Crystallogr.* **60**, 2126-2132 (2004).
216 Laskowski, R. A., MacArthur, M. W., Moss, D. S. & Thornton, J. M. PROCHECK: a program to check the stereochemical quality of protein structures. *Journal of Applied Crystallography* **26** 283-291 (1993).
217 Davis, I. W. *et al.* MolProbity: all-atom contacts and structure validation for proteins and nucleic acids. *Nucleic Acids Res* **35**, W375-383 (2007).
218 Kleywegt, G.J. (1996). Use of non-crystallographic symmetry in protein structure refinement. Acta Cryst. **D**52, 842-857 http://xray.bmc.uu.se/usf/lsqman_man.html.
219 DeLano, W.L. The PyMOL Molecular Graphics System (2002) DeLano Scientific, San Carlos, CA, USA. http://www.pymol.org.
220 Nicholls, A. Sharp, K.A. and Honig, B. (1991) Protein Folding and Association: Insights From the Interfacial and Thermodynamic Properties of Hydrocarbons. Proteins: Stuc. Func. and Genet. **11,** 281-296 http://trantor.bioc.columbia.edu/grasp/.
221 Jameson, D. M. & Eccleston, J. F. Fluorescent nucleotide analogs: synthesis and applications. *Methods Enzymol.* **278**, 363-390 (1997).
222 Lowry, O. H., Passonneau, J. V. & Rock, M. K. The stability of pyridine nucleotides. *J. Biol. Chem.* **236**, 2756-2759 (1961).
223 Stryer, L. & Haugland, R. P. Energy transfer: a spectroscopic ruler. *Proc Natl. Acad. Sci. U S A* **58**, 719-726 (1967).
224 Stryer, L. Fluorescence energy transfer as a spectroscopic ruler. *Annu. Rev. Biochem.* **47**, 819-846 (1978).
225 Woodward, S. K., Eccleston, J. F. & Geeves, M. A. Kinetics of the interaction of 2'(3')-O-(N-methylanthraniloyl)-ATP with myosin subfragment 1 and actomyosin subfragment 1: characterization of two acto-S1-ADP complexes. *Biochemistry* **30**, 422-430 (1991).
226 Mayhood, T. W. & Windsor, W. T. Ligand binding affinity determined by temperature-dependent circular dichroism: cyclin-dependent kinase 2 inhibitors. *Anal. Biochem.* **345**, 187-197 (2005).

227 Pantoliano, M. W. *et al.* High-density miniaturized thermal shift assays as a general strategy for drug discovery. *J. Biomol. Screen.* **6**, 429-440 (2001).
228 Adams, P. D. *et al.* PHENIX: building new software for automated crystallographic structure determination. *Acta Crystallogr. D Biol. Crystallogr.* **58**, 1948-1954 (2002).
229 Davies, S. P., Carling, D. & Hardie, D. G. Tissue distribution of the AMP-activated protein kinase, and lack of activation by cyclic-AMP-dependent protein kinase, studied using a specific and sensitive peptide assay. *European Journal of Biochemistry* **186**, 123-128 (1989).
230 Cook, P. F., Neville, M. E., Jr., Vrana, K. E., Hartl, F. T. & Roskoski, R., Jr. Adenosine cyclic 3',5'-monophosphate dependent protein kinase: kinetic mechanism for the bovine skeletal muscle catalytic subunit. *Biochemistry* **21**, 5794-5799 (1982).
231 Hiratsuka, T. New ribose-modified fluorescent analogs of adenine and guanine nucleotides available as substrates for various enzymes. *Biochim Biophys. Acta* **742**, 496-508 (1983).
232 Corkey, B. E., Duszynski, J., Rich, T. L., Matschinsky, B. & Williamson, J. R. Regulation of free and bound magnesium in rat hepatocytes and isolated mitochondria. *J. Biol. Chem.* **261**, 2567-2574 (1986).
233 Waldron, T. T. & Murphy, K. P. Stabilization of proteins by ligand binding: application to drug screening and determination of unfolding energetics. *Biochemistry* **42**, 5058-5064 (2003).
234 Linse, S., Helmersson, A. & Forsen, S. Calcium binding to calmodulin and its globular domains. *J. Biol. Chem.* **266**, 8050-8054 (1991).
235 Janosik, M., Kery, V., Gaustadnes, M., Maclean, K. N. & Kraus, J. P. Regulation of human cystathionine beta-synthase by S-adenosyl-L-methionine: evidence for two catalytically active conformations involving an autoinhibitory domain in the C-terminal region. *Biochemistry* **40**, 10625-10633 (2001).
236 Ying, W. NAD+/NADH and NADP+/NADPH in cellular functions and cell death: regulation and biological consequences. *Antioxid. Redox Signal.* **10**, 179-206 (2008).
237 Jin, X., Townley, R. & Shapiro, L. Structural insight into AMPK regulation: ADP comes into play. *Structure* **15**, 1285-1295 (2007).
238 Day, P. *et al.* Structure of a CBS-domain pair from the regulatory gamma1 subunit of human AMPK in complex with AMP and ZMP. *Acta Crystallogr. D Biol. Crystallogr.* **63**, 587-596 (2007).
239 Carling, D., Clarke, P. R., Zammit, V. A. & Hardie, D. G. Purification and characterization of the AMP-activated protein kinase. Copurification of acetyl-CoA carboxylase kinase and 3-hydroxy-3-methylglutaryl-CoA reductase kinase activities. *European Journal of Biochemistry* **186**, 129-136 (1989).